UNIVERSITÉ DE LILLE

ECOLE DOCTORALE BIOLOGIE SANTE DE LILLE (446)

Année : 2023

THÈSE

Pour l'obtention du diplôme

DE DOCTEUR DE L'UNIVERSITE DE LILLE

Caractérisation radiomics en IRM de l'infarctus et de la santé cérébrale des patients victimes d'AVC ischémique

Présentée et soutenue publiquement le 16 mai 2023

au Pôle Recherche

par Martin BRETZNER

Jury

Monsieur le Professeur Jean Pierre PRUVO	**Président**
Madame le Professeur Catherine OPPENHEIM	**Rapporteuse**
Madame le Professeur Laure FOURNIER	**Rapporteuse**
Madame le Professeur Myriam EDJLALI-GOUJON	**Examinatrice**
Monsieur le Professeur Xavier LECLERC	**Directeur**
Monsieur le Docteur Grégory KUCHCINSKI	**Co-Directeur**

Cette thèse a été préparée dans l'unité Inserm U1172 « Lille Neuroscience et Cognition » (Pr. Luc Buee) au sein de l'équipe « Troubles cognitifs dégénératifs et vasculaires » (Pr. David Devos) et dans l'UAR 2014 – US41 PLBS « Lille Invivo Imaging and Functional Exploration » (Pr. Jean-Pierre Pruvo).

Cette thèse a été également préparée dans le Rost Lab (Pr. Natalia Rost) au sein du J.P. Kistler Stroke Research Center (Pr. Steve Greenbeerg) au Mass General Brigham/Harvard Medical School (Boston, USA).

Remerciements

Aux organismes qui m'ont fait confiance

Ce travail n'aurait jamais vu le jour sans le soutien important des organismes qui m'ont fait confiance et financé. Je remercie donc la fondation ISITE-ULNE pour son soutien au travers de son programme *Health-PhD*, la Société Française de Neuroradiologie pour son soutien au travers de la bourse mobilité *Anne Bertrand*, La Société Française de Radiologie pour son soutien au travers de la bourse mobilité *Alain Rahmouni*, la Fondation Thérèse et René Planiol pour son soutien au travers de son programme d'aide à la mobilité, et l'European Society of Radiology et l'European Institute for Biomedical Imaging Research pour le soutien grâce à leur programme *Seed Grant*.

A mon Jury

Liste des tableaux

Liste des figures

Résumé

L'AVC ischémique (AVCi) est une cause majeure de handicap et de mortalité dans le monde et est ainsi un problème global de santé publique. Son pronostic est multifactoriel mais dépend principalement de la lésion ischémique et de l'état du cerveau sous-jacent. Leur caractérisation peut être réalisée en IRM mais son interprétation reste subjective et cette variabilité peut impacter le soin. Il est donc nécessaire de développer des biomarqueurs d'imagerie objectifs et quantitatifs de la lésion ischémique et de la santé cérébrale afin d'améliorer le diagnostic, le pronostic, et le traitement de l'AVCi. Les radiomics, l'extraction automatique de paramètres texturaux à partir d'imagerie médicale, peut fournir ces biomarqueurs, en décrivant quantitativement l'image IRM. Durant ma thèse, nous avons donc évalué les performances des radiomics pour caractériser l'infarctus et la santé cérébrale des patients victimes d'AVC ischémique.

L'objectif de notre premier travail a été de développer un biomarqueur pour quantifier la discordance DWI-FLAIR dans la caractérisation IRM des AVCi. En effet, dans les AVCi de début inconnu ou de présentation tardive, le traitement n'est indiqué que chez les patients ne présentant pas d'hypersignal FLAIR intra-lésionnel. Nous avons conduit une analyse radiomics des infarctus de 103 patients en FLAIR et en diffusion et avons prédit, grâce à un algorithme d'apprentissage machine, l'interprétation visuelle par deux experts du signal FLAIR lésionnel. Alors que l'accord inter-observateur était modeste (Cohen K=0.58), nous avons identifié deux variables radiomics (FLAIR kurtosis et Cluster Shade) prédictives de la positivité lésionnelle en FLAIR. Cette signature radiomics représente un potentiel biomarqueur thérapeutique innovant pour le soin des patients victimes d'AVCi.

Notre second travail nous a permis d'évaluer l'approche radiomics dans la quantification de la charge lésionnelle neurovasculaire. A partir de 4163 patients issus d'une cohorte multicentrique internationale de patients victimes d'AVCi, et grâce à un algorithme d'intelligence artificielle, nous avons montré que les radiomics T2-FLAIR du parenchyme d'allure saine étaient prédictifs du volume de leucopathie (R2=0.855±0.011). Ainsi, l'analyse radiomics des imageries T2-FLAIR permet d'identifier des altérations cérébrales au-delà des anomalies visibles sur les séquences

morphologiques. De plus, nous avons suggéré que certains profils de risques cardiovasculaires avaient une expression texturale spécifique. Enfin, l'âge était particulièrement bien capturé par les radiomics ce qui nous a permis de conceptualiser notre article suivant.

Durant notre troisième travail, nous avons étudié l'âge cérébral comme biomarqueur de santé cérébrale chez les patients victimes d'AVCi. En exploitant la même cohorte de 4163 patients avec un modèle d'apprentissage machine, nous avons prédit l'âge chronologique des patients à partir des radiomics T2-FLAIR. Puis, nous avons étudié la différence entre l'âge prédit, appelé âge cérébral, et l'âge chronologique et avons dérivé une variable indépendante de l'âge : l'âge cérébral relatif. Nous avons montré que les patients dont le cerveau avait l'air plus âgé avaient significativement plus de facteurs de risques cardiovasculaires (hypertension, diabète, tabagisme, antécédent d'AVC). Enfin, nous avons montré que l'âge cérébral relatif était associé au pronostic fonctionnel de l'AVC de manière indépendante à l'âge chronologique, au NIHSS, et aux antécédents d'AVC (Odds-ratios ajustés : 0.76, 0.58, 0.48, 0.55; p-values<0.001).

En conclusion, ma thèse montre des exemples applicatifs des radiomics et de l'intelligence artificielle dans la caractérisation des lésions ischémiques et de la santé cérébrale chez des patients victimes d'AVC ischémiques. Nos résultats suggèrent que ces techniques innovantes pourraient aider à orienter le soin de ces patients.

Abstract

Ischemic stroke (IS) is a major cause of disability and mortality worldwide and is therefore a global public health issue. Its prognosis depends on various factors but mainly on the extent of the ischemic injury and the condition of the underlying brain. While MRI can be used to characterize these aspects, its interpretation is subjective, which can impact treatment decisions. Therefore, there is a need to develop objective and quantitative imaging biomarkers for ischemic injury and brain health to improve the diagnosis, prognosis, and treatment of stroke. Radiomics, which involves the automatic extraction of texture parameters from medical imaging, can provide these biomarkers by quantitatively describing MRI images. In this thesis, we evaluated the performance of radiomics in characterizing infarcts and brain health in patients with ischemic stroke.

Our first study aimed to develop a biomarker to quantify the DWI-FLAIR mismatch in the MRI characterization of IS. In cases where the onset or presentation of IS is unknown or delayed, treatment is only indicated in patients without FLAIR intra-lesional hyperintensity. We conducted a radiomics analysis of infarcts in 103 patients using FLAIR and diffusion imaging and predicted the consensual visual interpretation of FLAIR lesion signal by two experts using a machine learning algorithm. Although the inter-observer agreement was modest (Cohen's K=.58), we identified two radiomics variables (FLAIR kurtosis and Cluster Shade) that were predictive of FLAIR lesion positivity. This radiomics signature represents an innovative potential therapeutic biomarker for the management of patients with IS.

Our second study allowed us to evaluate the radiomics approach in quantifying the cerebral burden of disease. Using an artificial intelligence algorithm on 4163 patients from an international multicenter cohort of patients with IS, we showed that T2-FLAIR radiomics of healthy-looking parenchyma predicted the volume of white matter hyperintensities ($R2=0.855\pm0.011$). Thus, radiomics analysis of T2-FLAIR imaging can identify brain alterations beyond those visible on morphological sequences. Additionally, we suggested that certain cardiovascular risk profiles had specific textural expressions. Finally, age was the clinical trait best represented by radiomics, which allowed us to conceptualize our next article.

In our third study, we investigated brain age as a biomarker of brain health in patients with IS. Using the same cohort of 4163 patients with a machine learning model, we predicted the chronological age of patients from T2-FLAIR radiomics. Then, we studied the difference between the predicted age, called brain age, and chronological age and derived an age-independent biomarker: relative brain age (RBA). We showed that patients with brains that appeared older had significantly more cardiovascular risk factors (hypertension, diabetes mellitus, smoking, history of stroke). Finally, we demonstrated that RBA was independently associated with poststroke functional prognosis, even after adjusting for chronological age, NIHSS, and history of stroke (respective adjusted odds ratios: 0.76, 0.58, 0.48, 0.55; all p-values<.001).

In conclusion, this thesis provides examples of the joint application of radiomics and artificial intelligence in characterizing ischemic lesions and brain health in patients with ischemic stroke. Our results suggest that these innovative techniques could help guide the management of these patients.

Table of Contents

Production scientifique

Publications scientifiques premier auteur

1. Bretzner M, Bonkhoff AK, Schirmer MD, et al. MRI Radiomic Signature of White Matter Hyperintensities Is Associated With Clinical Phenotypes. Front Neurosci. 2021;15:691244.

2. Regenhardt RW, Bretzner M, Zanon Zotin MC, et al. Radiomic signature of DWI-FLAIR mismatch in large vessel occlusion stroke. Journal of Neuroimaging. 2022;32:63–67. (co-premier)

3. Bretzner M, Bonkhoff AK, Schirmer MD, et al. Radiomics-Derived Brain Age Predicts Functional Outcome After Acute Ischemic Stroke. Neurology. Epub 2022 Nov 28.:10.1212/WNL.0000000000201596.

Communications orales en lien avec la thèse

1. 2023 – European Congress of Radiology – Présentation orale (5 minutes) : “The Brain Age Biomarker Initiative in Stroke”

2. 2023 – European Stroke Organisation Conference - Lecture Invitée (15 minutes) : “Role Of Radiomics In Stroke Outcome”.

3. 2022 – International Stroke Genetics Consortium Workshop – Lecture Invitée Avec Dr. Markus Schirmer (50 Min) : “Overview Of MRIGENIE Imaging Group Results – Summoning The Genie”.

4. 2022 – Lil’N Doc Day 2022 – Présentation orale (20 minutes) - “Radiomics Brain Age, A Novel Brain Health Imaging Biomarkers In Stroke Patients”.

5. 2022 – European Stroke Organization Conference – Présentation orale (10min) : “Radiomics Derived Brain Age Predicts Functional Outcome After Acute Ischemic Stroke”.

6. 2022 – Mass General Brigham Mccance Brain Health Seminar Series – Lecture Invitée (30min) : “Radiomics Brain Age, A Novel Brain Health Imaging Biomarkers In Stroke Patients”. (Https://Www.Youtube.Com/Watch?V=Ko4imbcxn6s)

7. 2021 – Mass General Brigham Stroke Research Center Seminar – Lecture Invitée (45min) : “Radiomics Brain Age Predicts Functional Outcome After Acute Ischemic Stroke”.

8. 2021 – International Stroke Conference – Abstract écrit (10min) : “Radiomics Signature Of Dwi-Flair Mismatch Correlates With Clinical Phenotype Of Patients With Large Vessel Occlusion Stroke”.

9. 2021 – International Stroke Conference – Abstract oral (10min) : “Radiomic Signature Of The Wmh Burden Correlates With Clinical Phenotypes”.

10. 2020 – European Stroke Organization Conference – Abstract oral (10min) : “The Impact Of MRI Textural Features On Stroke Outcome Prediction”.

Couverture médiatique en presse spécialisée

1. https://www.healthline.com/health-news/measuring-brain-age-biomarkers-may-better-predict-stroke-care-and-recovery
2. https://www.auntminnieeurope.com/index.aspx?sec=sup&sub=mri&pag=dis&ItemID=622465
3. https://www.medscape.com/viewarticle/973528?reg=1
4. https://2022.eso-conference.org/wp-content/uploads/2022/05/%E2%80%98Brain-age-biomarkers-predict-stroke-recovery_Thur5-May-0.01.pdf
5. https://vjneurology.com/speaker/martin-bretzner/

Couverture médiatique grand public

1. https://www.publico.pt/2022/05/04/ciencia/noticia/idade-cerebro-tambem-conta-prevencao-recuperacao-avc-2004845?ref=hp&cx=latest_news_a_v2--496639

Productions scientifiques associées durant la thèse

1. Bonkhoff AK, Schirmer MD, Bretzner M, et al. The relevance of rich club regions for functional outcome post-stroke is enhanced in women. Hum Brain Mapp. 2023;44:1579–1592.

2. Seners P, Scheldeman L, Christensen S, et al. Determinants of Infarct Core Growth During Inter-hospital Transfer for Thrombectomy. Ann Neurol. Epub 2023 Feb 7.

3. Dhoisne M, Puy L, Bretzner M, et al. Early reocclusion after successful mechanical thrombectomy for large artery occlusion-related stroke. Int J Stroke. Epub 2023 Jan 6.:17474930221148894.

4. Kraft AW, Regenhardt RW, Awad A, et al. Spoke-administered thrombolysis improves large vessel occlusion early recanalization: the real-world experience of a large academic hub-and-spoke telestroke network. Stroke Vasc Interv Neurol. 2023;3:e000427.

5. Regenhardt RW, Nolan NM, Rosenthal JA, et al. Understanding Delays in MRI-based Selection of Large Vessel Occlusion Stroke Patients for Endovascular Thrombectomy. Clin Neuroradiol. 2022;32:979–986.

6. Regenhardt RW, Rosenthal JA, Dmytriw AA, et al. Direct to angio-suite large vessel occlusion transfers achieve faster arrival-to-puncture times and improved outcomes. Stroke Vasc Interv Neurol. 2022;2:e000327.

7. Regenhardt RW, Awad A, Kraft AW, et al. Characterizing reasons for stroke thrombectomy ineligibility among potential candidates transferred in a hub-and-spoke network. Stroke Vasc Interv Neurol. 2022;2:e000282.

8. Forestier G, Agbonon R, Bricout N, et al. Small vessel disease and collaterals in ischemic stroke patients treated with thrombectomy. J Neurol. 2022;269:4708–4716.

9. Bonkhoff AK, Hong S, Bretzner M, et al. Association of Stroke Lesion Pattern and White Matter Hyperintensity Burden With Stroke Severity and Outcome. Neurology. Epub 2022 Jul 8.:10.1212/WNL.0000000000200926.

10. Marchal A, Bretzner M, Casolla B, et al. Endovascular Thrombectomy for Distal Medium Vessel Occlusions of the Middle Cerebral Artery: A Safe and Effective Procedure. World Neurosurgery. 2022;160:e234–e241.

11. Sveikata L, Vasung L, El Rahal A, et al. Syndrome of the trephined: clinical spectrum, risk factors, and impact of cranioplasty on neurologic recovery in a prospective cohort. Neurosurg Rev. 2022;45:1431–1443.

12. Kraft AW, Awad A, Rosenthal JA, et al. In a hub-and-spoke network, spoke-administered thrombolysis reduces mechanical thrombectomy procedure time and number of passes. Interv Neuroradiol. SAGE Publications Ltd; Epub 2022 Mar 23.:15910199221087498.

13. Regenhardt RW, Bonkhoff AK, Bretzner M, et al. Association of Infarct Topography and Outcome After Endovascular Thrombectomy in Patients With Acute Ischemic Stroke. Neurology. 2022;98:e1094–e1103.

14. Bonkhoff AK, Bretzner M, Hong S, et al. Sex-specific lesion pattern of functional outcomes after stroke. Brain Communications. Epub 2022 Feb 2.:fcac020.

15. Zanon Zotin MC, Schoemaker D, Raposo N, et al. Peak width of skeletonized mean diffusivity in cerebral amyloid angiopathy: Spatial signature, cognitive, and neuroimaging associations. Front Neurosci. 2022;16:1051038.

16. Bonkhoff AK, Ullberg T, Bretzner M, et al. Deep profiling of multiple ischemic lesions in a large, multi-center cohort: Frequency, spatial distribution, and associations to clinical characteristics. Front Neurosci. 2022;16:994458.

17. Hassen WB, Touloupas C, Benzakoun J, et al. Impact of Repeated Clot Retrieval Attempts on Infarct Growth and Outcome After Ischemic Stroke. Neurology. Wolters Kluwer Health, Inc. on behalf of the American Academy of Neurology; 2021;97:e444–e453.

18. Bonkhoff AK, Schirmer MD, Bretzner M, et al. Outcome after acute ischemic stroke is linked to sex-specific lesion patterns. Nat Commun. 2021;12:3289.

19. Etherton MR, Zachrison KS, Yan Z, et al. Regional Changes in Patterns of Stroke Presentation During the COVID-19 Pandemic. Stroke. American Heart Association; 2021;52:1398–1406.

20. Hong S, Marinescu R, Dalca AV, et al. 3D-StyleGAN: A Style-Based Generative Adversarial Network for Generative Modeling of Three-Dimensional Medical Images. In: Engelhardt S, Oksuz I, Zhu D, et al., editors. Deep Generative Models, and Data Augmentation, Labelling, and Imperfections. Cham: Springer International Publishing; 2021. p. 24–34.

21. Hong S, Giese A-K, Schirmer MD, et al. Excessive White Matter Hyperintensity Increases Susceptibility to Poor Functional Outcomes After Acute Ischemic Stroke. Front Neurol. 2021;12:700616.

22. Hong S, Bonkhoff AK, Hoopes A, et al. Hypernet-Ensemble Learning of Segmentation Probability for Medical Image Segmentation with Ambiguous Labels. arXiv; Epub 2021. Accessed at: https://arxiv.org/abs/2112.06693. Accessed February 21, 2023.

23. Hong S. Excessive White Matter Hyperintensity Increases Susceptibility to Poor Functional Outcomes After Acute Ischemic Stroke. Frontiers in Neurology. 2021;12:10.

24. Bonkhoff AK, Schirmer MD, Bretzner M, et al. Abnormal dynamic functional connectivity is linked to recovery after acute ischemic stroke. Human Brain Mapping. 2021;42:2278–2291.

25. Ben Hassen W, Tordjman M, Boulouis G, et al. Benefit of first-pass complete reperfusion in thrombectomy is mediated by limited infarct growth. European Journal of Neurology. 2021;28:124–131.

Avant-propos

En 2014, les résultats préliminaires des grands essais cliniques prouvant l'efficacité de la thrombectomie mécanique commençaient à être présentés. Je sortais alors des examens classant nationaux et j'entendais parler de ce traitement qui transformerait radicalement le pronostic des patients victimes d'AVC ischémique : c'est à ce moment que j'ai décidé de devenir neuroradiologue interventionnel.

Le CHU de Lille est un centre de référence dans la prise en charge de l'AVC ischémique, tant par la qualité des soins et du parcours patient, que par la quantité de patients traités. Il est notamment reconnu pour son traitement endovasculaire : la thrombectomie mécanique. En effet, 500 patients y sont admis chaque année pour bénéficier de cette intervention, faisant du CHU de Lille un des centres les plus actifs du monde. Une des particularités du CHU de Lille réside dans la place centrale qu'occupe l'IRM cérébrale à toutes les phases de la prise en charge. Bénéficiant d'une IRM 24/7 adossée au service des urgences et dédiée à l'imagerie de l'AVC, et forts de leur expertise clinique, les praticiens lillois ont pu identifier de nombreuses situations cliniques pour lesquelles la neuroimagerie peut aider à aiguiller ce parcours de soins particulier. Ce manuscrit a pour ambition d'explorer certaines d'entre elles.

J'ai eu l'opportunité de découvrir la recherche dans le cadre de mon Master 2 en traitement du signal à l'Université Paris-Est Créteil (Pr. Alain Luciani) sous la direction du Dr. Grégory Kuchcinski. J'émargeais déjà dans l'équipe « Troubles cognitifs dégénératifs et vasculaires » (Pr. David Devos) de l'unité Inserm U1172 « Lille Neuroscience et Cognition » (Pr. Luc Buee). Les travaux de notre laboratoire couvrent des thématiques variées comme l'impact des troubles vasculaires et de la ferroptose dans la pathophysiologie de la dégénération neuronale, la découverte de biomarqueurs cognitifs, et le développement de thérapies innovantes qui en découlent. J'ai alors découvert les analyses radiomics en analysant la texture d'analogues de caillots d'AVC en IRM 7T acquises dans la plateforme UAR 2014 – US 41 LIIFE « Lille Invivo Imaging and Functional Exploration » (Pr. Jean-Pierre Pruvo). Les ingénieurs de la plateforme LIIFE ont développé des outils spécifiques centrés autour de 3 axes : l'imagerie quantitative de la charge métabolique au sein du cerveau, la connectivité cérébrale multimodale

(IRM, PET, EEG) et multiparamétrique (fonctionnelle et structurelle), et l'intelligence artificielle pour la segmentation et la prédiction de déficits à l'échelle individuelle. C'est guidé par l'expertise et l'enthousiasme du Dr. Renaud Lopes, ingénieur de recherche et manager de la plateforme LIIFE, que j'ai pu m'approprier ces outils d'analyse de texture et d'intelligence artificielle sur lesquels les travaux du présent manuscrit sont largement appuyés.

Cette thèse est le fruit de quatre ans de travaux académiques conduits entre le Mass General Brigham – Harvard Medical School (Boston, USA) et le CHU de Lille – Université de Lille entre 2019 et 2022. Les articles scientifiques issus de cette collaboration ont tous eu pour origine des problématiques cliniques et radiologiques rencontrées quotidiennement dans la prise en charge de l'AVC ischémique à Lille. Ils ont nécessité de travailler de concert avec plus de cinquante radiologues, neurologues, et ingénieurs d'exception, répartis dans plus d'une douzaine de nations à travers l'Europe, les Etats-Unis, et l'Amérique du Sud autour de questions complexes interprofessionnelles et transdisciplinaires. Elle mobilise des moyens innovants comme l'intelligence artificielle et les analyses de texture radiomics en capitalisant sur les bénéfices de l'IRM cérébrale dans l'exploration de l'AVC.

Introduction

Généralités sur l'AVC ischémique

L'AVC est une pathologie fréquente et grave. En effet, chaque année en France, 150 000 nouvelles personnes sont touchées, soit un nouvel AVC toutes les 4 minutes. Il représente la première cause de handicap fonctionnel acquis, la deuxième cause de démence, et la troisième cause de mortalité. Il est de forme ischémique dans 85% des cas, et de forme hémorragique dans 15%.[1] Les travaux présentés dans ce manuscrit concernent l'AVC ischémique.

L'AVC ischémique résulte de l'occlusion d'une artère à destinée parenchymateuse cérébrale. L'occlusion vasculaire entraine un arrêt brutal de la perfusion d'aval et, en l'absence de recanalisation, cause la destruction progressive du territoire atteint. Ses étiologies sont multiples mais sont globalement regroupées dans cinq grands cadres étiologiques: athérosclérose des gros vaisseaux, cardio-embolique, occlusion d'une petite artère cérébrale, autre cause connue, et cause inconnue.[2] Il est influencé par de nombreux facteurs de risques, notamment cardiovasculaire. Ainsi, sa fréquence augmente avec l'âge, l'hypertension, le diabète, la fibrillation atriale, les coronaropathies, le tabagisme.[3]

Son diagnostic repose sur l'examen clinique et est confirmé par l'imagerie. Du fait de l'organisation fonctionnelle somatotopique du parenchyme cérébral, la traduction clinique est polymorphe et résulte en la perte d'une ou plusieurs fonctions cérébrales en fonction de la localisation de l'infarctus : motricité, sensibilité, proprioception, langage, compréhension, vigilance, vision, cognition ; à l'extrême, elle peut entrainer la mort. La sévérité du déficit clinique est quantifiée à l'aide du score NIHSS et traduit globalement la sévérité et la localisation de l'AVC. A la phase aigüe, l'imagerie a plusieurs rôles : distinguer AVC ischémique et hémorragique, faire le diagnostic positif de l'AVC ischémique, dépister une occlusion artérielle accessible à une thrombectomie mécanique.[4]

L'AVC se manifeste de plusieurs manières en imagerie à la phase aigüe. En IRM, l'AVC se traduit par un hypersignal sur les séquences pondérées en diffusion (DWI) avec une restriction du coefficient apparent de diffusion, c'est l'œdème cytotoxique. Après un délai variable mais généralement compris entre 4 heures et 6 heures, l'AVC se constitue, et apparait en hypersignal

FLAIR. En IRM de perfusion, En IRM de perfusion, on distingue le cœur ischémique (infarct core) endommagé de manière irréversible, de la pénombre ischémique (penumbra) qui peut bénéficier de la recanalisation.[5] En identifiant et caractérisant l'AVC, l'IRM permet de sélectionner les patients qui peuvent bénéficier d'un traitement thrombolytique ou endovasculaire.

Le traitement de l'AVC aigu repose sur 3 éléments : l'hospitalisation en milieu de soins spécialisés, la thrombolyse intraveineuse, et la thrombectomie mécanique. Le but est de recanaliser le plus rapidement possible l'occlusion vasculaire, soit chimiquement, soit mécaniquement, tout en prévenant les complications liées au déficit neurologique et à l'hospitalisation. La thrombolyse consiste en l'injection intraveineuse d'un agent recombinant activateur du plasminogène tissulaire dont l'objectif est la lyse du caillot responsable de l'occlusion artérielle cérébrale. Elle est indiquée dans les 4h30 suivant le début des symptômes, mais son efficacité décroit avec le temps. Pour obtenir un patient indépendant fonctionnellement après AVC, il faut traiter 10 patients par thrombolyse dans les 3h suivant le début des symptômes. et, entre 3h et 4h30, il faut en traiter 19. Ce nombre de patient à traiter grimpe à 50, si on traite les patients entre 4H30 et 6h. Son risque principal est l'hémorragie intracranienne, dont le risque est 1/40 avant 3h et de 1/50 entre 3h et 4h30.[6] La thrombectomie mécanique est une procédure endovasculaire dont l'objectif est également la recanalisation de l'artère occluse. L'opérateur vient alors retirer le caillot à l'aide d'un stent-retriever ou bien d'un cathéter d'aspiration. Lorsqu'il est indiqué, c'est le traitement le plus efficace de l'AVC. Ainsi, dans les 6 heures du déficit, il faut seulement traiter 2.6 patients pour obtenir un patient fonctionnellement indépendant après l'AVC.[7] Son efficacité décroit également avec le temps mais passé ce délai et en sélectionnant les bon candidats grâce à imagerie avancée IRM[8], ou en scanner de perfusion[9], le nombre de patient à traiter reste similaire (2.8 et 3.6 respectivement). Là encore, l'imagerie joue un rôle couperet dans la bonne indication du traitement.

Le temps, c'est du cerveau – *Time is brain* – le temps joue un rôle majeur dans le pronostic après un AVC ischémique. Les thérapeutiques sont plus efficaces et moins dangereuses lorsque l'AVC est traité rapidement. Cependant, l'expérience clinique montre que certains patients vont présenter un infarcissement précoce du territoire ischémié et rapidement perdre le bénéfice de la recanalisation, alors que d'autre vont progresser plus lentement et bénéficier d'un traitement

longtemps après le début des symptômes.[10] De ce fait, le paradigme d'indication de traitement en fonction du temps a longtemps interdit les traitements thrombolytique et endovasculaire à une large part de patients se présentant tardivement où dont le début des symptômes est inconnu. C'est pourquoi plusieurs méthodes ont été développées pour identifier les patients chez qui une recanalisation serait associée à une plus grande probabilité de récupération :

- Premièrement, on peut étudier la **discordance radio-clinique des symptômes** : une occlusion vasculaire proximale entrainant un déficit clinique cohérent et contrastant avec une lésion peu étendue en imagerie signifie qu'un large territoire est à risque et que seulement une fraction a subi des dommages irréversibles. Cette méthode nécessite une grande expertise clinique et d'imagerie et reste réservée aux centres experts.
- On peut également quantifier directement le volume du parenchyme en souffrance grâce **à l'imagerie de perfusion** : on cherche à quantifier la pénombre, la part du parenchyme qui est privée de sang mais qui reste viable. En scanner, on s'aidera de la profondeur de l'hypoperfusion, alors qu'en IRM on fera le ratio entre le parenchyme hypoperfusé et le volume lésionnel déjà visible en DWI.
- Enfin, on peut étudier la viabilité tissulaire grâce à la **discordance DWI-FLAIR** du signal de l'infarctus. C'est la méthode utilisée au CHU de Lille pour les décisions thérapeutiques en routine clinique. En aval de l'occlusion, et dès les premières minutes, un hypersignal DWI apparait témoignant d'un œdème cytotoxique. Puis, après 4 à 6 heures, un hypersignal FLAIR apparait, signalant l'œdème vasogénique. Les thérapeutiques thrombolytiques sont indiquées chez les patients se présentant avant 4.5 heures depuis le début des symptômes, on considère donc qu'un patient dont on ne connait pas le début des symptômes mais qui présente un infarctus visible en DWI mais pas en FLAIR est éligible à la thrombolyse intraveineuse : c'est la discordance DWI-FLAIR (figure 1).[11] De manière analogue, la thrombectomie mécanique chez les patients se présentant tardivement peut être indiquée quand une discordance DWI-FLAIR est identifiée.[8]

Figure 1 : Visibilité de la lésion en FLAIR en fonction du temps depuis le début des symptômes.

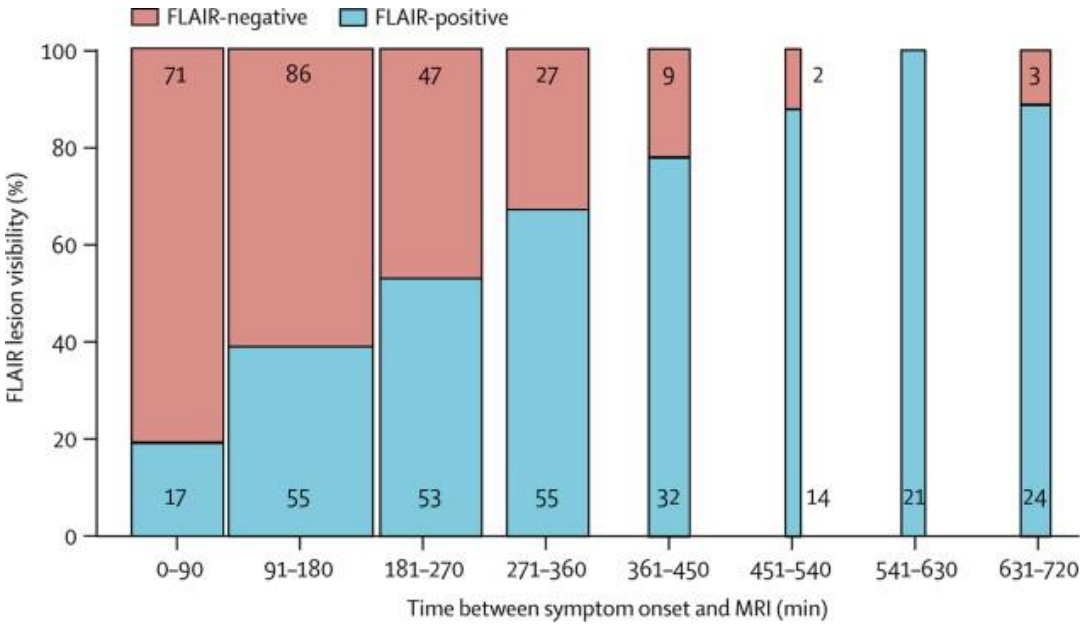

Source : G. Thomalla – Lancet Neurol (2011) - https://doi.org/10.1016/S1474-4422(11)70192-2

La séquence DWI bénéficie d'un fort contraste spontané. Ainsi, le caractère hyperintense de la lésion ischémique est globalement non équivoque. En revanche, l'analyse du signal FLAIR de l'infarctus peut être ambigüe et souffre d'une variabilité inter-lecteur substantielle.[12] La sanction thérapeutique est pourtant lourde : un patient dont l'AVC apparait en hypersignal FLAIR ne sera pas éligible à une recanalisation chimique ou mécanique pourtant déterminante pour son pronostic. La qualité de l'indication thérapeutique dépend alors de l'expérience du radiologue et du neurologue pour interpréter le signal de l'infarctus en IRM. Le développement d'une méthode objective pour aider à pour caractériser la discordance DWI-FLAIR est donc essentiel pour proposer une qualité de soins constante.

Outre le temps, d'autre facteurs peuvent influencer le pronostic après un infarctus cérébral. C'est notamment le cas des facteurs de risques cardiovasculaires. En effet, les patients présentant une hypertension artérielle, un diabète, un tabagisme, un âge avancé, ou encore un antécédent d'AVC ischémique ont moins de chance d'atteindre un bon pronostic post-AVC.[13] Cependant, lors de l'admission, il est parfois impossible de réaliser une anamnèse exhaustive. Néanmoins, ces facteurs de risques altèrent l'intégrité structurelle du parenchyme cérébral et se manifestent sous la forme de leucopathie, microsaignement cérébral, atrophie cérébrale, lacune,

et séquelle d'infarctus. Ces différents éléments sont particulièrement saillant en IRM, notamment sur la séquence T2-FLAIR réalisée de manière systématique durant le bilan initial d'un AVC à la phase aigüe. De plus, l'impact négatif sur le pronostic est médié par l'expression de ces facteurs de risques sur le parenchyme cérébral, notamment par la leucopathie et l'atrophie cérébrale.[14] Cette sémiologie radiologique permet d'estimer la santé cérébrale du patient mais est appréciée de manière largement subjective par les radiologues et neurologues. Son impact sur la décision thérapeutique n'est pourtant pas négligeable, notamment chez les patients situés aux bornes des indications thérapeutiques. Un patient présentant une fragilité cérébrale pourrait peut-être même bénéficier d'avantage d'une recanalisation vasculaire qu'un patient présentant une bonne santé cérébrale et qui récupérera seul. Par exemple, les patients de plus de 80 ans semblent plus bénéficier de la thrombectomie mécanique que les patients plus jeunes probablement car leur santé cérébrale leur permettrait une moins bonne récupération fonctionnelle.[7,15] Il semble donc utile de développer des méthodes qui permettent de mesurer l'état de santé cérébrale des patients victime d'AVC ischémique afin de développer des traitements personnalisés.

Les grandes avancées récentes dans la prise en charge endovasculaire des patients présentant un AVC ischémique ont identifié des biomarqueurs d'imagerie permettant une prise en charge individuelle. C'est le cas des critères volumétriques de perfusion et de la discordance DWI-FLAIR. Concernant la santé cérébrale, des biomarqueurs ont été mis en avant mais nécessitent souvent des techniques d'imagerie encore incompatibles avec le cadre de l'urgence, comme les marqueurs issus de l'IRM fonctionnelle ou de l'imagerie par tenseur de diffusion.[16] Certains biomarqueurs morphologiques IRM, comme les volumétries corticales ou de substance blanche, ont montré leur pertinence dans la modélisation pronostic après AVC.[17] Cependant, là encore, les séquences utilisées, les séquences tridimensionnelles pondérées T1, ne sont pas utilisées dans l'exploration des AVC à la phase aigüe. De plus, ces séquences nécessitent une résolution spatiale importante dont l'acquisition est incompatible avec des patients qui bien souvent ne peuvent maintenir un décubitus immobile. L'immense majorité de ces découvertes sont donc restées sans suites, confinées aux applications de recherche. Il est donc nécessaire de

développer des méthodes compatibles avec les séquences et la qualité des imageries acquises dans le cadre du soin afin de faciliter la transition de ces outils à un usage clinique.

Parmi les outils disponibles pour analyser les images de qualité clinique, les techniques d'analyse de la texture, encore appelées analyses radiomics, sont prometteuses pour une transition rapide à l'usage clinique.[18] Elles permettent de caractériser une image médicale en décrivant l'intensité et la relation spatiale qui existe entre les voxels qui la composent et peuvent analyser une image 2D ou 3D. En somme, elles quantifient la texture d'une image. En outre, elles sont économes en puissance de calcul et leur code source est disponible gratuitement ce qui facilite leur accès et utilisation. Elles sont devenues populaires dans le domaine de l'imagerie oncologique mais restent globalement sous-explorées dans les pathologies neurovasculaires et notamment l'AVC.[19] L'ensemble des travaux présentés dans ce manuscrit ont tous employés les analyses radiomics comme méthode d'analyse d'images..

Les analyses radiomics sont versatiles mais souffrent d'une contrainte de dimensionalité et de colinéarité. En effet, afin de décrire une image, ces techniques produisent de nombreuses variables, de quelques dizaines à plusieurs centaines, rendant les analyses statistiques traditionnelles trop restrictives. En effet, une analyse multivariée fréquentiste accepte généralement un risque d'erreur de 5%. Si, par exemple, on analysait un vecteur de 200 variables radiomics afin de prédire un unique trait clinique, on obtiendrait 10 fausses associations. Il devient alors nécessaire de corriger ce risque de fausse découvertes et ces corrections souvent sévères masquent parfois de réelles associations. Une autre limite des statistiques classiques pour explorer les données radiomics est leur difficulté à appréhender la multi-colinéarité constitutionnelle qui caractérise les radiomics. En effet, les nombreuses variables produites par l'analyse de texture sont souvent corrélées entre elles par catégorie de méthode de calcul. Les techniques de modélisation statistiques sont alors souvent mises en défaut pour l'estimation de leur coefficient. C'est pourquoi, il semble plus adapté d'utiliser des techniques issues du domaine de l'intelligence artificielle, plus particulièrement de l'apprentissage machine supervisé. Là encore, les travaux présentés ici sont tous basés sur des méthodes issues de l'apprentissage machine.

Au total, l'AVC est une pathologie fréquente et grave aux conséquences médicales, sociales et économiques importantes. L'imagerie y joue un rôle central, aiguillant la prise en charge à toutes ses étapes. Elle a permis de dépasser les critères de temps qui ont longtemps bridé les soins et ainsi d'ouvrir la porte à des prises en charges personnalisées. Cependant, il ressort un manque d'objectivité dans la lecture des imageries et une prise en compte insuffisante de la santé cérébrale de chaque patient.

Méthodologie générale

Objectif

Les travaux présentés ci-dessous ont pour objectif d'identifier des biomarqueurs objectifs de caractérisation de l'infarctus et de la santé cérébrale chez les patients explorés par IRM à la phase aiguë de l'AVC.

Contexte

Cette thèse s'est déroulée sur 4 ans, deux ans à Boston au Mass General Hospital sous la supervision du Pr. Natalia S. Rost, Professeur de neurologie à Harvard Medical School travaillant au Mass General Hospital, et deux ans à Lille au CHU de Lille et au sein de la plateforme LIIFE (responsable scientifique : Pr Jean-Pierre Pruvo), sous la direction du Pr. Xavier Leclerc, du Dr. Grégory Kuchcinski et du Dr. Renaud Lopes.

Cohortes

J'ai eu l'opportunité de travailler sur 2 cohortes durant cette thèse :

MRIGENIE

MRIGENIE est une cohorte multicentrique internationale incluant plus de 6000 patients victimes d'AVC ischémique à travers 20 centres répartis entre l'Amérique du Nord, l'Amérique du Sud, et l'Europe. Les patients ont bénéficié d'une IRM cérébrale à la phase aigüe (<48 heures) et d'un génotypage complet. L'objectif initial était de découvrir des variants génétiques de risque d'AVC et de leucopathie.[20]

Cohorte de thrombectomie mécanique du Mass General Hospital

Cette cohorte regroupe des patients traités par thrombectomie mécanique au Mass General Hospital à Boston et explorés par IRM cérébrale entre 2011 et 2019.

Radiomics

Les analyses de texture, encore appelées analyses radiomics lorsqu'appliquées au domaine de l'imagerie médicale, ont été décrites pour la première fois en 1973. Leurs applications initiales concernaient la classification de type de terrain sur photographie aérienne et satellite, et la classification de matériau géologique à partir de photomicrographies.[21] Mais, dans le domaine de l'imagerie médicale, ce n'est qu'à partir de 2012 que le terme radiomics apparait et que cette méthode gagne de l'intérêt.[22] Depuis, de nombreuses études ont étudié l'association entre ces descripteurs texturaux et différents phénotypes cliniques, biologiques, et génétiques.[23–25] Cependant, parmi les centaines d'études radiomics conduites, seule une poignée a eu pour sujet l'AVC.[19]

Méthode de calcul des radiomics

Les variables radiomics sont déclinées en grappes, selon leur méthode de calcul et ce qu'elles décrivent. On dénombre principalement 3 catégories de radiomics pour décrire une zone d'intérêt : les variables de forme décrivant les caractéristiques géométriques, les variables de premier-ordre décrivant l'histogramme, et les variables de second-ordre décrivant la texture.

Variables de forme

Les radiomics de forme vont mesurer la surface, le volume, les dimensions de la zone d'intérêt puis vont calculer différents ratios à partir de ces premières mesures comme le ratio surface/volume, la sphéricité, ou encore l'élongation.

Radiomics de premier-ordre

Ces descripteurs quantifient l'histogramme des valeurs d'intensité grâce au calcul des moments de sa distribution ainsi qu'à d'autres descripteurs de distribution statistiques :

- Moment d'ordre 0 : moyenne, et percentiles (dont la médiane)
- Moment d'ordre 1 : écart-type
- Moment d'ordre 2 : variance
- Moment d'ordre 3 : asymétrie (skewness)
- Moment d'ordre 4 : kurtosis
- Autres descripteurs : énergie, entropie, uniformité.

Radiomics de second-ordre

Les radiomics de second-ordre sont les variables caractéristiques des analyses radiomics. Elles décrivent la relation spatiale des voxels entre eux et donc leur texture. Ils sont divisés en plusieurs catégories selon leur méthode de calcul.

Matrices de co-occurrence de niveau de gris

Cette méthode quantifie le niveau de co-occurrence de niveau de gris dans une direction donnée à une distance spécifiée. Par exemple, combien y a-t-il de voxels de valeurs « 1 » à droite de voxels de valeur « 0 » à une distance de 1 pixel ? Cette méthode va créer n matrices de résultats avec i rangées et j colonnes, avec n le nombre d'angles de lectures, i l'intensité considérée et j l'intensité recherchée. Après avoir exploré l'ensemble des n angles, on reporte la moyenne de chacune des matrices. Enfin, sur cette matrice finale, des descripteurs statistiques sont calculés décrivant la co-occurrence des intensités de gris.

Matrices de zones de niveau de gris

Cette méthode quantifie le caractère contigu des voxels de même intensité. Par exemple, combien y a-t-il de zones de 5 voxels contigus de valeur d'intensité « 3 » ? Une matrice de résultats avec i rangées et j colonnes va être créée, avec i l'intensité étudiée et j la taille de la zone formée par les voxels contigus de même intensité. Ensuite, à partir de cette matrice, des descripteurs statistiques vont être calculés décrivant la tendance de l'image à contenir, par exemple, des petites zones de hautes intensités, ou bien des grandes zones de faibles intensités, ou encore des zones de taille très homogènes.

Matrices de longueur de chaines de niveau de gris

Cette méthode quantifie la présence de voxels de même intensité alignés dans l'image. Par exemple, combien y a-t-il de lignes verticales comportant « 6 » voxels de valeur « 2 » ? Ici, n matrices de résultats avec i rangées et j colonnes vont être créées, avec n la direction de lecture de l'alignement, i l'intensité de niveau de gris étudiée, et j la longueur de la chaine. Ensuite, on calcule la moyenne des n matrices et, enfin, des descripteurs statistiques sont calculés. Cette méthode décrit, par exemple, la propension de l'image à contenir des longues chaines, ou des petites chaines de niveau de gris, on bien des chaines de longueur très différentes.

Matrices de voisinages de différence de niveaux de gris

Cette méthode quantifie la différence de niveau de gris entre un voxel et la moyenne locale d'intensité. Par exemple, quelle est la différence de niveau de gris entre un voxel de valeur « 2 » et la valeur d'intensité moyenne dans un rayon de 1 voxel. Une matrice avec i rangées, *n*, *p*, et *s* colonnes est créée, avec i l'intensité considérée, n le nombre de voxels d'intensité dans l'image, *p* la probabilité de l'intensité *i* dans la zone d'intérêt, et s la somme des absolues des différences entre l'intensité *i* et la moyenne locale d'intensité dans un rayon donné. Sur cette matrice, des descripteurs statistiques sont calculés décrivant la granularité de l'image, par exemple, si les voxels changent d'intensité brutalement avec une grande fréquence spatiale, ou bien si l'image est plus homogène et que les changements d'intensités sont moins fréquents.

Matrice de dépendances de niveaux de gris

Cette méthode quantifie le niveau de dépendances entre niveau de gris d'une image. Par exemple, combien y a-t-il de voxels voisin d'un voxel de valeur « 2 » dont la valeur d'intensité est située entre « 1 » et « 3 » (différence de 1) ? Une matrice de i rangées, et n colonnes est créé, et on compte dans une distance de voisinage de *d* voxels, le nombre de voxels dont l'intensité ne diffère pas plus de *a* par rapport à un voxel d'intensité *i*. De cette matrice sont calculé des descripteurs statistiques qui décrivent l'homogénéité de la texture au sein de la zone d'intérêt de manière globale, ou plus spécifiquement si l'image est plus homogène vers les régions où des voxels de hautes intensités ou basses intensités sont présents.

Méthodologie générale des analyses radiomics

Les analyses radiomics sont généralement divisées en 4 étapes :

La collecte de données d'imagerie

Comme toute analyse d'image, la qualité et la robustesse des analyses dépendent de la qualité et de la standardisation des images. En effet, malgré des méthodes d'harmonisation et de standardisation toujours plus performantes, une harmonisation préalable des paramètres d'acquisition améliore et facilite de manière substantielle les analyses.[26] Cette remarque est à pondérer par le nombre de patients analysés car si avoir peu de patient et beaucoup de variabilité entre sources d'image peut desservir l'analyse, bénéficier d'une grande cohorte peut constituer

une force en termes de généralisabilité. L'unique contrainte de l'analyse radiomics est le format de l'image qui doit être numérisé et matriciel. En effet, le calcul des variables étudie la distribution et la relation entre voxels d'une même image.

La segmentation

Comme pour la collecte d'image, la variabilité entre méthodes de segmentation est une source importante de variabilité non souhaitable.[27] Il faut alors être vigilant à la qualité des segmentations et à l'éventuelle variabilité entre sources différentes de segmentations. La réduction des variabilités de segmentation est aidée par la standardisation de la qualité des imageries et l'établissement d'un protocole strict de segmentation. Au mieux, on peut utiliser un algorithme de segmentation automatique, qui s'il n'est pas parfait introduira un biais constant plus facile à interpréter.

L'extraction de variables radiomics

L'extraction des variables radiomics est une étape cruciale de l'analyse. Cette étape comporte deux sous étapes : la préparation de l'image, puis l'extraction des radiomics. La préparation de l'image permet d'atténuer des variabilités qui peuvent exister et qui peuvent concerner la dimensionalité de la matrice de voxels ou les bornes de son intensité. C'est particulièrement utile dans les acquisitions IRM où les matrices, l'épaisseur de coupe, l'espacement inter-coupes peut largement varier d'un centre à l'autre et même d'une année à l'autre au sein d'un même centre. Il est donc souvent nécessaire d'harmoniser les matrices d'échantillonnage entre les images (resampling) avant de réaliser l'extraction.

L'IRM pose également le problème du profil d'intensité. En effet, en scanner, les valeurs de densités sont absolues car étalonnées sur la densité de l'eau, alors qu'en IRM les valeurs d'intensité sont abstraites. Il est donc nécessaire de borner et de centrer les profils d'intensités afin de standardiser l'extraction. Un point important concerne également l'échantillonnage des intensités de niveaux de gris, ainsi, le choix du nombre et de la largeur des classes de l'histogramme de l'image influence l'analyse radiomics.[28]

Enfin, on peut filtrer et transformer l'image avant de réaliser l'extraction des radiomics afin d'accentuer certains traits. On peut citer les filtres Laplacien de Gaussienne, les décompositions

en vaguelettes, l'analyse en motifs binaires locaux, et les transformations par fonction exponentielle ou logarithmique.

L'extraction des radiomics est dépendantes de nombreux paramètres qu'il faut spécifier, explorer, et optimiser. Il faut définir pour chaque classe de radiomics certains paramètres et ces paramètres doivent être cohérents avec la question posée et la résolution spatiale de l'image après rééchantillonnage.

L'analyse et la modélisation.

La première étape de l'analyse est de vérifier que les variables radiomics sont homogènes et qu'il n'existe pas de source de variabilité non souhaitée. Ensuite, il faut résoudre le problème de la dimensionalité et de la multi colinéarité des données radiomics. Cet aspect est important pour conduire l'analyse et dépend de la taille de l'échantillon de patients. En l'absence d'une cohorte de taille importante permettant l'analyse de l'ensemble des variables, il existe deux stratégies : la réduction de dimension et la sélection de variables.

La réduction de dimension permet de représenter les données radiomics par des variables combinatoires synthétiques, comme dans l'analyse en composantes principales. Il existe de nombreuses méthodes linéaires (analyse en composante principales, analyse factorielle, analyse discriminante linéaire, analyse en composante indépendante, décomposition en valeur singulière) ou non-linéaires (t-SNE, umap…) qui permettent de projeter les données radiomics sur quelques nouvelles dimensions. Ainsi, on passe de plusieurs centaines de variables à analyser à moins d'une dizaine. Ces techniques permettent une très grande efficience de calcul, une excellente gestion de la multi colinéarité, et une représentation graphique facilitée rendant les analyses exploratoires aisées. Cependant, ces méthodes sacrifient une partie de la variance et surtout rendent l'interprétation des résultats périlleuse.

La sélection de variables est une autre stratégie, similaire à celles appliquées en statistiques traditionnelles. On cherche à éliminer les variables redondantes et à sélectionner les variables les plus pertinentes pour l'analyse. Dans ce cas, dans un sous-groupe séparé de patients, on sélectionne les variables radiomics pertinentes grâce à un modèle dont les coefficients sont accessibles et quantifiable. Du fait de la dimensionalité des radiomics, il est nécessaire d'utiliser

des modèles adaptés comme les régression pénalisé L1 (LASSO), régression pénalisée L2 (Ridge), régression pénalisé L1 et L2 (ElasticNet), ou encore des modèles de forêts aléatoires d'arbres décisionnels (Random Forest, XGboost). Ces méthodes sont largement plus couteuses en puissance de calcul et nécessitent une plus grande taille d'échantillon. Cependant, elles permettent d'interpréter les résultats et c'est pourquoi elles sont populaires dans les analyses radiomics.[29]

Une fois le problème de la dimensionalité réglé, la modélisation peut débuter. Cette étape n'est pas différente d'une analyse classique et dépend de la ou des variables à modéliser. Souvent, il faut adopter un plan d'analyse caractéristique des analyses en apprentissage machine, comme la validation croisée imbriquée (figure 2). Dans la validation croisée, le jeu de données est successivement scindé en échantillons d'entrainement et de test, on réalise la sélection des variables et la modélisation sur l'échantillon d'entrainement et l'évaluation sur l'échantillon de test. Si on opte pour une validation croisée imbriquée, l'échantillon d'entrainement est lui-même scindé successivement en échantillons de sélection de donnée et de validation et la sélection des variables s'effectue dans une validation croisée imbriquée dans la première validation croisée. Les modèles d'apprentissage machine ont également la particularité de nécessiter l'optimisation d'hyperparamètres. Par exemple, dans le modèle ElasticNet, il existe deux paramètres L1 et L2 dont il faut choisir des valeurs. Ces paramètres doivent être réglés pour chaque analyse et dépendent de la distribution de la variable indépendante et du nombre de variables. Il eest difficile de définir de manière optimale ces paramètres manuellement, c'est pourquoi cette étape intervient au sein de la validation croisée imbriquée, lors de la sélection des variables.

Figure 2 : exemple de plan d'analyse croisée imbriquée

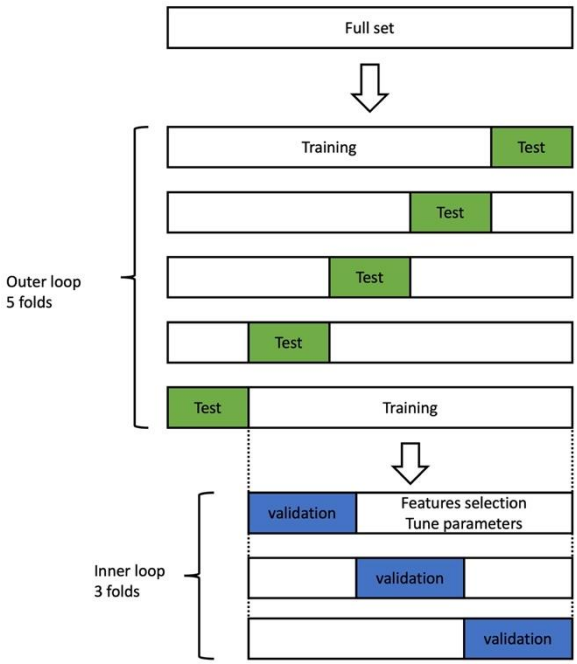

Source : figure adaptée de Bretzner et al.[30]

DOI : https://doi.org/10.1212/WNL.0000000000201596

Résultats

Caractérisation DWI-FLAIR de la lésion ischémique

Ces dix dernières années, un changement de paradigme dans l'AVC s'est opéré, passant de l'horloge à l'horloge biologique. Désormais, lorsqu'un patient se présente à plus de 6 heures d'un déficit, on peut tenter estimer la viabilité tissulaire de la lésion ischémique en imagerie afin d'identifier les patients qui bénéficieront d'une revascularisation chimique ou mécanique.[4] Au CHU de Lille, tous les patients présentant une suspicion d'AVC ischémique bénéficient d'une IRM en urgences. Notre protocole standardisé comporte des séquences de diffusion, T2-FLAIR, 3D TOF, et T2*. A Lille, la méthode de première intention pour analyser la viabilité tissulaire est la discordance DWI-FLAIR. Une acquisition en technique de perfusion complémentaire est réalisée en cas de discordance entre l'examen neurologique et les constatations radiologiques. Le neurologue et le radiologue examinent les séquences de diffusion pour identifier l'infarctus puis le T2-FLAIR afin de dépister un hypersignal intra lésionnel. Cette étape est cruciale pour la suite de la prise en charge du patient tant elle guide l'indication thérapeutique. Cependant, elle reste principalement basée sur l'appréciation visuelle du radiologue et du neurologue et souffre d'une variabilité substantielle.[12] Trouver une méthode objective pour aider à la décision thérapeutique en urgence semble donc nécessaire.

Les analyses radiomics peuvent décrire le signal dans une zone d'intérêt et constituent donc une méthode candidate pour aborder ce problème. Pour explorer cette hypothèse nous avons analysé une cohorte de patients traités par thrombectomie mécanique au Mass General Brigham à Boston et exploré par IRM cérébrale. Nous avons segmenté manuellement les lésions ischémiques sur les images b1000 des séquences de diffusion puis avons réalisé un recalage spatial des masques et des lésions ischémiques avec les séquences T2-FLAIR. Nous avons ensuite extrait les variables radiomics sur les séquences b1000 et FLAIR au sein des masques de lésion ischémiques. En parallèle, nous avons réalisé une double lecture visuelle des séquences T2-FLAIR par deux neuroradiologues afin de caractériser le signal de la lésion, les cas discordants ont été adjudiqué par consensus. Ces lésions étaient gradées FLAIR négatif, FLAIR subtile, ou FLAIR évident. Puis les variables radiomics extraites ont été utilisées pour prédire le grade de positivité

en FLAIR grâce à un modèle de régression pénalisée ElasticNet. Enfin, les variables sélectionnées par le modèle ont été collectées et analysées pour constituer une signature radiomics de la discordance DWI-FLAIR.

Nous avons confirmé que l'accord inter-lecteur était modéré malgré un protocole d'entrainement rigoureux, confirmant les données de la littérature et la pertinence de la question posée.[12] Deux variables sont ressorties comme pertinentes pour la prédiction de la positivité en FLAIR : le T2-FLAIR kurtosis et le T2-FLAIR Cluster Shade (de la matrice de co-occurrences de niveau de gris) après décomposition en motifs binaires locaux. Parmi les résultats notables, aucune variables radiomics issues de l'image b1000 n'a été sélectionnée par le modèle, ce qui est cohérent avec la question posée de la prédiction du signal T2-FLAIR intra-lésionnel. Deuxièmement, le kurtosis décrit le caractère pointu de la distribution d'un histogramme d'intensité et l'épaisseur des queues de la distribution. Ici, le kurtosis bas, était prédicteur d'une positivité en FLAIR. Étant donné qu'une distribution platikurtique (avec un kurtosis bas) est plus plate autour de la moyenne, on peut en déduire qu'appliquée au cas du signal FLAIR de la lésion, elle décrit une plus grande diversité de signal FLAIR dans la lésion et donc la présence d'un hypersignal en plus du pic de normal de signal FLAIR. Malheureusement, l'interprétation du Cluster Shade après décomposition en motifs binaires locaux est plus périlleuse. Le Cluster Shade décrit l'asymétrie par rapport à la moyenne et pourrait donc décrire un contingent différent présentant un hypersignal FLAIR au sein de parenchyme de signal proche de la moyenne. Ces deux variables radiomics constitue notre signature radiomics de la discordance DWI-FLAIR.

Les perspectives de ce travail sont de valider cette signature sur une cohorte externe, comme celle du CHU de Lille. Puis, une fois validée et couplée à un algorithme de segmentation de lésion ischémique, un index radiomics de positivité en FLAIR pourrait être produit pour les patients admis à l'IRM des urgences puis une valeur seuil de positivité pourrait être recherchée secondairement. In fine, elle pourrait aider à la décision thérapeutique de revascularisation à la phase hyper aigüe loirs du bilan IRM initial.

Received: 10 July 2021 | Revised: 2 August 2021 | Accepted: 19 August 2021

DOI: 10.1111/jon.12928

JOURNAL OF NEUROIMAGING | WILEY

SHORT COMMUNICATION

Radiomic signature of DWI-FLAIR mismatch in large vessel occlusion stroke

Robert W. Regenhardt[1,2] | Martin Bretzner[2,3] | Maria Clara Zanon Zotin[2,4] | Anna K. Bonkhoff[2] | Mark R. Etherton[2] | Sungmin Hong[2] | Alvin S. Das[2] | Naif M. Alotaibi[1] | Justin E. Vranic[1,5] | Adam A. Dmytriw[1,5] | Christopher J. Stapleton[1] | Aman B. Patel[1] | Gregory Kuchcinski[3] | Natalia S. Rost[2] | Thabele M. Leslie-Mazwi[1,2]

[1] Department of Neurosurgery, Massachusetts General Hospital, Boston, Massachusetts, USA

[2] Department of Neurology, Massachusetts General Hospital, Boston, Massachusetts, USA

[3] Univ. Lille, CHU Lille, Inserm U1172, Lille, France

[4] Ribeirão Preto Medical School, University of São Paulo, São Paulo, Brazil

[5] Department of Radiology, Massachusetts General Hospital, Boston, Massachusetts, USA

Correspondence
Robert W. Regenhardt, Department of Neurosurgery, Massachusetts General Hospital, 55 Fruit St, WACC 720, Boston, MA 02114, USA.
Email: Robert.Regenhardt@mgh.harvard.edu.

Funding information
The National Institute of Neurological Disorders and Stroke supported RWR (R25NS065743) and NSR (R01NS086905, R01NS082285, U19NS115388). The ISITE-ULNE Fundation, Sociétés Françaises de Neuroradiologie et de Radiologie, and Planiol Fundation supported MB.

Robert W. Regenhardt and Martin Bretzner contributed equally as co-first authors.

Natalia S. Rost and Thabele M. Leslie-Mazwi contributed equally as co-senior authors.

Abstract

Background and Purpose: Ischemic diffusion-weighted imaging-fluid-attenuated inversion recovery (DWI-FLAIR) mismatch may be useful in guiding acute stroke treatment decisions given its relationship to onset time and parenchymal viability; however, it relies on subjective grading. Radiomics is an emerging image quantification methodology that may objectively represent continuous image characteristics. We propose a novel radiomics approach to characterize DWI-FLAIR mismatch.

Methods: Ischemic lesions were visually graded for FLAIR positivity (absent, subtle, obvious) among consecutive large vessel occlusion stroke patients who underwent hyperacute MRI. Radiomic features were extracted from within the lesions on DWI and FLAIR. The DWI-FLAIR mismatch radiomics signature was built with features systematically selected by a cross-validated ElasticNet linear regression model of mismatch.

Results: We identified 103 patients with mean age 68 ± 16 years; 63% were female. FLAIR hyperintensity was absent in 25%, subtle in 55%, and obvious in 20%. Inter-rater agreement for visual grading was moderate ($K = .58$). The radiomics signature of DWI-FLAIR mismatch included native FLAIR histogram kurtosis and local binary pattern-filtered FLAIR gray-level cluster shade; both correlated with visual grading ($\rho = -.42$, $p < .001$ and $\rho = .40$, $p < .001$, respectively).

Conclusions: Radiomics can describe DWI-FLAIR mismatch and may provide objective, continuous biomarkers for infarct evolution using clinical-grade images. These novel biomarkers may prove useful for treatment decisions and future research.

KEYWORDS
acute ischemic stroke, DWI-FLAIR mismatch, large vessel occlusion, MRI, neuroimaging, radiomics

INTRODUCTION

In the era of image-guided reperfusion stroke therapies, there is growing interest in diffusion-weighted imaging-fluid-attenuated inversion recovery (DWI-FLAIR) mismatch. DWI-FLAIR mismatch is often used as a proxy for the time since onset of ischemia as FLAIR hyperintensity may reflect vasogenic edema that does not occur until 4–6 h.[1] FLAIR hyperintensity may also represent tissue that is destined for necrosis, whereas a tissue signature with DWI-FLAIR mismatch may not be so definitive.[2] Randomized trials have shown that FLAIR characterization

allows treatment selection for thrombolytic therapy, and MRI selection for endovascular therapy (EVT) is well-described.[1,3]

In routine clinical practice, DWI-FLAIR mismatch is graded visually and suffers from poor inter-reader agreement.[4] Moreover, infarction is a continuous process that cannot be perfectly captured on a discrete scale. Radiomics are emerging image quantification methodologies that objectively represent continuous image characteristics by describing the spatial distribution of signal intensities and pixel interrelationships to enhance clinical decision-making.[5] We propose a novel radiomics approach to describe DWI-FLAIR mismatch.

METHODS

This study was compliant with the Health Insurance Portability and Accountability Act and was approved by the local institutional review board. Informed consent was waived based on minimal patient risk and practical inability to perform the study without the waiver. The data that support the findings of this study will be made available from the corresponding author upon reasonable request and pending approval of local institutional review board.

Consecutive anterior circulation large vessel occlusion (LVO) stroke patients who underwent pre-EVT DWI and FLAIR imaging were selected for this analysis given the hyperacute timing of MRI, likelihood of large DWI lesions, and translatable results. They were identified from a prospectively maintained database at a referral center from 2011 to 2019.[6] Demographics, history, presentations, and treatments were recorded.[7]

MRIs were obtained on a Siemens 3T MRI or a GE 1.5T MRI. DWI sequences had echo time 60–120 ms, repetition time 5300–5600 ms, *b*-values of 1000, and slice thickness 5 mm with a 1-mm gap. FLAIR sequences had median echo time 145 ms, repetition time 10 seconds, and slice thickness 5 mm with 1-mm gap.

Infarct lesion masks were manually traced on DWI using Slicer 4.8.1.[8] DWI and infarct masks were linearly co-registered to FLAIR (SPM12, http://www.fil.ion.ucl.ac.uk/spm/; Matlab, The Mathworks 2019b). Images were visually inspected for appropriate registration and artifacts (26 patients excluded). DWI-FLAIR mismatch was graded by two independent fellowship-trained neuroradiologists trained on a training set until 100% accuracy was achieved. Intralesional FLAIR signal was defined as absent (0), subtle (+), or obvious (++) (Figure 1). Inter-reader agreement was calculated using Cohen's K. Readers achieved consensus in discordant cases.

Radiomic features were extracted using PyRadiomics 2.2.0 from DWI and FLAIR images within the infarct masks.[5] The same parameters were used for the extraction of radiomics from DWI and FLAIR images. The full parameter file is available at: https://github.com/MBretzner/Radiomics/blob/main/extraction_params_DWI_FLAIR.yaml. Briefly, all features were extracted in axial plane from resampled 1 mm × 1 mm × 6 mm images; image intensities were normalized. Radiomic features were extracted from native images and prefiltered images. Filters included Laplacian of Gaussian with sigmas of 1, 2 and 3, wavelet decompositions, and local binary patterns (LBP). As a result, 1487 rotation invariant radiomics were extracted.

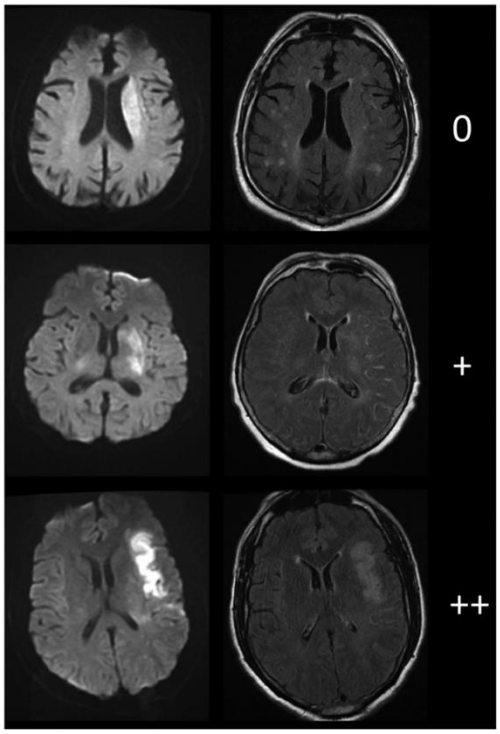

FIGURE 1 Diffusion-weighted imaging (left) and fluid-attenuated inversion recovery imaging (right) examples of visual gradings. Intralesional fluid-attenuated inversion recovery hyperintensities were graded as absent (0), subtle (+), or obvious (++)

Prediction of the consensual DWI-FLAIR mismatch was done using an ElasticNet linear regressor. Radiomics-based prediction of the DWI-FLAIR mismatch was performed in a 100-time repeated fivefold nested cross-validation scheme. The radiomic signature of the DWI-FLAIR mismatch was built with the features that were consistently selected across all repetitions. Correlations of the signature's radiomics with the consensual visual grading were assessed using Spearman correlation.

RESULTS

We identified 103 patients with mean age 68 ± 16 years; 63% were female. Median admission NIHSS was 16 (interquartile range: 12–19). Mean infarct volume was 29 ± 30 cc. FLAIR hyperintensity was absent in 25%, subtle in 55%, and obvious in 20%. Inter-rater agreement was moderate with Cohen's $K = .58$; raters did not disagree on obvious versus absent (Figure 2). Interestingly, agreement was better for patients

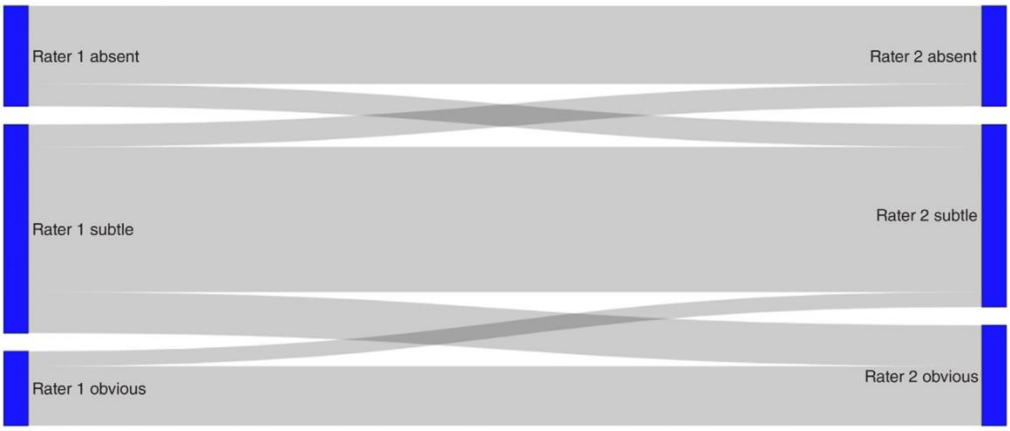

FIGURE 2 Flow diagram of inter-rater agreement for visual grading. There was no disagreement between absent and obvious fluid-attenuated inversion recovery hyperintensity within infarcted areas between rater 1 and rater 2. All disagreement affected subtle hyperintensity and either absent or obvious hyperintensity

TABLE 1 Clinical and imaging characteristics ($n = 103$)

Characteristic	Data
Age, years	68 ± 16
Female	63%
Prestroke mRS, median (IQR)	0 (0-1)
Hypertension	74%
Atrial fibrillation	34%
Diabetes	20%
Coronary disease	20%
Transient ischemic attack	16%
Smoking	17%
Presenting NIHSS, median (IQR)	16 (12-19)
Intravenous alteplase	48%
LKW-to-MRI, min	369 ± 277
Infarct volume	29 ± 30
Infarct FLAIR hyperintensity	
Absent	25%
Subtle	55%
Obvious	20%

Note: All the data represent mean ± standard deviation unless otherwise indicated.
Abbreviations: IQR, interquartile range; mRS, modified Rankin Scale; NIHSS, National Institutes of Health Stroke Scale; LKW, last known well.

with last known well (LKW) < 6 h ($n = 66$, $K = .65$) than for patient with LKW > 6 h ($n = 37$, $K = .46$). Demographic and clinical information are shown (Table 1).

The coefficient of determination for the repeated out-of-sample cross-validated predictions for DWI-FLAIR mismatch was $R^2 = .20$

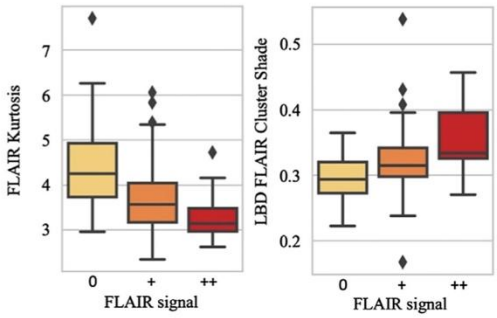

FIGURE 3 Correlation box plots of the diffusion-weighted imaging-fluid-attenuated inversion recovery (DWI-FLAIR) mismatch radiomic signature versus consensual FLAIR gradings. LBD, local binary pattern

(95% confidence interval: .12–.27), with an average of 33.8 ± 8.6 features selected per repetition. The radiomic signature of DWI-FLAIR mismatch included two systematically selected radiomic features: FLAIR histogram kurtosis and LBP-FLAIR gray-level cluster shade. No DWI feature characteristics were retained. Both correlated with visual grading ($\rho = -.42$, $p < .001$ and $\rho = .40$, $p < .001$, respectively) (Figure 3).

DISCUSSION

In a cohort of LVO stroke patients, we have developed a novel radiomics approach to quantify DWI-FLAIR mismatch on hyperacute pre-EVT MRI. Two radiomic features, FLAIR histogram kurtosis and LBP-FLAIR gray-level cluster shade, describe infarct FLAIR hyperintensity in an objective and continuous fashion from clinical-grade images.

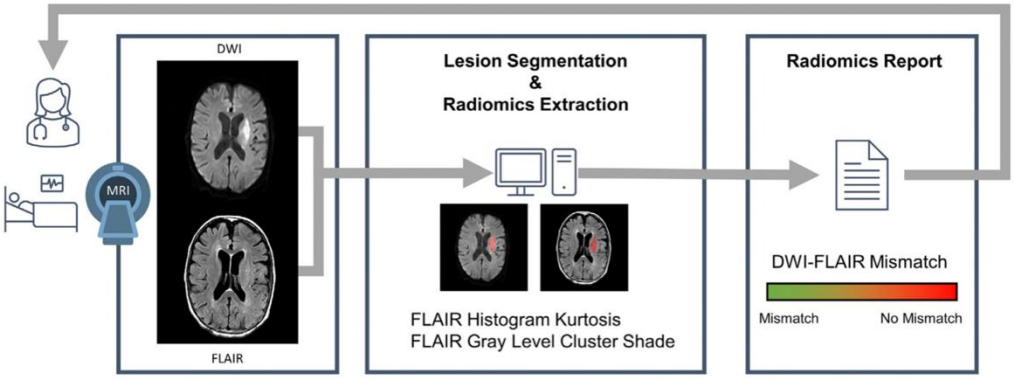

FIGURE 4 Conceptual framework outlining a proposed imaging and processing workflow for acute stroke clinical care. A stroke patient is evaluated emergently and undergoes MRI. DWI and FLAIR sequences are obtained. Software allows the automatic lesion segmentation and radiomics extraction. A report is produced in seconds to minutes that can aid acute clinical decision making. DWI, diffusion-weighted imaging; FLAIR, fluid-attenuated inversion recovery

A major strength of this approach is its objectivity, providing a potential solution to settle ambiguous cases. By relying on consensual agreement between readers, radiomics were selected in a robust way, mimicking clinical practice where images are adjudicated by neuroradiologists, neurologists, and neurointerventionalists. Our cohort was composed of patients with large ischemic lesions demonstrating a broad spectrum of infarct FLAIR signal. It was, therefore, well-suited for the identification of textural descriptors of the range of infarct progression on FLAIR.

This radiomics approach offers several advantages for quantifying DWI-FLAIR mismatch compared to other tools, such as the signal intensity ratio.[3] The signal intensity ratio is calculated by dividing the mean signal intensity from a region within the lesion's most intense FLAIR signal by that from a region in normal-appearing contralateral tissue.[9] Although this ratio describes the most progressed region of infarct, which may best estimate time from symptom onset, it fails to capture information about the entire infarct in the case of heterogenous lesions and relies on manual, subjective placement of regions of interests both within the infarct and contralateral parenchyma. Although its creators caution the inclusion of chronic infarction, leukoaraiosis, and cerebrospinal fluid in regions of interest,[9] these distinctions can be difficult to establish even when limiting FLAIR evaluation to DWI hyperintense tissue. Others used this method to analyze images from the WAKE-UP trial but failed to identify a relevant cutoff as FLAIR hyperintensity within the lesion was an exclusion criterion.[10]

Furthermore, an important advantage and goal of radiomics is automation. Our technique can be integrated into a computerized radiology pathway that provides output data within seconds to minutes. This is critical for clinical translation given the acute nature of stroke and need to make rapid clinical decisions (Figure 4).

We identified FLAIR histogram kurtosis and LBD-FLAIR gray-level cluster shade as key radiomic features quantifying DWI-FLAIR mismatch. The kurtosis of a distribution describes aggregation around the mean. We showed that FLAIR kurtosis was inversely correlated with intralesional FLAIR hyperintensity. A high kurtosis distribution has a peak around the mean with heavy tails. This describes a lesion without FLAIR hyperintensity as most voxels have normal intensity values distributed around the mean. In contrast, a low kurtosis distribution has a flat top with light tails; a uniform distribution is the extreme case. A lesion with frank FLAIR hyperintensity is composed of voxels with varying intensity values, flattening the distribution and thus reducing kurtosis.

Interpretation of the gray-level cluster shade of the LBP-filtered FLAIR image is more challenging. Gray-level cluster shade is a second-order textural descriptor of skewness and uniformity of the gray-level co-occurrence matrix. A higher cluster shade implies a greater asymmetry in the image. LBP is a gray-level- and rotation-invariant filter that is performant for describing uniform patterns. It may detect a bright uniform hyperintensity skirted by normal appearing parenchyma.

Interestingly, no DWI textural features were selected within the radiomic signature of DWI-FLAIR mismatch. This corroborates with our methods, as readers only identified the presence of FLAIR hyperintensity within the infarcted area. Furthermore, this approach corresponds to the routine assessment of strokes where DWI identifies ischemic lesions and FLAIR better characterizes their parenchyma.

As stated above, other radiomics features describing more subtle textural patterns were not predictive of DWI-FLAIR mismatch visual gradings in our cohort. Exploring larger cohorts with our method could potentially uncover more detailed textural aspects specific of the infarction process. It stands to reason that FLAIR kurtosis was most robustly predictive. Intuitively, DWI-FLAIR mismatch may be represented solely by the mean intensity of the FLAIR lesion. However, because MRI signal is relative, normal cerebral and lesion intensities

may vary from one patient to another. Kurtosis describes the fourth moment of a distribution and is independent from the mean. Therefore, it represents an appropriate metric to describe MRI signal because it is robust to its relative characteristic.

Our study presents several limitations. First, all limitations inherent to single-center and retrospective studies apply. Future studies could assess the robustness of radiomic features across other scanners and imaging protocols. As only eight MRIs were acquired with a 3T coil in our study, we did not stratify groups by scanner a priori. Furthermore, our method was developed utilizing LVO stroke patients eligible for EVT given availability of hyperacute MRI and relatively large infarct volumes (mean: 29 ml). A potential pitfall could exist when extrapolating these data to smaller infarcts, such as those occurring with lacunar stroke.[11] Also, as with any imaging-based technique, its performance might be influenced by image quality such as the presence of major motion artifacts. Future studies could include replication of this analysis utilizing patients with other stroke etiologies and patients with motion artifacts. Ultimately, the DWI-FLAIR mismatch radiomic signature could be evaluated in a clinical trial to select stroke patients for reperfusion therapies. In addition, our inter-rater agreement was only moderate albeit consistent with previously published performances.[4] Interestingly, it was slightly worse for MRIs from patients with LKW > 6 h; this may be related to our limited sample size and further highlights the need for an objective method. Importantly, subsequent radiomic signature analyses were based on consensus agreement. Lastly, in this exploratory work, we present two candidate MRI biomarkers to quantify DWI-FLAIR mismatch. However, the nature of our cohort prevented the suggestion of clear cutoff values for selecting patients for reperfusion therapy. Further work analyzing data on late presenting or wake-up stroke patients is warranted to validate our results and identify cutoff values.

In conclusion, radiomics can describe ischemic DWI-FLAIR mismatch and may provide an objective, continuous biomarker for infarct evolution using clinical-grade images. The novel imaging biomarkers of FLAIR histogram kurtosis and LBP-FLAIR gray-level cluster shade may prove useful for acute treatment decisions and future research, particularly when time of stroke onset is unknown.

ACKNOWLEDGMENTS AND DISCLOSURE

Joyce McIntyre maintained the stroke database. The authors declare no conflict of interest.

ORCID

Robert W. Regenhardt https://orcid.org/0000-0003-2958-3484
Martin Bretzner https://orcid.org/0000-0002-7594-4159
Alvin S. Das https://orcid.org/0000-0003-2313-977X

REFERENCES

1. Thomalla G, Simonsen CZ, Boutitie F, et al. MRI-guided thrombolysis for stroke with unknown time of onset. N Engl J Med 2018;379:611-22.
2. Welch KMA, Windham J, Knight RA, et al. A model to predict the histopathology of human stroke using diffusion and t sub 2-weighted magnetic resonance imaging. Stroke 1995;26:1983-9.
3. Schwamm LH, Wu O, Song SS, et al. Intravenous thrombolysis in unwitnessed stroke onset: MR WITNESS trial results. Ann Neurol 2018;83:980-93.
4. Thomalla G, Cheng B, Ebinger M, et al. DWI-FLAIR mismatch for the identification of patients with acute ischaemic stroke within 4·5 h of symptom onset (PRE-FLAIR): a multicentre observational study. Lancet Neurol 2011;10:978-86.
5. Van Griethuysen JJM, Fedorov A, Parmar C, et al. Computational radiomics system to decode the radiographic phenotype. Cancer Res 2017;77:e104-7.
6. Regenhardt RW, Etherton MR, Das AS, et al. White matter acute infarct volume after thrombectomy for anterior circulation large vessel occlusion stroke is associated with long term outcomes. J Stroke Cerebrovasc Dis 2021;30:105567.
7. Regenhardt RW, Young MJ, Etherton MR, et al. Toward a more inclusive paradigm: thrombectomy for stroke patients with pre-existing disabilities. J Neurointerv Surg 2020. https://doi.org/10.1136/neurintsurg-2020-016783.
8. Regenhardt RW, Etherton MR, Das AS, et al. Infarct growth despite endovascular thrombectomy recanalization in large vessel occlusive stroke. J Neuroimaging 2020;31:155-64.
9. Song SS, Latour LL, Ritter CH, et al. A pragmatic approach using magnetic resonance imaging to treat ischemic strokes of unknown onset time in a thrombolytic trial. Stroke 2012;43:2331-5.
10. Cheng B, Boutitie F, Nickel A, et al. Quantitative signal intensity in fluid-attenuated inversion recovery and treatment effect in the WAKE-UP trial. Stroke 2020;51:209-15.
11. Regenhardt RW, Das AS, Ohtomo R, et al. Pathophysiology of lacunar stroke: history's mysteries and modern interpretations. J Stroke Cerebrovasc Dis 2019;28:2079-97.

How to cite this article: Regenhardt RW, Bretzner M, Zanon Zotin MC, Bonkhoff AK, Etherton MR, Hong S, et al. Radiomic signature of DWI-FLAIR mismatch in large vessel occlusion stroke. *J Neuroimaging*. 2022;32:63–67. https://doi.org/10.1111/jon.12928

Caractérisation de la santé cérébrale des patients victimes d'AVC ischémique

La capacité du parenchyme à endurer l'insulte ischémique varie d'un individu à un autre : toutes choses égales par ailleurs, un cerveau en bonne santé survivra mieux à un infarctus qu'un cerveau en mauvaise santé.[31] Il est donc nécessaire prendre en compte la santé cérébrale individuelle pour approcher une estimation qualitative de la résilience d'un patient vis-à-vis d'un AVC.[1] Bien qu'elle ne soit pas étudiée directement, plusieurs caractéristiques démographiques ou cliniques sont utilisées afin d'estimer la capacité de résilience cérébrale d'un individu. On peut citer l'âge, les antécédents médicaux, ou encore les facteurs de risques cardiovasculaires comme biomarqueurs témoignant de l'état général et cérébral attendus d'un patient. Par essence, ces biomarqueurs indirects ne peuvent décrire précisément l'état de santé cérébrale véritable d'un patient. En effet, bien qu'ils soient associés à la santé d'un patient à l'échelle d'une cohorte, ils ne peuvent en mesurer les particularités individuelles. De plus, les conséquences de ces facteurs de risques sur la santé des patients peuvent être mitigées par l'effet des traitements, c'est notamment le cas des traitement antidiabétiques ou antihypertenseurs. C'est seulement parce qu'ils sont simples et faciles d'accès qu'ils sont utilisés en clinique. Cependant, grâce à la puissance toujours grandissante des moyens d'imagerie et numériques à notre disposition, il devient à présent possible d'envisager de sonder directement la santé cérébrale des patients.

La santé cérébrale recouvre de nombreux concepts qui s'attachent ultimement à symboliser l'intégrité structurelle et fonctionnelle du cerveau. Ce thème, pourtant dynamique dans le domaine de la recherche, peine à trouver sa place dans la prise en charge clinique des patients atteints d'une pathologie touchant à la sphère neurologique. Ce retard à l'application clinique peut s'expliquer de différentes manières. La première raison est méthodologique : les méthodes développées pour sonder la santé cérébrale des patients ne s'appuient pas sur des moyens disponibles en routine clinique. En effet, dans le domaine de l'imagerie médicale, de plus en plus de travaux portent sur l'IRM fonctionnelle de tâche ou de repos ou encore sur l'IRM de tenseur de diffusion. Leur acquisition est longue et nécessite la coopération du patient, au moins pour maintenir un décubitus strict et au mieux pour exécuter des ordres. En outre, lorsque la méthode s'appuie sur de l'imagerie morphologique, celle-ci bénéficie généralement d'une très haute définition affranchie de tout artéfact, notamment de mouvement. Il existe donc une

incompatibilité entre les méthodes existantes pour mesurer la santé cérébrale individuelle et la réalité des situations cliniques d'application. Cette discordance est d'autant plus frappante dans les pathologies où la prise en charge doit être mise en œuvre en urgence et où la coopération du patient ne peut pas être obtenue, comme dans l'AVC. Il semble donc essentiel de changer de paradigme dans le développement de méthodes innovantes pour l'inférence de la santé cérébrale en remettant l'applicabilité au centre, et en se basant sur les technologies d'imagerie déjà déployées ou accessibles en clinique.

La santé cérébrale dépend de la santé cardiovasculaire et cette dernière peut se manifester sur l'imagerie encéphalique.[32] La leucopathie est une des expressions classiques du vieillissement et des facteurs de risque cardiovasculaire en faisant un biomarqueur classique de santé cérébrale particulièrement saillant à la lecture d'imagerie IRM T2-FLAIR. En outre, certains auteurs ont montré que cette leucopathie ne représentait que la fraction visible d'une charge lésionnelle plus diffuse, comprenant une pénombre infra-radiologique au pourtour.[33] Si cette pénombre de leucopathie est difficilement individualisable à l'œil nu, des méthodes qui relèvent de l'analyse et du traitement du signal peuvent la mettre en évidence.[34] Les radiomics, décrivant l'image de manière standard et objective sont alors susceptibles de quantifier cette charge lésionnelle, au-delà de son contingent évident. Nous avons exploré cette hypothèse en prédisant la charge de leucopathie en analysant la texture de la substance d'allure normale, faisant ainsi la preuve de la continuité entre ces deux contingents de la même lésion. Puis, nous avons exploré si l'expression texturale en T2-FLAIR pouvait être spécifique de certains facteurs de risque cardiovasculaire.

Nous avons analysé plus de 4000 patients issus la cohorte MRIGENIE pour lesquels une imagerie T2-FLAIR était disponible. Nous avons sélectionné les patients pour lesquels une segmentation satisfaisante de la leucopathie, du parenchyme cérébral, et des ventricules cérébraux avait été obtenue grâce à un algorithme d'apprentissage profond dédié.[35] Puis, nous avons extrait les variables radiomics de la substance blanche d'allure normale, en dehors de la leucopathie. Nous avons analysé si les radiomics extraits en dehors de la leucopathie pouvaient prédire le volume de leucopathie. Enfin, nous avons exploré si les radiomics qui étaient pertinents

pour la prédiction de la leucopathie étaient corrélés aux facteurs de risques cardiovasculaires en utilisant une analyse canonique des corrélations.

Premièrement, nous avons montré que les radiomics extraits dans le parenchyme d'allure saine, en dehors de la leucopathie, étaient prédictifs du volume de leucopathie et pouvaient donc capturer des altérations invisibles à l'œil nu. Ce résultat vient conforter l'hypothèse de la pénombre de leucopathie et montre que cette dernière ne représente que la partie visible d'un contingent pathologique plus étendu. Deuxièmement, nous avons pu identifier 68 variables radiomics qui étaient pertinentes pour la prédiction, ces variables ont constitué notre signature radiomics de la leucopathie. Enfin, nous avons montré que les radiomics de la signature de la leucopathie étaient corrélée avec les facteurs de risques cardiovasculaires.

Ce travail nous a permis d'identifier la performance particulièrement élevée des radiomics pour capturer les altérations parenchymateuses cérébrales liée à l'âge sur le T2-FLAIR et a directement inspiré notre travail sur l'âge cérébral.

Publication 2: MRI radiomic signature of white matter hyperintensity is correlated with clinical phenotypes

frontiers in Neuroscience

ORIGINAL RESEARCH
published: 12 July 2021
doi: 10.3389/fnins.2021.691244

OPEN ACCESS

Edited by:
Danny J. J. Wang, University of Southern California, Los Angeles, United States

Reviewed by:
Dafna Ben Bashat, The Wohl institute for Advanced Imaging, Israel
Yong Fan, University of Pennsylvania, United States

***Correspondence:**
Martin Bretzner
mbretzner@mgh.harvard.edu;
martin.bretzner@gmail.com

†*The members of the MRI-GENIE GISCOME Investigators and the International and Stroke Genetics Consortium are given in Supplementary Table 1.*

Specialty section:
This article was submitted to Brain Imaging Methods, a section of the journal Frontiers in Neuroscience

Received: *05 April 2021*
Accepted: *15 June 2021*
Published: *12 July 2021*

Citation:
Bretzner M, Bonkhoff AK, Schirmer MD, Hong S, Dalca AV, Donahue KL, Giese A-K, Etherton MR, Rist PM, Nardin M, Marinescu R, Wang C, Regenhardt RW, Leclerc X, Lopes R, Benavente OR, Cole JW, Donatti A, Griessenauer CJ, Heitsch L, Holmegaard L, Jood K, Jimenez-Conde J, Kittner SJ, Lemmens R, Levi CR, McArdle PF, McDonough CW, Meschia JF, Phuah C-L, Rolfs A, Ropele S, Rosand J, Roquer J, Rundek T, Sacco RL, Schmidt R, Sharma P, Slowik A, Sousa A, Stanne TM, Strbian D, Tatlisumak T, Thijs V, Vagal A, Wasselius J, Woo D, Wu O, Zand R, Worrall BB, Maguire JM, Lindgren A, Jern C, Golland P, Kuchcinski G and Rost NS (2021) MRI Radiomic Signature of White Matter Hyperintensities Is Associated With Clinical Phenotypes. Front. Neurosci. 15:691244. doi: 10.3389/fnins.2021.691244

MRI Radiomic Signature of White Matter Hyperintensities Is Associated With Clinical Phenotypes

Martin Bretzner[1,2], Anna K. Bonkhoff[1], Markus D. Schirmer[1], Sungmin Hong[1], Adrian V. Dalca[1,3,4], Kathleen L. Donahue[1], Anne-Katrin Giese[1], Mark R. Etherton[1], Pamela M. Rist[1,5], Marco Nardin[1], Razvan Marinescu[1,4], Clinton Wang[1,4], Robert W. Regenhardt[1], Xavier Leclerc[2], Renaud Lopes[2,6], Oscar R. Benavente[7], John W. Cole[8], Amanda Donatti[9], Christoph J. Griessenauer[10,11], Laura Heitsch[12,13], Lukas Holmegaard[14], Katarina Jood[14], Jordi Jimenez-Conde[15], Steven J. Kittner[8], Robin Lemmens[16,17], Christopher R. Levi[18,19], Patrick F. McArdle[20], Caitrin W. McDonough[21], James F. Meschia[22], Chia-Ling Phuah[13], Arndt Rolfs[23], Stefan Ropele[24], Jonathan Rosand[25], Jaume Roquer[26], Tatjana Rundek[26], Ralph L. Sacco[26], Reinhold Schmidt[24], Pankaj Sharma[27,28], Agnieszka Slowik[29], Alessandro Sousa[8], Tara M. Stanne[14], Daniel Strbian[30], Turgut Tatlisumak[31,32], Vincent Thijs[33], Achala Vagal[34], Johan Wasselius[35,36], Daniel Woo[37], Ona Wu[3], Ramin Zand[38], Bradford B. Worrall[39], Jane M. Maguire[40], Arne Lindgren[41,42], Christina Jern[14], Polina Golland[4], Grégory Kuchcinski[2], Natalia S. Rost[1] and on behalf of the MRI-GENIE GISCOME Investigators the International and Stroke Genetics Consortium†*

[1] *J. Philip Kistler Stroke Research Center, Massachusetts General Hospital, Boston, MA, United States,* [2] *Inserm, CHU Lille, U1172 - LilNCog (JPARC) - Lille Neurosciences and Cognition, University of Lille, Lille, France,* [3] *A. A. Martinos Center for Biomedical Imaging, Massachusetts General Hospital, Harvard Medical School, Boston, MA, United States,* [4] *Computer Science and Artificial Intelligence Laboratory, Massachusetts Institute of Technology, Cambridge, MA, United States,* [5] *Division of Preventive Medicine, Department of Medicine, Brigham and Women's Hospital and Harvard Medical School, Boston, MA, United States,* [6] *CNRS, Institut Pasteur de Lille, US 41 - UMS 2014 - PLBS, Lille, France,* [7] *Department of Medicine, Division of Neurology, University of British Columbia, Vancouver, BC, Canada,* [8] *Department of Neurology, University of Maryland School of Medicine and Veterans Affairs Maryland Health Care System, Baltimore, MD, United States,* [9] *School of Medical Sciences, University of Campinas (UNICAMP) and the Brazilian Institute of Neuroscience and Neurotechnology (BRAINN), Campinas, Brazil,* [10] *Department of Neurosurgery, Geisinger, Danville, PA, United States,* [11] *Research Institute of Neurointervention, Paracelsus Medical University, Salzburg, Austria,* [12] *Division of Emergency Medicine, Washington University School of Medicine, St. Louis, MO, United States,* [13] *Department of Neurology, Washington University School of Medicine and Barnes-Jewish Hospital, St. Louis, MO, United States,* [14] *Institute of Biomedicine, Sahlgrenska Academy at University of Gothenburg, Gothenburg, Sweden,* [15] *Department of Neurology, Neurovascular Research Group (NEUVAS), Institut Hospital del Mar d'Investigacions Mèdiques (IMIM), Universitat Autonoma de Barcelona, Barcelona, Spain,* [16] *Department of Neurosciences, Experimental Neurology and Leuven Research Institute for Neuroscience and Disease (LIND), KU Leuven – University of Leuven, Leuven, Belgium,* [17] *VIB, Vesalius Research Center, Laboratory of Neurobiology, Department of Neurology, University Hospitals Leuven, Leuven, Belgium,* [18] *School of Medicine and Public Health, University of Newcastle, Newcastle, NSW, Australia,* [19] *Department of Neurology, John Hunter Hospital, Newcastle, NSW, Australia,* [20] *Division of Endocrinology, Diabetes and Nutrition, Department of Medicine, University of Maryland School of Medicine, Baltimore, MD, United States,* [21] *Department of Pharmacotherapy and Translational Research and Center for Pharmacogenomics, University of Florida, Gainesville, FL, United States,* [22] *Department of Neurology, Mayo Clinic, Jacksonville, FL, United States,* [23] *Centogene AG, Rostock, Germany,* [24] *Department of Neurology, Clinical Division of Neurogeriatrics, Medical University of Graz, Graz, Austria,* [25] *Henry and Allison McCance Center for Brain Health, Center for Genomic Medicine, Massachusetts General Hospital, Boston, MA, United States,* [26] *Department of Neurology and Evelyn F. McKnight Brain Institute, Miller School of Medicine, University of Miami, Miami, FL, United States,* [27] *Institute of Cardiovascular Research, Royal Holloway University of London (ICR2UL), Egham, United Kingdom,* [28] *Ashford and St. Peter's Hospitals, Chertsey and Ashford, United Kingdom,* [29] *Department of Neurology, Jagiellonian University Medical College, Krakow, Poland,* [30] *Division of Neurocritical Care and Emergency Neurology, Department of Neurology, Helsinki University Central Hospital, Helsinki, Finland,* [31] *Department of Clinica Neuroscience, Institute of Neuroscience and Physiology, Sahlgrenska Academy at University of Gothenburg, Gothenburg, Sweden,* [32] *Department of Neurology, Sahlgrenska University Hospital, Gothenburg, Sweden,* [33] *Stroke Division, Florey Institute of Neuroscience and Mental*

Health, Department of Neurology Austin Health, Heidelberg, VIC, Australia, [34] Department of Radiology, University of Cincinnati College of Medicine, Cincinnati, OH, United States, [35] Department of Clinical Sciences Lund, Radiology, Lund University, Lund, Sweden, [36] Department of Radiology, Neuroradiology, Skåne University Hospital, Malmö, Sweden, [37] Department of Neurology and Rehabilitation Medicine, University of Cincinnati College of Medicine, Cincinnati, OH, United States, [38] Department of Neurology, Geisinger, Danville, PA, United States, [39] Department of Neurology and Public Health Sciences, University of Virginia, Charlottesville, VA, United States, [40] Faculty of Health, University of Technology Sydney, Ultimo, NSW, Australia, [41] Department of Neurology and Rehabilitation Medicine, Skåne University Hospital, Lund, Sweden, [42] Department of Clinical Sciences Lund, Neurology, Lund University, Lund, Sweden

Objective: Neuroimaging measurements of brain structural integrity are thought to be surrogates for brain health, but precise assessments require dedicated advanced image acquisitions. By means of quantitatively describing conventional images, radiomic analyses hold potential for evaluating brain health. We sought to: (1) evaluate radiomics to assess brain structural integrity by predicting white matter hyperintensities burdens (WMH) and (2) uncover associations between predictive radiomic features and clinical phenotypes.

Methods: We analyzed a multi-site cohort of 4,163 acute ischemic strokes (AIS) patients with T2-FLAIR MR images with total brain and WMH segmentations. Radiomic features were extracted from normal-appearing brain tissue (brain mask–WMH mask). Radiomics-based prediction of personalized WMH burden was done using ElasticNet linear regression. We built a radiomic signature of WMH with stable selected features predictive of WMH burden and then related this signature to clinical variables using canonical correlation analysis (CCA).

Results: Radiomic features were predictive of WMH burden ($R^2 = 0.855 \pm 0.011$). Seven pairs of canonical variates (CV) significantly correlated the radiomics signature of WMH and clinical traits with respective canonical correlations of 0.81, 0.65, 0.42, 0.24, 0.20, 0.15, and 0.15 (FDR-corrected $p\text{-values}_{CV1-6} < 0.001$, $p\text{-value}_{CV7} = 0.012$). The clinical CV1 was mainly influenced by age, CV2 by sex, CV3 by history of smoking and diabetes, CV4 by hypertension, CV5 by atrial fibrillation (AF) and diabetes, CV6 by coronary artery disease (CAD), and CV7 by CAD and diabetes.

Conclusion: Radiomics extracted from T2-FLAIR images of AIS patients capture microstructural damage of the cerebral parenchyma and correlate with clinical phenotypes, suggesting different radiographical textural abnormalities per cardiovascular risk profile. Further research could evaluate radiomics to predict the progression of WMH and for the follow-up of stroke patients' brain health.

Keywords: stroke, cerebrovascular disease (CVD), MRI, radiomics, machine learning, brain health

INTRODUCTION

White matter hyperintensities (WMH) are a cardinal manifestation of small vessel disease (SVD) (Wardlaw et al., 2013). Increased WMH burden is associated with incident ischemic stroke and worse clinical outcome (Arsava et al., 2009). Beyond ischemic stroke, WMH are also associated with vascular cognitive impairment and dementia (Au et al., 2006). WMH prevalence increases with age but is also directly influenced by individual small vessel risk factors: the aggregation of cardiovascular risk factors leads to an increased WMH burden (Wardlaw et al., 2015). Hence, WMH are an imaging biomarker of brain health suggestive of neurodegeneration beyond normal brain aging (Brugulat-Serrat et al., 2019).

Structural injury of the brain has been shown to occur at the macrostructural level, in the form of WMH, but also at the microstructural level. Advanced diffusion tensor imaging (DTI) studies have shown an age-related loss of parenchymal microstructural integrity in normal-appearing white matter (NAWM) (Etherton et al., 2017a). Furthermore, perfusion-weighted imaging (PWI)-based research has also revealed age-related alterations of the blood-brain barrier with increased contrast agents' leakage (Topakian et al., 2010). However, such microstructural injuries are not visualized with conventional structural MRI sequences, and as DTI and PWI require special

acquisition times, the outlined imaging biomarkers are not currently used in clinical routine for SVD patients. Consequently, we are in need of conventional MRI-based methodologies that better quantify SVD and brain health to ensure a widespread application and translation to clinical practice.

Radiomic analyses cover a broad ensemble of high-throughput quantification methods applicable to digitalized medical images (Gillies et al., 2015). These methods automatically extract high-dimensional data, called radiomic features, by describing a given region of interest by its size, shape, histogram, and relationship between voxels. Because these techniques can capture slight differences in intensities and patterns that would remain undetected to a human reader, radiomics bear the potential to describe neuroimaging beyond what meets the naked eye, and thus might help to phenotype SVD (Lambin et al., 2012). Conceivably, they may identify early underlying brain injury at the individual level with rapid clinical translatability and thus enhance personalized care in stroke and SVD.

The aim of the current study was to assess the structural integrity of the brain using a texture analysis approach and to understand the infra-radiological footprint of WMH by exploring its relationship with cardiovascular risk profiles. To do so, we analyzed 4,163 T2 FLAIR images from a large multi-site international collaborative effort studying stroke and WMH. We sought to (a) build a robust radiomic signature of the subvisible manifestations of WMH and (b) to apply canonical correlation analysis (CCA) to investigate the relation between this latent textural expression in relation to sociodemographic information and cardiovascular risk factors, providing a potentially novel approach to improve SVD and stroke care.

MATERIALS AND METHODS

Participants

We reviewed all ischemic stroke patients included in the MRI-GENetics Interface Exploration (MRI-GENIE) study, a large international multi-site collaboration of 20 sites gathering clinical, MRI imaging, and genetic data, built on top of the NINDS Stroke Genetics Network (SiGN) study. Both study design, data collection protocols, and populations have been previously described (Giese et al., 2020).

Ethics

The MRI-GENIE project has been approved by the MGH Institutional Review Board (IRB, Protocol #: 2001P001186 and Protocol #: 2003P000836), as well as ethics boards of the collaborating institutions. All participants or health care proxy provided signed informed consent.

Data Collection and Neuroimaging Pre-processing

Clinical data were acquired within the SiGN study and comprised information on age, sex, hypertension (HTN), history of smoking, diabetes mellitus (DM), atrial fibrillation (AF). Among the 6,627 patients included across 20 sites, FLAIR images were available for 6,389 patients. Axial T2-FLAIR images were acquired between 2003 and 2011 within 48 h of the initial stroke. They had a mean in-plane resolution of 0.7 mm (range: 0.3–1.0 mm) and a through-plane resolution of 6.2 mm (range: 3.0–30.0 mm). Total brain, ventricle, and WMH segmentations were accomplished using deep learning methods described in detail previously (Schirmer et al., 2019; Dubost et al., 2020). Briefly, total brain segmentation was done using a tailored 2D-convolutional neural network for clinical T2-FLAIR data. T2-FLAIR image intensities were normalized and scaled. Successively, WMH and ventricles were automatically segmented using distinct convolutional neural network frameworks. A total of 1,353 patients were excluded after final quality control of all T2-FLAIR images and respective segmentations; this control process is described in great detail in a previous publication (Schirmer et al., 2019). To capture the underlying processes of SVD in brain parenchyma not overtly affected by WMH, we computed masks for normal-appearing brain parenchyma by subtracting ventricles and WMH masks from total brain masks, resulting in 5,031 masks. To remove any stray voxels that could impact radiomics extraction, a morphological opening operation with a 3 × 3 voxel kernel was performed on the final masks. Among those 5,031 patients, 868 were excluded for missing major clinical data (age and sex), remaining missing values (89 patients included, see **Supplementary Table 2**) were imputed using medians of distributions. As a result, a total of 4,163 patients were included across 17 different sites.

Radiomic Feature Extraction

Radiomic features were extracted using the open-source toolbox PyRadiomics V2.2.0. The full list of the radiomics extraction parameters can be found online at https://github.com/MBretzner/WMH_radiomicSign.

Briefly, to account for the discrepancy in voxel sizes and to reduce unwanted variance that could be originating from differences between centers and scanners, all features were extracted in-plane from down-sampled 1 mm × 1 mm × 6 mm T2-FLAIR images. Quantization was set to a fixed bin width of 5. Features extraction was performed outside of WMH on native and pre-filtered images. Filters included Laplacian of Gaussian (LoG) filters (with sigmas of 1, 2, and 3 mm), wavelet decompositions, and 2D Local Binary Patterns (2D-LBD). For each patient, 118 features were computed including mask statistics, shape features, first-order histogram statistics, GLCM (Gray Level Co-occurrence Matrix) features, GLRLM (Gray Level Run Length Matrix), GLDM (Gray Level Dependence Matrix), and NGTDM (Neighboring Gray Tone Difference Matrix) features. Exhaustive and didactic descriptions and formulas of every radiomic feature and filter can be found online

at https://pyradiomics.readthedocs.io/en/latest/features.html. As a result, we extracted 763 rotation invariant radiomic features per patient.

Machine Learning Approach to Build the Radiomic Signature of the WMH

To account for cerebral size differences, each WMH volume was divided by the corresponding brain volume to obtain a percentage of WMH per total brain volume. As the resultant distribution was highly skewed, it was transformed using a Box-Cox transform and is referred to as "WMH burden" in the next paragraphs.

To address the high dimensionality of the data, prediction of the WMH burden was done using an ElasticNet linear regressor. Since ElasticNet coefficient estimates are not scale-invariant, we standardized predictors, i.e., radiomics variables, to be 0 centered and have variances of the same order.

Radiomics-based predictions of WMH burden were performed in 30-times repeated nested fivefold stratified cross-validation scheme, resulting in a total of 24,990 out-of-sample predictions. Predictions were plotted against ground truth values, and R^2 values were computed with standard deviation.

To better understand the role of each class of radiomics and to rule out an association based solely on the size of the extraction mask and thus reflecting only atrophy, an ancillary prediction of the WMH burden was performed using only the radiomics features that only reflected the size and the shape of the analyzed brains. As NIHSS has been shown to be a surrogate marker of stroke volume, and to assess a hypothetical impact of stroke lesions on radiomics features, residual of the WMH burden predictions were studied per NIHSS score when available (Tong et al., 1998). To explore the potential impact of data heterogeneity across all sites, a second ancillary analysis was performed predicting WMH burden in a leave-one-site-out cross-validation scheme.

TABLE 1 | Demographic and clinical characteristics of the study population (n = 4,163).

Age	**Mean (SD)**	**62.8 (15.0)**
Female	n (%)	1,748 (42.0%)
Hypertension	n (%)	2,825 (67.9%)
Diabetes mellitus	n (%)	687 (16.5%)
Atrial fibrillation	n (%)	595 (14.3%)
Coronary artery disease	n (%)	772 (18.5%)
History of smoking	n (%)	1,331 (32.0%)
Prior stroke	n (%)	539 (12.9%)
WMH volume	Median (IQR)	4.2 mL (1.4–11.2)
NIHSS*	Median (IQR)	3 (1–6)

NIHSS, NIH Stroke Scale.
**NIHSS was available for 2,234 (53.7%) patients included.*
"Prior stroke" refers to a stroke preceding the one that led to the inclusion in the study.

The shrinkage ability of the ElasticNet regressor was leveraged to select the most predictive features of the WMH burden. The radiomic signature of the WMH was built with the features that were consistently selected across each of the 30 repetitions and therefore represented the most robust and stable predictors of WMH burden.

Understanding the Textural Footprint of Clinical Phenotypes

Association of clinical variables and the radiomic signature of WMH burden were done *via* CCA, which allows studying two multivariate variable sets concomitantly (Hotelling, 1936; Wang et al., 2020). Indeed, traditional analyses explore relationships between many to one variable, whereas CCA can study complex many-to-many correlations, truly leveraging the power of multivariate datasets. CCA can be conceived as similar to principal component analyses in the way that each side of the data (here clinical and radiomics) undergoes a factorization into a latent representation of the variables, called canonical variates (CV). The canonical correlation score of a canonical function represents the correlation between the two CV that composes it. To extract each canonical function, CCA finds combinations of factors of the two sets so that they are maximally correlated. Canonical loadings represent the correlations between variables and their latent representation (CV) and can be interpreted as the relative contribution of variables to the variates: a variable with a large loading has more impact on a variate than a variable with a smaller loading.

Radiomic features and continuous clinical variable (age) normality was assessed using the Shapiro–Wilks test and, if needed, were transformed using the R toolbox *BestNormalize* (Peterson and Cavanaugh, 2020). Significance of canonical correlations was determined *via* permutation testing (1,000 permutations) and assessed using Wilks' Lambda computed with Rao's F-approximation, p-values were corrected for multiple testing with Benjamini–Hochberg procedure (Hotelling, 1936; Wang et al., 2020). Explained variances of the canonical functions were calculated and figured in a scree plot. Loadings were calculated to discover and characterize the impact of clinical and radiomic features on each canonical function and thus to provide support for the interpretation of the relationship between the radiomics and clinical domains.

Overall, the goal of CCA is to find underlying representations that best describe the correlations between the two multi-dimensional datasets. Thus, this technique permits the estimation of the sources of maximal covariance between the clinical and the radiomics domains, highlighting the subvisible contribution of cardiovascular risk factors to T2 FLAIR imaging.

Code Availability

Radiomic features extraction, feature selection, and machine learning analyses were performed in python

3.7.6 using the toolbox *scikit-learn* (Pedregosa et al., 2011). CCA was performed in R V1.3.1056 using the toolboxes *CCA*, *vegan* (González et al., 2008; Oksanen et al., 2019). The complete codes used to perform the radiomics extraction as well as the extraction parameters and the data analysis are available here: https://github.com/MBretzner/WMH_radiomicSign.

RESULTS

Population

All patients included in MRI-GENIE have suffered an ischemic stroke. Population demographics are shown in **Table 1**. The mean age was 62.8, and there were 42% females, median WMH volume was 4.2 mL [interquartile range (IQR): 1.4–11.2]. Admission NIH stroke scale (NIHSS) was available for 2,234 (53.7%) patients; median NIHSS was 3 (IQR: 1–6). Comparison of included and excluded patients' available clinical characteristics is shown in **Supplementary Table 2**. Briefly, excluded patients were younger, had less hypertension, less coronary artery disease (CAD), less AF, but had more prior strokes. There was no difference in sex or diabetes status. Importantly NIHSS scores did not differ.

Building the Latent Radiomic Signature of the WMH Burden

The coefficient of determination of the repeated out-of-sample cross-validated predictions of the WMH burden was $R^2 = 0.855 \pm 0.011$ (**Figure 1**). The average (SD) number of selected features per repetition was 150.3 (5.6). These features represented the most relevant ones in the prediction of WMH burden. To reduce the redundancy and multicollinearity of radiomic features, we built a signature of the WMH burden by only including the features that were systematically selected in every repetition. This step resulted in the automatic selection of 68 features, which are referred to as the "radiomic signature of WMH." These features are listed in **Supplementary Table 1**.

Prediction performance of the WMH burden using radiomics that only capture the shape and size of the extraction mask but not voxel intensities was substantially lower with an R^2 of 0.41 ± 0.03. The analysis of the residual of the WMH burden predictions per available NIHSS score showed no trend suggesting an impact of stroke lesions on the predictions (**Supplementary Figure 1**).

Results of the predictions recursively holding one site out are reported in **Supplementary Table 3**. Distributions of patients Age and WMH volume per site are reported in **Supplementary Figure 2**. Briefly, when the center held-out was showing large clinical differences (mainly younger patient and/or neglectable loads of WMH), prediction performances were lower.

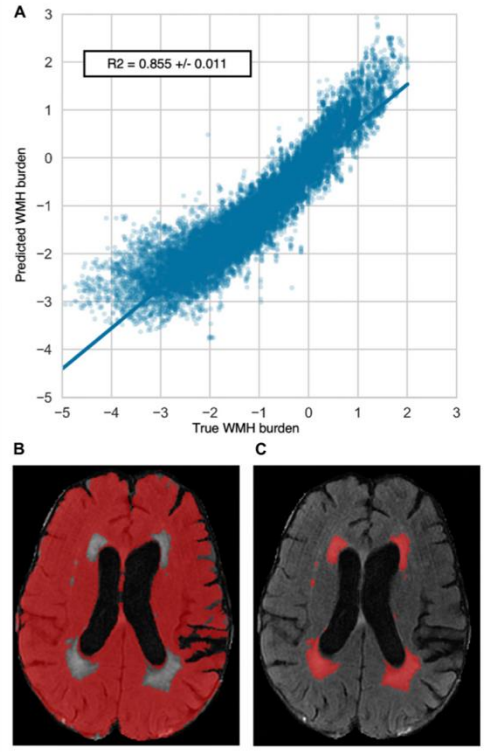

FIGURE 1 | Repeated out-of-sample cross-validated predictions of WMH burden. **(A)** Predictions of the WMH burden resulted in a coefficient of determination of $R^2 = 0.855 \pm 0.011$. Predicted and true WMH burdens show negative values due to the Box-Cox transformation of the WMH burden distribution. The bottom panels provide an illustrative example of a radiomics extraction mask **(B)** and a WMH mask **(C)**.

Clinical Phenotypes Captured by Radiomics

Aiming to discover possible links between clinical phenotypes and textural features of the radiomic signature of WMH burden, we performed a CCA.

The CCA could identify seven canonical functions (CF 1–7) correlating the radiomics with clinical variates. All seven canonical functions were significant (False discovery rate corrected p-values $CF_{1-6} < 10^{-3}$; $CF_7 = 0.012$) with respective canonical correlations of 0.81, 0.65, 0.42, 0.24, 0.20, 0.15, and 0.15. **Figure 2** contains the scree plot of the explained variance of each CF and the correlation plot of the clinical and radiomic variates of the first canonical function with patients points colored according to their age. Loadings of the clinical and the five most impactful radiomic variables (highest loadings) of the first two canonical functions are reported in **Table 2**. The bi-loading

plot in **Figure 3** provides a graphical interpretation relationship between the most impactful variables of the first two canonical functions. Loadings of the clinical variate of all canonical functions are shown in **Table 3**; loadings of the radiomics variate are presented in **Supplementary Table 1**. Variables that share the same direction along a given function have a positive covariance, whereas variables that show opposing directions have negative covariance. The magnitude of the loading reflects the strength of the association.

DISCUSSION

Radiomic features, extracted outside of the visible WMH, captured latent characteristics of WMH and could accurately predict WMH burden. Upon further analysis, seven distinct combinations of radiomics features were associated seven distinct combinations of clinical traits relevant to WMH, such as age, sex, hypertension, history of smoking, DM, and CAD. Therefore, the methods presented here provide new tools to help to understand and quantify the microstructural portion of the parenchymal deterioration due to SVD in stroke and give a radiological snapshot of brain health. Importantly, our analyses relied on basic T2-FLAIR images, as commonly acquired in clinical routine and thus do not require any advanced, more costly additional imaging sequences.

White matter hyperintensities represent a cardinal feature among radiological manifestations of brain aging and SVD. However, DTI-(Etherton et al., 2016) and PWI-based studies suggested (Promjunyakul et al., 2018) that WMH represent an end-stage macrostructural injury, embodying a surreptitious disease altering brain parenchyma. Our results support the hypothesis of WMH penumbra in cerebral SVD with a continuum between visible and invisible parenchymal damage (Maillard et al., 2011; Wardlaw et al., 2013). A major caveat of traditional advanced imaging biomarkers is their acquisition. Indeed, DTI sequences are rarely acquired routinely because of long scanning times, and PWI necessitates the injection of Gadolinium-based contrast agents. In contrast, our method can capture parenchymal microstructural integrity and hence, promises to replace additional dedicated imaging as a candidate approach to follow-up SVD progression in the clinic.

Cerebral atrophy has been shown to be associated with WMH burden (Aribisala et al., 2013). However, little is known about the relationship between the texture of the brain and WMH accumulation. By showing a twofold improvement of predictions leveraging exhaustive textural information compared to predictions restricted to radiomics describing only shape and size, our findings suggest that, beyond atrophy, textural analysis of the brain might better document WMH related damage of the brain. Therefore, one hypothesis would be that radiomics might be able to capture early-stage infra-radiological abnormalities prior to their evolution into irreversible cerebral loss, potentially bearing implications for future studies targeting WMH progression prevention.

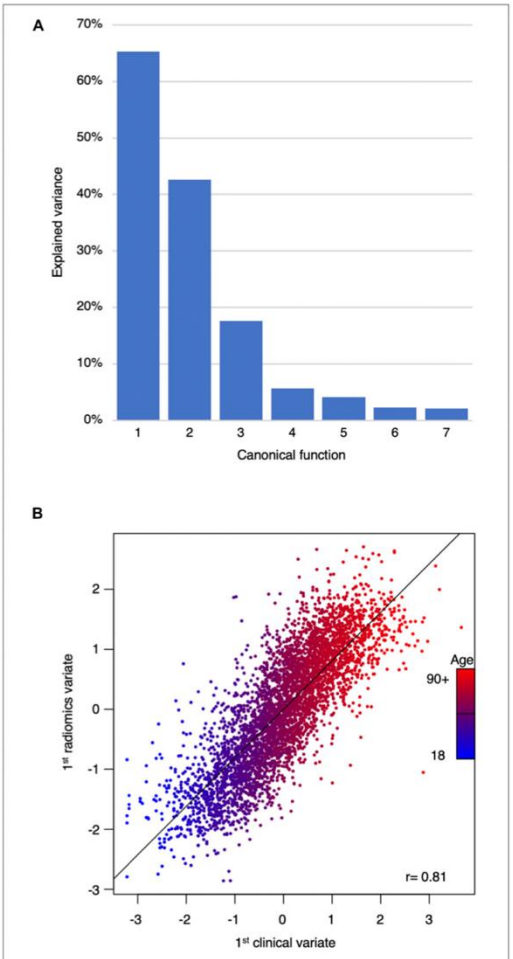

FIGURE 2 | Scree plot of the explained variance per canonical function and correlation plot between the first clinical and radiomic variates. **(A)** Scree plot of the explained variance by canonical functions. **(B)** Correlation plot of the first clinical and radiomics canonical variates. Each dot represents a patient and is colored according to age. The first canonical function mainly represented age. There was a very strong correlation between the clinical and the radiomics variates of $r = 0.81$.

By means of our CCA, we estimated the associations between the radiomic signature of WMH and SVD risk factors. The influence of cardiovascular risk factors on brain tissue was previously investigated in neuropathology and advanced imaging studies yet was rarely described by analyzing the texture of conventional imaging (Gouw et al., 2011; Wardlaw et al., 2013). Our work complement and support previous studies on MRI

TABLE 2 | Clinical and most impactful radiomic loadings of the first two canonical functions.

Clinical loadings			Radiomics loadings		
	CF 1	**CF 2**		**CF 1**	**CF 2**
AF	0.310	0.005	LoG-1mm histogram 10 percentile	−0.254	−0.128
Age	0.990	0.008	LoG-1mm GLSZM large area high gray level emphasis	−0.747	−0.008
CAD	0.260	0.097	LoG-1mm GLSZM large area low gray level emphasis	−0.743	−0.005
DM	0.127	0.009	LoG-2mm GLDM gray level non uniformity	−0.514	0.671
Hypertension	0.381	−0.057	LoG-2mm GLRLM run variance	−0.241	−0.124
Female sex	0.089	−0.993	LoG-2mm GLRLM short run low gray level emphasis	0.734	0.097
Smoking	0.069	0.180	LoG-3mm GLRLM gray level non uniformity normalized	0.300	−0.167
			LoG-3mm GLRLM short run low gray level emphasis	0.767	0.073
			Original histogram 10 percentile	−0.733	−0.071
			Original GLRLM run length non uniformity	0.662	0.221
			Original GLRLM run length non uniformity normalized	0.658	0.051
			Original GLRLM run variance	−0.801	−0.013
			Original shape major axis length	−0.263	0.696
			Original shape maximum 2D diameter column	−0.162	0.745
			Original shape mesh volume	−0.608	0.581
			Original shape minor axis length	0.046	0.709
			Original shape sphericity	−0.759	−0.172
			Original shape surface volume ratio	0.778	0.044
			Wavelet-LH GLSZM Small area high gray level emphasis	−0.413	−0.161

AF, atrial fibrillation; CAD, coronary artery disease; DM, diabetes mellitus; LoG, Laplacian of Gaussian; GLCM, Gray Level Co-occurrence matrix; GLRLM, Gray Level Run Length Matrix; GLDM, Gray Level Dependence Matrix; NGTDM, Neighboring Gray Tone Difference Matrix. Loadings assess the relative contribution of a variable to a canonical function.

textural analysis applied to SVD by Valdés et al. (2017) on gadolinium-enhanced T2-FLAIR, Bernal et al. (2020) on dynamic spectral gadolinium-enhanced T1 weighted imaging, Tozer et al. (2018) on T1 and T2-FLAIR cognitive textural biomarkers, and Shu et al. (2020) and Shao et al. (2018) who could predict the progression of WMH using radiomics extracted from, respectively, T1-FLAIR and T2-FLAIR images. Our analyses were based on a large collection of clinical T2-FLAIR images, a routine MRI sequences acquired during both acute screening and follow-up of patients with stroke and cerebrovascular disease. Therefore, it argues for the overall clinical relevance of radiomics in stroke and SVD.

Age was the clinical aspect correlating most strongly with the radiomic signature of WMH burden and is a well-established predictor of WMH (Rost et al., 2010; Giese et al., 2020). Similarly, blood-brain barrier studies using PWI highlight an age-associated increased leakage of contrast agents within WMH, but also beyond, in NAWM, showcasing a possible preclinical pathogenic step leading to cognitive decline (Wardlaw et al., 2017). Our findings also suggest the presence of age-related subvisible abnormalities that can notably be quantified on structural T2-FLAIR images. Radiomic features describing atrophy (brain size and lower sphericity) and T2-FLAIR heterogeneity, were the most strongly correlated with age. On the first canonical function, age was the main variable, however, HTN, AF, and CAD were also moderately represented, painting the picture of vascular pathological brain aging. The heterogeneity and hyperintensities of the parenchyma could have maybe captured lacunes, enlarged perivascular spaces, or microbleed, which is, along with WMH, radiological hallmarks of SVD (Wardlaw et al., 2013). Radiomics presented here could therefore portray a representation of a pathological brain aging process in stroke patients, depicting atrophic and heterogeneous parenchyma.

The second canonical function illustrated sex differences in tissue aspects in T2-FLAIR. The association of the radiomic signature with sex was mainly driven by shape radiomics capturing differences in brain size. This finding remains, however, independent from age-related atrophy since canonical functions analyze the unexplained variance from the previous function. Nevertheless, the female sex was also associated with greater linear edge density (GLRLM after LoG filtering), which might indicate some sex-specific textural differences in the loss of microstructural integrity, as suggested in DTI with previous findings reporting sex-specific fractional anisotropy values (Etherton et al., 2017b).

The third canonical function captured a profile representing mainly patients with a history of smoking, and, to a lesser extent, diabetes, which shared common textural features describing more high spatial frequency changes in intensities which could represent diffuse and fine heterogeneity throughout the brain.

The fourth canonical function characterized a specific relation between hypertension and some textural features highlighting inhomogeneity on a lower spatial frequency after wavelet decomposition, thus describing a patchy texture. Since no other cardiovascular risk factor was represented on this dimension, it describes an age-independent specific textural manifestation of hypertension on T2-FLAIR.

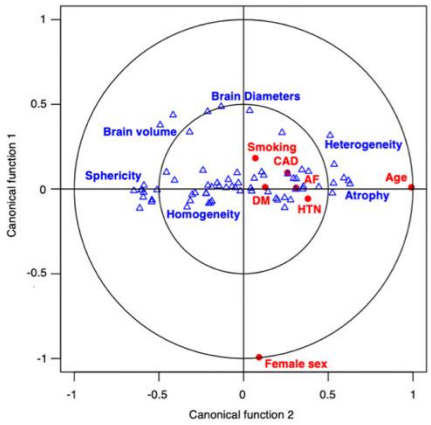

FIGURE 3 | Bi-loading plot of the variables projected over the two first canonical functions. A bi-loading plot graphically represents both the correlation of variables with canonical functions, and the correlation between variables of each set. The position of a variable relative to an axis describes the strength of the correlation of that variable with the axis, the closer to the outer circle, the stronger the correlation. Clinical variables (red dot) and radiomic features (blue triangle) are positively correlated if close or negatively correlated if diagonally opposed. Blue tags were positioned next to correlated radiomic features representing common textural concepts. On T2 FLAIR images, younger patients had larger brains and more homogeneous brain tissue (left side of the plot) whereas older patients had more atrophic and heterogeneous brains (right side of the plot).

Diabetes mellitus was mainly represented in the fifth dimension, correlating with textural features that illustrated overall less hyperintense parenchyma and especially those obtained after filtering with LoG filters. Since those filters are known to act as blob detectors, they potentially captured isolated islets of damage.

The sixth canonical function related the presence of CAD and AF to a more homogeneous texture, which was, however, combined with a high impulse response to the LoG filters of 1, 2, and 3 mm sigma that could signify the presence of spots of subvisible damage of varying size of presupposed embolic origin. On the contrary, the seventh canonical function pictured the differences separating AF from CAD and DM patients, where AF patients seemed to exhibit more patches of high spatial frequency intensity changes, which could represent zones of subtly lesioned brain.

Diabetes and AF were represented by several dimensions meaning that the diseases in question could manifest in several distinctive aspects or stages in our data. Conditional factors that could influence such diversity in presentations include the relative control of disease by treatment or lifestyle, the patient's stage of disease severity, genetic predispositions, and endophenotypes of varying severity.

As with any work on radiomics, the main pitfall remains the *curse of dimensionality*, which refers to a very high number of variables. Consequently, one of the strengths of our study was the available sample size, allowing us to truly leverage both machine learning methodologies and multivariate modeling to select and characterize relevant radiomic variables in a data-driven fashion. In fact, to date and to the best of our knowledge, this is the largest radiomics study performed on any topic. Previous work on radiomics of SVD studied smaller datasets (<250 participants) and thus did not permit powerful unsupervised feature selections (Valdés et al., 2017; Tozer et al., 2018; Bernal et al., 2020). Another added value of the present study is its multicentric design. Our study is the first to explore radiomics of SVD in a large and multicentric population including diverse ischemic stroke cohorts with patients presenting a large spectrum of age and WMH burdens. While the heterogeneity of our dataset could be perceived as a limitation for prediction performances, we think it is on the contrary strength of our study. Indeed, our algorithm was trained on very diverse patients therefore theoretically increasing its chance of success if applied to an external dataset. By implementing multiple measures, such as down-sampling and intensity normalization, to prevent differences originating from acquisition parameters discrepancies, we could reach homogeneous results across all centers while capturing relevant sources of variance, as depicted by the low error of our WMH burden predictions. Another source of unwanted variance in radiomics analyses is segmentation. Indeed, underestimation of the WMH burden, brain parenchyma, or ventricles could have impacted our radiomics based WMH burden prediction. However, we here built upon previous results obtained with state-of-the-art deep learning-based, fully automated segmentation methods that could produce consistent outlines of brains, WMH, and ventricles from T2-FLAIR (Schirmer et al., 2019; Dubost et al., 2020). Preventive measures we implemented, especially down-sampling and intensity normalization, may have come at the cost of losing pertinent information. However, that impact might have been mitigated thanks to our large sample size. We thus emphasize the capital importance of international collaborations, such as the MRI-GENIE consortium, to gather large datasets, especially in the era of quantitative imaging and personalized medicine.

Limitations and Future Directions

We acknowledge several limitations; first, stroke lesion outlines were not available and thus not accounted for. Overall, the median size of ischemic stroke lesions in this cohort is expected to be small, as the median NIHSS was 3. Moreover, the radiomic analysis conducted here provides a single value per radiomic variable per patient, averaging the textural presentation over the whole extraction zone and thus largely decreasing the impact of small lesions. Regarding large lesions, the corresponding perturbated radiomic value could have been assimilated to an outlier and then mitigated by the ElasticNet model, which includes an L1 regularization that improves its robustness to extreme values. The absence of clear trend in the analysis of the residual of WMH burden prediction per NIHSS score is in favor of a limited impact of stroke lesions on the predictions. Other SVD imaging features were also not accounted for, such as microbleeds or enlarged perivascular space, which have been previously linked to radiomic features (Valdés et al., 2017; Tozer et al., 2018).

TABLE 3 | Clinical loadings for all seven canonical functions.

	Clinical loadings						
Canonical function	**1**	**2**	**3**	**4**	**5**	**6**	**7**
AF	0.310	0.005	0.102	0.020	0.313	−0.596	0.663
Age	0.990	0.008	0.096	0.080	−0.045	0.034	0.017
CAD	0.260	0.097	0.169	−0.157	−0.214	−0.744	−0.521
DM	0.127	0.009	−0.443	−0.117	0.781	−0.050	−0.401
Hypertension	0.381	−0.057	0.067	−0.916	0.055	0.058	0.030
Female sex	0.089	−0.993	−0.015	0.056	−0.004	−0.030	0.039
Smoking	0.069	0.180	−0.903	−0.055	−0.347	−0.132	0.081

AF, atrial fibrillation; CAD, coronary artery disease; DM, diabetes mellitus.
A high loading coefficient implies a higher contribution to a canonical function. For instance, age was the most important variable when establishing the clinical variate of the first canonical function.

Secondly, we could not study the relationship between radiomics and other known WMH biomarkers such as dyslipidemia.

Thirdly, we here suggest a novel biomarker to assess the structural integrity of the brain on routine T2-FLAIR imaging. However, as with every new biomarker, the results presented here would need external validation, especially to appreciate the robustness of the features included in the radiomic signature of WMH.

Fourthly, a substantial number of patients were excluded from the analysis because of failed segmentation mainly due to image quality. While this might bias the analysis, it also highlights the challenges of processing clinical imaging in a real-world setting.

Lastly, radiomics were extracted outside of the WMH but not specifically within the white matter. Future research could evaluate the impact of co-registration and resampling on radiomics of SVD, then benchmark radiomics of NAWM against more traditional DTI metrics in the prediction of clinical outcomes and therefore provide a more straightforward method to quantify microstructural integrity.

CONCLUSION

In a large cohort of ischemic stroke patients, we demonstrated that radiomic features predicted WMH burden and were associated with clinical factors. By applying machine learning methods to radiomics analyses of T2-FLAIR images from a large multi-site ischemic stroke cohort, we could characterize the latent expression of SVD that extends beyond the visible WMH and subsequently uncover links associating cardiovascular risk factors to distinct textural patterns. Radiomics analysis may hold promise to become a cost-effective tool to quantify microstructural damage on routinely acquired images in the follow-up of SVD and stroke patients, once externally validated.

DATA AVAILABILITY STATEMENT

Data will be made available upon reasonable request and with approval from local IRBs, to replicate the results presented in this manuscript. Requests to access the data should be directed to NR: nrost@partners.org.

ETHICS STATEMENT

The studies involving human participants were reviewed and approved by the MRI-GENIE project and by the MGH Institutional Review Board (IRB, Protocol #: 2001P001186 and Protocol #: 2003P000836), as well as ethics boards of the collaborating institutions: (Albrecht-Kossel Institute for Neuroregeneration (AKOS) University of Rostock, Germany; University of Cincinnati (UC) College of Medicine, USA; Geisinger Institute, USA; Helsinki University Central Hospital, Finland; IMIM - Hospital del Mar, Spain; Imperial college of London, UK; Mayo Clinic Florida, USA; Medical University Graz, Austria; Sahlgrenska Academy at University of Gothenburg, Sweden; Skane University Hospital, Sweden; Leuven University Hospitals, Belgium; University of British Columbia, Canada; University of Maryland School of Medicine, USA; University of Miami, USA; University of Newcastle, Australia). All participants or health care proxy provided signed informed consent. The patients/participants provided their written informed consent to participate in this study.

AUTHOR CONTRIBUTIONS

MB, AB, MS, SH, ME, PR, RM, CW, RR, XL, RL, GK, and NR: conception and design of the study. MB, AB, MS, SH, ADa, KD, A-KG, ME, PR, MN, OB, JC, ADo, CG, LHo, LHe, KJ, JJ-C, SK, RL, CL, PM, CM, JMe, C-LP, AR, SR, JRs, JRq, TR, RSa, RSc, PS, ASl, ASo, TS, DS, TT, VT, AV, JC, DW, OW, RZ, BW, JM, AL, CJ, PG, and NR: acquisition and analysis of data. MB, AB, MS, ME, RM, CW, RR, XL, ReL, CG, JMe, JW, GK, and NR: drafting a significant portion of the manuscript or figures. All authors contributed to the article and approved the submitted version.

FUNDING

The MRI-GENIE study was funded by NIH NINDS (R01NS086905). MB was supported by the ISITE-ULNE

Fundation, the Société Française de Neuroradiologie, the Société Française de Radiologie, the Thérèse and René Planiol Fundation. ME was supported by the American Academy of Neurology and MGH Executive Council on Research. PR was supported by NIH K01 HL128791. TT was supported by the Helsinki University Central Hospital, Sigrid Juselius Foundation, Sahlgrenska University Hospital, and University of Gothenburg. The funders had no role in design and conduct of the study; collection, management, analysis, and interpretation of the data; preparation, review, or approval of the manuscript; and decision to submit the manuscript for publication.

ACKNOWLEDGMENTS

A copy of a public version of this manuscript has been made available on https://www.biorxiv.org (Bretzner et al., 2021).

SUPPLEMENTARY MATERIAL

The Supplementary Material for this article can be found online at: https://www.frontiersin.org/articles/10.3389/fnins.2021.691244/full#supplementary-material

REFERENCES

Aribisala, B. S., Valdés Hernández, M. C., Royle, N. A., Morris, Z., Muñoz Maniega, S., Bastin, M. E., et al. (2013). Brain atrophy associations with white matter lesions in the ageing brain: the Lothian Birth Cohort 1936. *Eur. Radiol.* 23, 1084–1092. doi: 10.1007/s00330-012-2677-x

Arsava, E. M., Rahman, R., Rosand, J., Lu, J., Smith, E. E., Rost, N. S., et al. (2009). Severity of leukoaraiosis correlates with clinical outcome after ischemic stroke. *Neurology* 72, 1403–1410. doi: 10.1212/wnl.0b013e3181a18823

Au, R., Massaro, J. M., Wolf, P. A., Young, M. E., Beiser, A., Seshadri, S., et al. (2006). Association of white matter hyperintensity volume with decreased cognitive functioning: the Framingham heart study. *Arch. Neurol.* 63, 246–250. doi: 10.1001/archneur.63.2.246

Bernal, J., Valdés-Hernández, M. D. C., Escudero, J., Viksne, L., Heye, A. K., Armitage, P. A., et al. (2020). Analysis of dynamic texture and spatial spectral descriptors of dynamic contrast-enhanced brain magnetic resonance images for studying small vessel disease. *Magn. Reson. Imaging* 66, 240–247. doi: 10.1016/j.mri.2019.11.001

Bretzner, M., Bonkhoff, A. K., Schirmer, M. D., Hong, S., Dalca, A., Donahue, K. L., et al. (2021). MRI radiomic signature of white matter hyperintensities is associated with clinical phenotypes. *bioRxiv*[Preprint] 2021.01.24.427986,

Brugulat-Serrat, A., Salvadó, G., Operto, G., Cacciaglia, R., Sudre, C. H., Grau-Rivera, O., et al. (2019). White matter hyperintensities mediate gray matter volume and processing speed relationship in cognitively unimpaired participants. *Hum. Brain Mapp.* 41, 1309–1322. doi: 10.1002/hbm.24877

Dubost, F., de Bruijne, M., Nardin, M., Dalca, A. V., Donahue, K. L., Giese, A.-K., et al. (2020). Multi-atlas image registration of clinical data with automated quality assessment using ventricle segmentation. *Med. Image Anal.* 63:101698. doi: 10.1016/j.media.2020.101698

Etherton, M. R., Wu, O., Cougo, P., Giese, A.-K., Cloonan, L., Fitzpatrick, K. M., et al. (2017a). Integrity of normal-appearing white matter and functional outcomes after acute ischemic stroke. *Neurology* 88, 1701–1708. doi: 10.1212/wnl.0000000000003890

Etherton, M. R., Wu, O., Cougo, P., Giese, A.-K., Cloonan, L., Fitzpatrick, K. M., et al. (2017b). Structural integrity of normal appearing white matter and sex-specific outcomes after acute ischemic stroke. *Stroke* 48, 3387–3389. doi: 10.1161/strokeaha.117.019258

Etherton, M. R., Wu, O., and Rost, N. S. (2016). Recent advances in leukoaraiosis: white matter structural integrity and functional outcomes after acute ischemic stroke. *Curr. Cardiol. Rep.* 18:123.

Giese, A.-K., Schirmer, M. D., Dalca, A. V., Sridharan, R., Donahue, K. L., Nardin, M., et al. (2020). White matter hyperintensity burden in acute stroke patients differs by ischemic stroke subtype. *Neurology* 95, e79–e88.

Gillies, R. J., Kinahan, P. E., and Hricak, H. (2015). . Radiomics: images are more than pictures, they are data. *Radiology* 278, 563–577. doi: 10.1148/radiol.2015151169

González, I., Déjean, S., Martin, P. G. P., and Baccini, A. C. C. A. (2008). An R package to extend canonical correlation analysis. *J. Stat. Softw.* 23, 1–14.

Gouw, A. A., Seewann, A., van der Flier, W. M., Barkhof, F., Rozemuller, A. M., Scheltens, P., et al. (2011). Heterogeneity of small vessel disease: a systematic review of MRI and histopathology correlations. *J. Neurol. Neurosurg. Psychiatry* 82, 126–135. doi: 10.1136/jnnp.2009.204685

Hotelling, H. (1936). Relations between two sets of variates. *Biometrika* 28, 321–377. doi: 10.2307/2333955

Lambin, P., Rios-Velazquez, E., Leijenaar, R., Carvalho, S., van Stiphout, R. G. P. M., Granton, P., et al. (2012). Radiomics: extracting more information from medical images using advanced feature analysis. *Eur. J. Cancer* 48, 441–446. doi: 10.1016/j.ejca.2011.11.036

Maillard, P., Fletcher, E., Harvey, D., Carmichael, O., Reed, B., Mungas, D., et al. (2011). White matter hyperintensity penumbra. *Stroke* 42, 1917–1922. doi: 10.1161/strokeaha.110.609768

Oksanen, J., Kindt, R., Legendre, P., Hara, B., Simpson, G., Solymos, P., et al. (2019). *vegan: Community Ecology Package*. Available online at: https://CRAN.R-project.org/package=vegan (accessed November 29, 2020).

Pedregosa, F., Varoquaux, G., Gramfort, A., Michel, V., Thirion, B., Grisel, O., et al. (2011). Scikit-learn: machine learning in python. *J. Mach. Learn. Res.* 12, 2825–2830.

Peterson, R. A., and Cavanaugh, J. E. (2020). Ordered quantile normalization: a semiparametric transformation built for the cross-validation era. *J. Appl. Stat.* 47, 2312–2327. doi: 10.1080/02664763.2019.1630372

Promjunyakul, N.-O., Dodge, H. H., Lahna, D., Boespflug, E. L., Kaye, J. A., Rooney, W. D., et al. (2018). Baseline NAWM structural integrity and CBF predict periventricular WMH expansion over time. *Neurology* 90, e2119–e2126.

Rost, N. S., Rahman, R., Sonni, S., Kanakis, A., Butler, C., Massasa, E., et al. (2010). Determinants of white matter hyperintensity volume in patients with acute ischemic stroke. *J. Stroke Cerebrovasc. Dis.* 19, 230–235. doi: 10.1016/j.jstrokecerebrovasdis.2009.05.007

Schirmer, M. D., Dalca, A. V., Sridharan, R., Giese, A.-K., Donahue, K. L., Nardin, M. J., et al. (2019). White matter hyperintensity quantification in large-scale clinical acute ischemic stroke cohorts – the MRI-GENIE study. *Neuroimage Clin.* 23:101884. doi: 10.1016/j.nicl.2019.101884

Shao, Y., Chen, Z., Ming, S., Ye, Q., Shu, Z., Gong, C., et al. (2018). Predicting the development of normal-appearing white matter with radiomics in the aging brain: a longitudinal clinical study. *Front. Aging Neurosci.* 10:393. doi: 10.3389/fnagi.2018.00393

Shu, Z., Shao, Y., Xu, Y., Ye, Q., Cui, S., Mao, D., et al. (2020). Radiomics nomogram based on MRI for predicting white matter hyperintensity progression in elderly adults. *J. Magn. Reson. Imaging* 51, 535–546. doi: 10.1002/jmri.26813

Tong, D. C., Yenari, M. A., Albers, G. W., O'Brien, M., Marks, M. P., and Moseley, M. E. (1998). Correlation of perfusion- and diffusion-weighted MRI with NIHSS score in acute (<6.5 hour) ischemic stroke. *Neurology* 50, 864–869. doi: 10.1212/wnl.50.4.864

Topakian, R., Barrick, T. R., Howe, F. A., and Markus, H. S. (2010). Blood–brain barrier permeability is increased in normal-appearing white matter in patients with lacunar stroke and leucoaraiosis. *J. Neurol. Neurosurg. Psychiatry* 81, 192–197. doi: 10.1136/jnnp.2009.172072

Tozer, D. J., Zeestraten, E., Lawrence, A. J., Barrick, T. R., and Markus, H. S. (2018). Texture analysis of T1-weighted and fluid-attenuated inversion recovery images detects abnormalities that correlate with cognitive decline in small vessel disease. *Stroke* 49, 1656–1661. doi: 10.1161/strokeaha.117.019970

Valdés, M. H., González-Castro, V., Chappell, F. M., Sakka, E., Makin, S., Armitage, P. A., et al. (2017). Application of Texture analysis to study small vessel disease

and blood-brain barrier integrity. *Front. Neurol.* 8:327. doi: 10.3389/fneur.2017.00327

Wang, H.-T., Smallwood, J., Mourao-Miranda, J., Xia, C. H., Satterthwaite, T. D., Bassett, D. S., et al. (2020). Finding the needle in a high-dimensional haystack: canonical correlation analysis for neuroscientists. *Neuroimage* 216:116745. doi: 10.1016/j.neuroimage.2020.116745

Wardlaw, J. M., Makin, S. J., Valdés Hernández, M. C., Armitage, P. A., Heye, A. K., Chappell, F. M., et al. (2017). Blood-brain barrier failure as a core mechanism in cerebral small vessel disease and dementia: evidence from a cohort study. *Alzheimers Dement.* 13, 634–643. doi: 10.1016/j.jalz.2016.09.006

Wardlaw, J. M., Smith, C., and Dichgans, M. (2013). Mechanisms of sporadic cerebral small vessel disease: insights from neuroimaging. *Lancet Neurol.* 12, 483–497. doi: 10.1016/s1474-4422(13)70060-7

Wardlaw, J. M., Valdés Hernández, M. C., and Muñoz-Maniega, S. (2015). What are white matter hyperintensities made of? Relevance to vascular cognitive impairment. *J. Am. Heart Assoc.* 4:001140.

Conflict of Interest: AR was employed by the company Centogene GmbH.The remaining authors declare that the research was conducted in the absence of any commercial or financial relationships that could be construed as a potential conflict of interest.

L'âge cérébral – le biomarqueur idéal de santé cérébral ?

L'estimation de la santé cérébrale peut être réalisée par plusieurs méthodes. La plupart vont comparer une mesure, clinique, biologique, génétique, ou tirée de l'imagerie, avec une valeur de référence. Fréquemment, cette valeur de référence évolue avec l'âge : la santé attendue d'un individu, et donc sa santé cérébrale, évolue avec le temps. Dans le domaine de la neuroradiologie, on peut, par exemple, mesurer le volume de structures cérébrales, relever des anomalies, comme la leucopathie cérébrale, ou encore analyser des cartes de tenseur de diffusion.[36–39] On compare alors ces valeurs à des références et on constate si le patient dévie de la trajectoire d'accumulation attendue due au vieillissement - à l'instar des courbes de croissances. Si certains biomarqueurs, comme le volume cérébral, sont faciles à manipuler et à interpréter, d'autres sont, par essence, indéchiffrables. De plus, du fait de la complexité croissante des moyens numériques appliqués, ce dernier cas de figure est amené à être de plus en plus fréquent. Il existe donc un besoin de développer des biomarqueurs synthétiques et facile à conceptualiser pour décrire l'état de santé cérébrale des patients, sans quoi, l'entreprise de leur déploiement dans le domaine du soin sera difficile.

Parmi les concepts existants pour décrire la santé cérébrale, l'âge cérébral est un candidat particulièrement attrayant. L'âge cérébral est un biomarqueur qui résulte de la prédiction de l'âge du patient à partir d'éléments tirés de son imagerie cérébrale, généralement une IRM. Cette IRM est alors le lieu, soit d'application directe d'algorithmes d'intelligence artificielle, soit, le plus souvent, d'une extraction de biomarqueurs sur lesquelles s'appuie la prédiction d'âge cérébral.[40–42] Ce biomarqueur a bénéficié d'une attention particulière dans les pathologies psychiatriques et neurodégénératives mais son intérêt dans l'AVC est globalement inconnu.[17,43,44] Malheureusement, toutes les méthodes développées utilisent des séquences tridimensionnelles pondérées en T1 haute résolution. Outre le fait que les séquences T1 ne sont pas acquises lors de l'exploration de la pathologie ischémique cérébrale, la qualité requise pour dériver l'âge cérébral est incompatible avec des patients qui peuvent rarement se soumettre à une décubitus strict immobile. Il est donc nécessaire de développer des méthodes d'inférence de l'âge cérébral à partir d'imagerie acquises de manière routinières lors du bilan aigu et lors du suivi des patients victimes d'AVC, comme le T2-FLAIR.

Le vieillissement cérébral se manifeste de plusieurs manières en IRM mais est particulièrement appréciable en T2-FLAIR. En effet, cette séquence morphologique permet d'apprécier la trophicité du parenchyme, la leucopathie, l'hétérogénéité du parenchyme, la présence de lacunes, de séquelles. De plus, notre premier travail sur la cohorte MRIGENIE nous a permis de montrer le potentiel de l'analyse radiomics du T2-FLAIR pour capturer l'âge chronologique. Cependant, les radiomics n'ont jamais été évalué dans l'inférence de l'âge cérébral, a fortiori chez les patients victimes d'AVC ischémique.

Nous avons analysé plus de 4000 patients de la cohorte MRIGENIE et extrait les radiomics de l'imagerie T2-FLAIR dans l'ensemble du parenchyme cérébral. Puis, à partir des variables radiomics, nous avons prédit l'âge chronologique. L'âge cérébral prédit était encore impropre à l'analyse car était corrélé à l'âge chronologique, biais quasi-systématique des études sur l'âge cérébral.[45] Nous avons corrigé ce biais et dérivé l'âge cérébral relatif, biomarqueur qui compare du cerveau d'un patient avec ceux d'autres patients du même âge chronologique afin de déterminer s'il apparait plus âgé ou plus jeune. Afin de comprendre les déterminants cliniques du vieillissement cérébral, nous avons conduit une analyse multivariée de l'âge cérébral relatif. Enfin, pour déterminer si l'âge cérébral relatif est un biomarqueur pertinent pour le pronostic après un AVC, nous avons conduit une analyse multivariée du pronostic après l'AVC à partir des variables cliniques et de neuroimagerie.

Premièrement, nous avons montré la faisabilité de l'inférence radiomics de l'âge cérébral à partir d'images acquises durant le soin. Deuxièmement, nous avons montré l'impact négatif des facteurs de risque cardiovasculaire sur le vieillissement cérébral. Enfin, nous avons montré qu'avoir un cerveau d'allure plus âgée était un facteur de risque indépendant de mauvais pronostic après AVC ischémique.

Les perspectives de ce travail sont multiples et commencent par une réplication des résultats sur une cohorte externe et surtout représentative des modalités modernes de la prise en charge de l'AVC ischémique. En effet, ces résultats préliminaires ont eu pour sujets des patients pris en charge pour un AVC entre 2003 et 2011 et qui pour la plupart n'ont pas bénéficié de traitement. Il faut donc répéter cette étude sur une cohorte moderne représentative afin de réévaluer la pertinence de ce biomarqueur de santé cérébrale dans une prise en charge moderne.

Une fois validé, ce biomarqueur pourrait être étudié afin de déterminer s'il peut permettre de personnalisation la prise en charge, et surtout, proposer un traitement à d'avantage de patients.

RESEARCH ARTICLE

Radiomics-Derived Brain Age Predicts Functional Outcome After Acute Ischemic Stroke

Martin Bretzner, MD, Anna K. Bonkhoff, MD, Markus D. Schirmer, PhD, Sungmin Hong, PhD, Adrian Dalca, PhD, Kathleen Donahue, BS, Anne-Katrin Giese, MD, Mark R. Etherton, MD, PhD, Pamela M. Rist, ScD, Marco Nardin, BS, Robert W. Regenhardt, MD, PhD, Xavier Leclerc, MD, PhD, Renaud Lopes, PhD, Morgan Gautherot, PhD, Clinton Wang, PhD, Oscar R. Benavente, MD, John W. Cole, MD, MS, Amanda Donatti, PhD, Christoph Griessenauer, MD, Laura Heitsch, MD, Lukas Holmegaard, MD, Katarina Jood, MD, Jordi Jimenez-Conde, MD, Steven J. Kittner, MD, Robin Lemmens, MD, Christopher R. Levi, PhD, Patrick F. McArdle, PhD, Caitrin W. McDonough, PhD, James F. Meschia, MD, Chia-Ling Phuah, MD, Arndt Rolfs, MD, Stefan Ropele, MD, Jonathan Rosand, MD, MSc, Jaume Roquer, MD, Tatjana Rundek, MD, PhD, Ralph L. Sacco, MD, MS, Reinhold Schmidt, MD, Pankaj Sharma, MD, PhD, FRCP, Agnieszka Slowik, MD, PhD, Alessandro Sousa, MD, Tara M. Stanne, MD, Daniel Strbian, MD, Turgut Tatlisumak, MD, Vincent Thijs, PhD, Achala Vagal, MD, Johan Wasselius, MD, PhD, Daniel Woo, MD, Ona Wu, PhD, Ramin Zand, MD, Bradford B. Worrall, MD, MSc, Jane Maguire, PhD, Arne G. Lindgren, MD, PhD, Christina Jern, MD, Polina Golland, PhD, Grégory Kuchcinski, MD, PhD, and Natalia S. Rost, MD, MPH, and the MRI-GENIE and GISCOME Investigators and the International Stroke Genetics Consortium

Correspondence
Dr. Bretzner
mbretzner@mgh.harvard.edu or martin.bretzner@univ-lille.fr

Neurology® 2023;100:e822-e833. doi:10.1212/WNL.0000000000201596

Abstract

Background and Objectives

While chronological age is one of the most influential determinants of poststroke outcomes, little is known of the impact of neuroimaging-derived biological "brain age." We hypothesized that radiomics analyses of T2-FLAIR images texture would provide brain age estimates and that advanced brain age of patients with stroke will be associated with cardiovascular risk factors and worse functional outcomes.

Methods

We extracted radiomics from T2-FLAIR images acquired during acute stroke clinical evaluation. Brain age was determined from brain parenchyma radiomics using an ElasticNet linear regression model. Subsequently, relative brain age (RBA), which expresses brain age in comparison with chronological age-matched peers, was estimated. Finally, we built a linear regression model of RBA using clinical cardiovascular characteristics as inputs and a logistic regression model of favorable functional outcomes taking RBA as input.

From the J. Philip Kistler Stroke Research Center (M.B., A.K.B., M.D.S., S.H., A. Dalca, K.D., A.-K.G., M.R.E., P.M.R., M.N., R.W.R., C.W., N.S.R.), A.A. Martinos Center for Biomedical Imaging (A. Dalca, O.W.), and Henry and Allison McCance Center for Brain Health (J. Rosand), Massachusetts General Hospital, Harvard Medical School, Boston; Lille Neuroscience & Cognition (M.B., X.L., R. Lopes, G.K.), Inserm, CHU Lille, U1172 and Institut Pasteur de Lille (M.G.), CNRS, Inserm, CHU Lille, US 41 - UMS 2014 - PLBS, Lille University, France; Computer Science and Artificial Intelligence Lab (A. Dalca, C.W., P.G.), Massachusetts Institute of Technology, Cambridge; Division of Preventive Medicine (P.M.R.), Department of Medicine, Brigham and Women's Hospital, Boston, MA; Department of Medicine (O.R.B.), Division of Neurology, University of British Columbia, Vancouver, Canada; Department of Neurology (J.W.C., S.J.K.), University of Maryland School of Medicine and Veterans Affairs Maryland Health Care System, Baltimore, MD; School of Medical Sciences (A. Donatti, A. Sousa), University of Campinas (UNICAMP) and the Brazilian Institute of Neuroscience and Neurotechnology (BRAINN), Campinas, São Paulo; Departments of Neurosurgery (C.G.) and Neurology (R.Z.), Geisinger, Danville, PA; Department of Neurosurgery (C.G.), Christian Doppler Klinik, Paracelsus Medical University, Salzburg, Austria; Division of Emergency Medicine (Laura Heitsch), Washington University School of Medicine, St. Louis; Department of Neurology (Laura Heitsch, C.-L.P.), Washington University School of Medicine & Barnes-Jewish Hospital, St. Louis, MO; Department of Clinical Neuroscience (L. Holmegaard, K.J., T.M.S., T.T.), Institute of Neuroscience and Physiology, Sahlgrenska Academy at University of Gothenburg, Sweden; Department of Neurology, Sahlgrenska University Hospital, Gothenburg, Sweden; Department of Neurology (J.J.-C.), Neurovascular Research Group (NEUVAS), IMIM-Hospital del Mar (Institut Hospital del Mar d'Investigacions M ́ediques), Universitat Autonoma de Barcelona, Spain; Department of Neurosciences (R. Lemmens), Experimental Neurology and Leuven Research Institute for Neuroscience and Disease (LIND), KU Leuven - University of Leuven, Belgium; Department of Neurology (R. Lemmens), Laboratory of Neurobiology, VIB Vesalius Research Center, University Hospitals Leuven, Belgium; School of Medicine and Public Health (C.R.L.), University of Newcastle, New South Wales; Department of Neurology, John Hunter Hospital, Newcastle, New South Wales, Australia; Division of Endocrinology (P.F.M.), Diabetes and Nutrition, Department of Medicine, University of Maryland School of Medicine, Baltimore; Department of Pharmacotherapy and Translational Research and Center for Pharmacogenomics (C.W.M.), University of Florida, Gainesville; Department of Neurology (J.F.M.), Mayo Clinic, Jacksonville, FL; Klinik und Poliklinik für Neurologie (A.R.), Universitätsmedizin Rostock, Germany; Department of Neurology (S.R., R.S.), Clinical Division of Neurogeriatrics, Medical University Graz, Austria; Center for Genomic Medicine (J. Rosand), Massachusetts General Hospital, Boston; Broad Institute (J. Rosand), Cambridge, MA; Department of Neurology and Evelyn F. McKnight Brain Institute (J. Roquer, T.R., R.L.S./M.S.), Miller School of Medicine, University of Miami, FL; Institute of Cardiovascular Research (P.S.), Royal Holloway University of London (ICR2UL), UK St Peter's and Ashford Hospitals, Egham, United Kingdom; Department of Neurology (A. Slowik), Jagiellonian University Medical College, Krakow, Poland; Division of Neurocritical Care & Emergency Neurology (D.S.), Department of Neurology, Helsinki University Central Hospital, Finland; Stroke Division (V.T.), Florey Institute of Neuroscience and Mental Health, Heidelberg; Department of Neurology (V.T.), Austin Health, Heidelberg, Australia; Departments of Radiology (A.V.) and Neurology and Rehabilitation Medicine (D.W.), University of Cincinnati College of Medicine, OH; Department of Clinical Sciences Lund, Radiology (J.W.) and Neurology (A.G.L.), Lund University, Sweden; Department of Radiology, Neuroradiology, Skåne University Hospital, Malmö, Sweden; Departments of Neurology and Public Health Sciences (B.B.W.), University of Virginia, Charlottesville, VA; University of Technology Sydney (J.M.), Australia; Section of Neurology (A.G.L.), Skåne University Hospital, Lund, Sweden; Department of Laboratory Medicine (C.J.), Institute of Biomedicine, the Sahlgrenska Academy, University of Gothenburg, Sweden; and Department of Clinical Genetics and Genomics (C.J.), Sahlgrenska University Hospital, Region Västra Götaland, Gothenburg, Sweden.

Go to Neurology.org/N for full disclosures. Funding information and disclosures deemed relevant by the authors, if any, are provided at the end of the article.

Glossary

AF = atrial fibrillation; **DM** = diabetes mellitus; **HTN** = hypertension; **MRI-GENIE** = MRI-GENetics Interface Exploration; **MAE** = mean absolute error; **mRS** = modified Rankin scale; **NIHSS** = NIH Stroke Scale; **RBA** = relative brain age; **WMH** = white matter hyperintensity.

Results

We reviewed 4,163 patients from a large multisite ischemic stroke cohort (mean age = 62.8 years, 42.0% female patients). T2-FLAIR radiomics predicted chronological ages (mean absolute error = 6.9 years, $r = 0.81$). After adjustment for covariates, RBA was higher and therefore described older-appearing brains in patients with hypertension, diabetes mellitus, a history of smoking, and a history of a prior stroke. In multivariate analyses, age, RBA, NIHSS, and a history of prior stroke were all significantly associated with functional outcome (respective adjusted odds ratios: 0.58, 0.76, 0.48, 0.55; all p-values < 0.001). Moreover, the negative effect of RBA on outcome was especially pronounced in minor strokes.

Discussion

T2-FLAIR radiomics can be used to predict brain age and derive RBA. Older-appearing brains, characterized by a higher RBA, reflect cardiovascular risk factor accumulation and are linked to worse outcomes after stroke.

While chronological age is one of the most influential determinants of poststroke outcomes,[1] little is known about the impact of neuroimaging-derived brain age, a recently developed biomarker of personalized brain health.[2] Stroke has devastating effects on both functional and cognitive outcomes.[3] However, the resilience of an individual to ischemic insults might vary depending on the status of the underlying brain. In fact, older-appearing brains on MRI, defined by a higher neuroimaging-predicted brain age rather than chronological age, have been associated with diverse diseases, risk factors, lifestyles, and cognitive performances.[4,5] By contrast, patients with younger-appearing brains are believed to undergo a healthier aging process with better brain maintenance, featuring a decreased pathologic age-related structural degeneration.[6] While a variety of studies focused on the brain age of patients suffering from neurodegenerative or psychiatric diseases, the aging process of the brains of patients with stroke and its impact on stroke outcomes remain largely undescribed.[2]

Although chronological time passes at the same speed for everyone, individuals age at different paces; thus, individuals can be more sensitive or, on the contrary, more resilient to the effects of biological aging. Quantifying the deviation from an expected brain aging distribution could prove relevant for assessing brain health and health prognoses, especially in diseases heavily influenced by age, such as stroke. Some authors showed that the brains of stroke survivors appeared older than those of age-matched healthy controls, highlighting the detrimental impact of the ischemic insult on the aging trajectory of the brain.[7,8] Moreover, other authors found an association between higher brain age and a greater risk of stroke, trapping stroke survivors in a vicious circle.[9] However, the clinical determinants of brain age in patients with stroke are currently unknown, warranting further imaging studies in stroke populations to identify potentially preventable risk factors.

The resilience of a brain to an ischemic insult varies between individuals and depends on numerous factors which overall describe individuals' brain health. Nevertheless, while good brain health might help to withstand a circumscribed stroke, this benefit could become insignificant when suffering from a more severe stroke. The influence of brain age on functional outcome should consequently be examined as a function of stroke severity to better understand the extent to which brain health plays a role in ischemic lesion mitigation. This could help select patients before acute therapeutic interventions. Indeed, identifying good responder patients lying at the borders of the therapeutic indication's spectrum is the central question of ongoing clinical trials, namely minor strokes (NIH Stroke Scale [NIHSS] less than 5). For instance, patients suffering from a minor stroke on a vulnerable brain might potentially benefit more from revascularization therapies than patients with better brain health. Identifying new noninvasive biomarkers available on admission, such as brain age, could help select additional patients for acute stroke treatment.

Capturing radiologic hallmarks of aging has been a dynamic field of neuroimaging research over the past few decades.[2] Nevertheless, established methods to quantify this process mainly leveraged atrophy, disregarding other cerebral imaging manifestations of age-related degeneration. Radiomics, an emergent method of image quantification providing standardized quantitative variables describing the global texture of an image, could provide a better estimate of age-related imaging alterations.[10] However, performances of radiomics to produce brain age biomarkers are unknown, a fortiori from acute MRI scans of patients with stroke.

In this large multicentric retrospective imaging study of patients with ischemic stroke, we aimed to (1) assess performances of brain T2-FLAIR MRI radiomics to predict brain age from clinical imaging, (2) understand the clinical determinants of brain age, and (3) study its relevance to poststroke outcome. We hypothesized that patients with stroke with a higher radiomics-predicted brain age than their chronological age would have more cardiovascular risk factors and worse poststroke functional outcomes, especially as observed in minor strokes.

Methods

Participants

We reviewed all neuroimaging data of patients with stroke included in a large international multisite collaborative effort: the MRI-GENetics Interface Exploration (MRI-GENIE) study. Sites shared clinical, MRI imaging, and genetic data. Both study design, data collection protocols, and populations have been previously published.[11-13]

Standard Protocol Approvals, Registrations, and Patient Consents

All participants or health care proxies provided signed informed consent. The MRI-GENIE project has been approved by the MGH Institutional Review Board (IRB, Protocol No.: 2001P001186 and Protocol #: 2003P000836) and the ethics boards of the collaborating institutions.

Data Collection and Neuroimaging Preprocessing

We reviewed a total of 4,163 patients across 17 different sites, for which cardiovascular risk factor phenotypes, T2-FLAIR imaging, and successful brain and ventricles segmentations were available.[14,15] Demographic and cardiovascular phenotypes included age, sex, hypertension (HTN), history of smoking, diabetes mellitus (DM), atrial fibrillation (AF), and a history of prior stroke. Acute stroke severity was measured with the NIHSS. Functional outcome was measured with the modified Rankin scale (mRS) at 60–180 days after stroke.

Axial T2-FLAIR images were acquired between 2003 and 2011 within 48 hours of the hospital admission, mostly on 1.5 T MRI scanners. Mean in-plane resolution was 0.7 mm (range: 0.3–1.0 mm), and the mean through-plane resolution was 6.2 mm (range: 3.0–30.0 mm). Total brain, ventricle, and white matter hyperintensities (WMH) were automatically segmented using dedicated state-of-the-art deep-learning frameworks; raw values were reported. Thorough control of the quality of the segmentations was performed and is already published.[14,15] To reduce interscanner unwanted variance, T2-FLAIR images intensities were normalized using a mean-shift algorithm.[14] We computed parenchymal masks by subtracting the ventricle masks from the total brain masks. Then, we performed a morphologic opening operation with a 3×3 kernel to each axial slice to prevent any segmentation noise from perturbating radiomics extraction.

Radiomic Feature Extraction

Radiomic features were extracted using the open-source toolbox PyRadiomics V2.2.0 from brain parenchyma on T2-FLAIR.[10] In brief, 760 features were extracted describing the shape, histogram, and texture of the brains. To reduce interscanner variability, images were downsampled to a $1 \times 1 \times 6$ mm matrix. The list of the extraction parameters can be found in the supplemental materials (eMethods, links.lww.com/WNL/C494).

Chronological Age, Brain Age, and Relative Brain Age

Radiomics-derived predictions of patients' chronological age were performed by an ElasticNet linear regression model in a 5-fold nested stratified cross-validation scheme (eFigure 1, links.lww.com/WNL/C494). First, the whole data set was split into 5 equivalent training and test samples (80/20%) to produce one single out-of-training-sample age prediction for every patient. Then, for each of the 5 train-test splits, feature selection was performed on the training set by an ElasticNet linear regression model in a 3-fold cross-validation scheme (inner loop). Selected features were subsequently entered into another ElasticNet model that was fitted on the entire training set where its L1 and L2 hyperparameters were optimized and then finally tested on the unseen test set (outer loop). Radiomics-based predicted ages are subsequently referred to as "brain age." Prediction performances were evaluated with Pearson correlation (r) and coefficient of determination (R^2). Intercenter variability in brain age prediction performances was studied (eAppendix 1, eFigure 2, eTable 1). To better understand which radiomics variables were relevant for brain age prediction, we recorded radiomics selected across all folds of the nested cross-validation and their respective ElasticNet linear regression coefficients (eAppendix 2, eTable 2). The results of the radiomics and machine learning results were reported according to the RQS and CLAIM statements (eAppendices 3 and 4).[16,17]

To evaluate the specific added value of brain age to chronological age, we calculated the residuals of predictions (brain age—chronological age). However, these residuals are known to be negatively correlated with chronological age because of a regression dilution bias induced by the accumulation of random measurement errors, which can be encountered in radiomics analyses.[18] An established solution suggested by the authors of a study[4] is to calculate relative brain age (RBA) by regressing out any correlation with chronological age as follows:

$$RBA = Predicted\ Age - Expected\ (Predicted\ Age \mid Chronological\ Age)$$

The expected predicted age as a function of chronological age is obtained by fitting a linear regression model with chronological age as an input and the predicted age as a response variable. RBA represents the appearance of an individual brain in comparison with chronological age-matched peers within the cohort: A higher brain age at a given chronological age will have a positive RBA and will reflect an older-looking brain,

whereas a younger-appearing brain on neuroimaging will have a negative RBA.

To evaluate the added value of detailed textural brain information on top of simple volumetric information of the brain mask, an ancillary analysis was performed: We here predicted brain age using only those radiomics features describing the size and the shape of the parenchyma but not the more detailed texture. This analysis was performed to produce brain age biomarkers based only on the cerebral parenchymal volumetric data and to compare it with the ones predicted from both volumetric and T2-FLAIR intensity profile data. No prediction was done using only advanced textural radiomics because they are inherently correlated to shape radiomics. To further help the interpretation of the neuroimaging underpinnings of radiomics RBA, we calculated the correlation between RBA and brain volume and WMH burden.

Identifying Clinical Determinants of Accelerated Aging

To quantify the impact of patients' clinical phenotypes on their brain, RBA were compared using a two-sided *t*-test for each categorical clinical variable (sex, HTN, DM, AF, CAD, history of smoking, history of prior stroke) and using Pearson correlation for continuous variables (age) (level of significance: $p < 0.05$). Variables for which RBA significantly differed in univariate analyses were then entered into a multiple linear regression model of RBA.

Evaluating the Impact of Accelerated Brain Aging on Poststroke Functional Outcome

Good functional outcome was defined as an mRS ≤ 2 at follow-up. Comparison of patients' RBA by dichotomized outcome groups was performed using a two-sided *t*-test. To compare the effect of RBA on functional outcome with traditional variables, a multiple logistic regression of dichotomized functional outcome was built. Feature selection for this model was performed using a 5-fold cross-validated recursive feature elimination process. Candidate predictors were age, sex, HTN, DM, AF, CAD, history of smoking, prior stroke, brain volume, WMH volume, NIHSS at index stroke, and RBA. The final model's coefficients were estimated, and odds ratios were calculated. To further evaluate the impact of RBA beyond dichotomized functional outcome (good vs bad), full-scale mRS distributions (0–6) were examined by quartiles of RBA.

In ancillary analyses, we investigated the hypothesis that RBA would only be impactful on functional outcomes in minor strokes because severe strokes may lead to unfavorable outcomes regardless of the underlying brain status. To explore this hypothesis, we studied the effect sizes of RBA on dichotomized outcome groups by incrementally adding patients by the rank of NIHSS (0, 0–1, 0–2, 0–3, etc.) and estimated the effect sizes by calculating the standardized adjusted odds ratios of multiple logistic regression models built with the variables previously identified as significantly associated with good functional outcome.

Data Availability

On reasonable request to the corresponding author and pending approval from local IRBs, data will be made available to replicate the results presented in this article. Radiomic features extraction, feature selection, and machine learning analyses were performed in Python 3.7.6 using the toolbox *scikit-learn* and *pyradiomics*.[10,19] Logistic regression coefficients estimations were performed using *statsmodels*.[20]

Results

Population

All included patients had suffered an ischemic stroke. Population demographics are shown in Table 1. There were 42% female patients, and the mean age was 62.8 (standard deviation 15.0) years. Admission NIHSS scores and follow-up mRS scores were available for 2,234 and 1,871 patients, respectively. Exhaustive ordinal mRS scale (0–6) data were available for 871 patients. Median NIHSS was 3 (interquartile range: 1–6); good functional outcome was achieved by 72.5% of patients.

Radiomics Brain Age Predictions and RBA

The mean predicted brain age was 62.8 years with a mean absolute error (MAE) of 6.9 years. Pearson correlation and coefficient of determination between predicted brain age and chronological age were $r = 0.81$ $p < 0.001$ and $R^2 = 0.65$, respectively (Figure 1). Prediction performances using only radiomics describing the shape and size of the brain parenchyma were lower: $r = 0.66$ $p < 0.001$, $R^2 = 0.45$, mean predicted brain

Table 1 Clinical and Radiological Characteristics of the Study Population (n = 4,163)

Age	Mean (SD)	62.8 (15.0)
Female	n (%)	1,748 (42.0%)
Hypertension	n (%)	2,825 (67.9%)
Diabetes mellitus	n (%)	687 (16.5%)
Atrial fibrillation	n (%)	595 (14.3%)
Coronary artery disease	n (%)	772 (18.5%)
History of smoking	n (%)	1,331 (32.0%)
Prior stroke	n (%)	539 (12.9%)
WMH volume	Median (IQR)	4.2 mL (1.4–11.2)
Brain volume	Mean (SD)	1,467.5 mL
Brain ventricular volume	Median (IQR)	31.8 (18.9–42.6)
NIHSS at baseline[a]	Median (IQR)	3 (1–6)
Good functional outcome at 60–180 d[b]	n (%)	1,356 (72.5%)

[a] NIHSS was available for 2,234 patients.
[b] Dichotomized functional outcome (mRS ≤ 2 vs mRS > 2) was available for 1,871 patients.
Abbreviations: IQR = interquartile range; mRs = modified Rankin scale; NIHSS = NIH Stroke Scale; WMH = white matter hyperintensities.

Figure 1 Brain Age Prediction Performances and Relative Brain Age

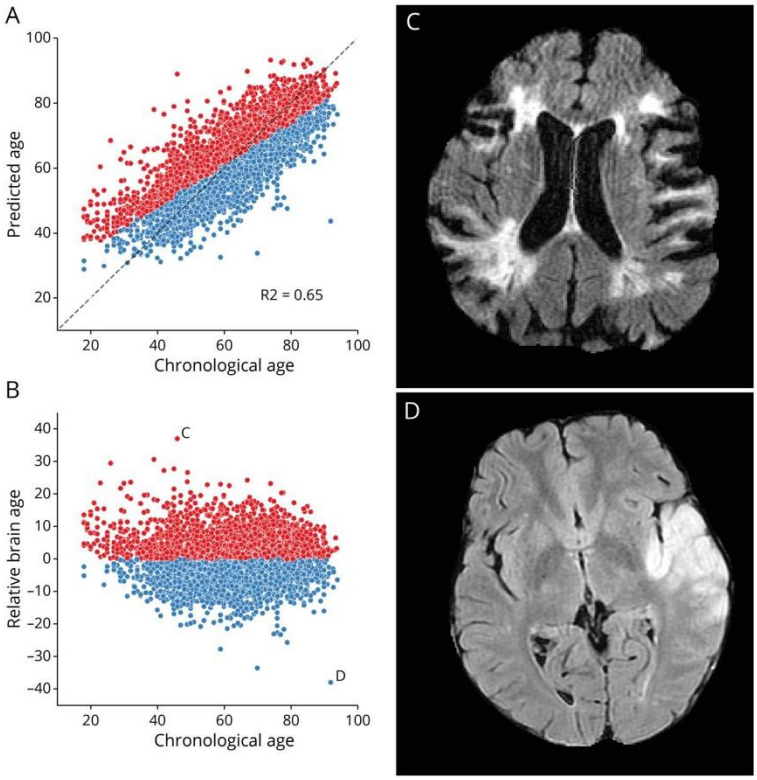

Scatter plots of the T2-FLAIR radiomics (A) predicted brain age and (B) relative brain age (RBA) per chronological age. Patients were colored in red if they had a positive RBA and thus a brain that appeared older to their age-matched peers or in blue if they had a negative RBA and a younger-looking brain. (C) T2-FLAIR axial image of a patient with a positive RBA: predicted brain age = 88, chronological age = 46, RBA = 36.2; this patient's brain exhibits multiple cortical and subcortical sequelae, moderate-to-severe parenchymal atrophy with enlarged ventricles and sulci, and confluent white matter hyperintensities, which extents are unexpectedly large for a 46-year-old patient. (D) T2-FLAIR axial image of a patient with a negative RBA: predicted brain age = 43, chronological age = 92, RBA = −38.6; notwithstanding the left middle cerebral artery lesion, this patient's brain trophicity is maintained; the cortex and the deep gray nuclei are sharply defined, overall describing a healthy brain for this 92-year-old patient.

age: 62.8 years, and MAE = 9.0 years. Additional radiographic examples of brain age predictions are shown in eFigure 3 (links.lww.com/WNL/C494). Relevant radiomics for brain age prediction, their correlation with imaging characteristics, and the results of the intersite prediction performances are presentedal materials (eAppendices 2 and 4). In brief, brain age prediction performances were lower when producing brain age in a site where patients' age significantly differed from the training sites. T2-FLAIR radiomics that captured neuroimaging aspects of atrophy, hyperintensities, and heterogeneity were predictive of higher brain age and therefore older-appearing brain, whereas radiomics representative of parenchymal trophicity and homogeneity were predictive of lower brain age and thus, younger-appearing brain. Moreover, this was confirmed by analyzing RBA with more traditional radiological hallmarks of brain aging: patients with older-appearing brains had a higher WMH burden and a lower brain volume.

Clinical Phenotype and Brain Aging

In univariable analysis, patients with HTN, DM, AF, CAD, a history of smoking, and a history of prior stroke had a significantly higher RBA. RBA did not differ between male patients and female patients (Table 2). As expected, there was no significant correlation between chronological age and RBA: $r = 0.03$, $p = 0.145$.

Table 2 Comparison of Patients' Relative Brain Age (RBA) by Clinical Phenotype (n = 4,163)

	No	Yes	*p* Value
Female	0.02 ± 7.16	−0.02 ± 7.23	0.863
Hypertension	−0.61 ± 7.45	0.29 ± 7.05	<0.001
Diabetes mellitus	−0.18 ± 7.16	0.92 ± 7.03	<0.001
Atrial fibrillation	−0.10 ± 7.14	0.60 ± 7.48	0.034
Coronaropathy	0.13 ± 7.29	0.58 ± 6.74	0.014
History of smoking	−0.15 ± 7.07	0.33 ± 7.43	0.045
Prior stroke	−0.42 ± 7.07	2.85 ± 7.33	<0.001

Two-sided *t*-test, alpha = 5%. RBA values are expressed by their mean ± standard deviation. Patients with positive RBA have older-looking brains, whereas patients with negative RBA have younger-looking brains.

Table 3 Multivariable Linear Regression of the Clinical Predictors of Relative Brain Age (RBA) (n = 4,163)

	RBA coefficient	95% CI		p Value
		Lower	Upper	
Hypertension	0.5615	0.085	1.038	0.021
Diabetes mellitus	0.9098	0.318	1.502	0.003
Atrial Fibrillation	0.4911	−0.133	1.115	0.123
Coronary artery disease	0.1824	−0.387	0.752	0.530
History of Smoking	0.5367	0.07	1.003	0.024
Prior Stroke	3.2134	2.566	3.861	<0.001

Two-sided *t*-test, alpha = 5%. A positive coefficient implies older-looking brains.

In multiple regression analyses, RBA was higher and therefore expressed accelerated brain aging in patients with HTN, DM, a history of smoking, and a history of prior stroke (Table 3).

RBA and Poststroke Functional Outcome

Patients who achieved a good functional outcome had a significantly lower RBA (−0.44 vs 1.45, $p < 0.001$) and therefore a younger-looking brain than their chronological age-matched peers.

Among the evaluated predictors of poststroke outcome, the automated cross-validated recursive feature elimination process selected 4 clinical variables to enter the final logistic regression model: age, baseline NIHSS, prior stroke, and RBA. The results of the logistic regression of good functional outcomes are summarized in Table 4. In brief, in multivariable analysis, higher chronological age, higher RBA, higher baseline NIHSS score, or the presence of a history of prior stroke was independently associated with worse poststroke outcomes (respective adjusted odds ratios for good outcome: 0.58, 0.76, 0.48, 0.55; all *p*-values < 0.001). Distributions of mRS scores by quartile of RBA are shown in Figure 2. There was a higher proportion of favorable mRS in the lower quartiles of RBA in patients exhibiting younger-looking brains.

Table 4 Logistic Regression of Good Functional Outcome

	Unstandardized aOR			Standardized aOR			
		95% CI for aOR			95% CI for aOR		
Variables	aOR	Lower	Upper	aOR	Lower	Upper	p Value
Age	0.96	0.95	0.97	0.58	0.51	0.65	<0.001
NIHSS	0.87	0.85	0.89	0.48	0.43	0.54	<0.001
Prior stroke	0.55	0.41	0.74	0.55	0.41	0.74	<0.001
RBA	0.96	0.95	0.98	0.76	0.68	0.86	<0.001

NIHSS = NIH Stroke Scale; RBA = relative brain age; aOR = adjusted odds ratio.

Multivariable effect sizes of RBA on the dichotomized poststroke outcome by the rank of baseline NIHSS are shown in Figure 3. After adjustment for covariates (age, NIHSS, history of prior stroke), the detrimental effect size of RBA on achieving a good functional outcome was maximal for NIHSS = 0 (aOR = 0.61, n = 295) and decreased until NIHSS ≤ 9 (aOR = 0.75, n = 1,642).

Discussion

By leveraging a large ischemic stroke clinical imaging cohort, we successfully used brain MRI T2-FLAIR radiomics to predict brain age and derived RBA, a biomarker describing patients' brain health relative to their peers. Older-appearing brains were associated with cardiovascular risk factors, highlighting their detrimental impact on brain health. Finally, we showed that high RBA had a negative impact on poststroke functional outcomes. This effect was especially pronounced in patients presenting with lower stroke severity.

Chronological age quantifies the length of time a person has lived but is unlikely to affect stroke prognosis directly. It may best serve as a surrogate marker for age-related cerebral parenchymal alterations. In some patients, such deleterious alterations accumulate more rapidly or more slowly than the expected pace. Our results suggest that quantifying the deviation from expected brain age in patients with stroke can be relevant for assessing brain health and prognostication. Indeed, in our cohort, patients who did not achieve a favorable outcome had brains that appeared older on T2-FLAIR compared with their chronological age-matched peers. Moreover, our results show that RBA affected stroke outcomes independently from chronological age, NIHSS, and history of prior stroke. Indeed, patients with an older-appearing brain were more likely to develop an unfavorable poststroke outcome at any given age. This finding indicates that radiomics-derived RBA could assess the brain health of patients with stroke and quantify the resilience of brains in a way that chronological age cannot. In previous analyses of randomized control trials, chronological age–defined older patients (older than 80 years) were identified as a subgroup that benefitted more from endovascular recanalization than their younger counterparts, with the hypothesis that they had less brain reserve to withstand ischemia.[21,22] Future studies could evaluate whether patients with older-appearing brains would benefit more from recanalization[23] and assess whether brain age imaging biomarkers can help to identify new candidates for reperfusion therapies. For instance, patients with an NIHSS lower than 5 are currently not eligible for mechanical thrombectomy and are the topic of numerous randomized controlled trials. Our results could suggest that in this specific stroke population, patients with an older-appearing brain are less likely to reach a good functional poststroke outcome and could maybe benefit more from reperfusion therapies.

Figure 2 mRS Shift Plot per Quartile of RBA

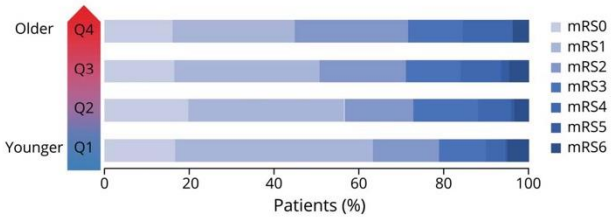

Q1-Q4 quartiles of RBA, mRS modified Rankin Scale. Q1-Q2 represents patients with lower RBA and thus younger-looking brains, whereas Q3-Q4 represents older-looking brains. mRS = modified Rankin scale; RBA = relative brain age.

Individual lifestyles, genetics, and environment can also set a different course for brain aging.[4,24] We found that high RBA was associated with HTN, DM, and a history of smoking, in line with the results based on large cohorts such as UK Biobank and Whitehall II.[4,5,9,24] This adds to the body of evidence that cardiovascular health and brain health are intertwined and stresses the importance of preventative medicine.[25] Our results also showed that a history of prior stroke was the most influential clinical factor affecting RBA, with an effect size 3-fold larger than other clinical variables. The second most detrimental clinical trait for brain aging in our sample was diabetes, which also emerged as a significant condition accelerating brain aging in previous work.[26] Identifying potentially modifiable factors affecting brain health yields relevance for prevention interventions.[27] For instance, body mass index and daily exercise were previously identified as predictive of younger brain age and are potentially modifiable.[24,28] RBA and brain age could furthermore be used as follow-up brain health biomarkers.

Figure 3 Effect Sizes of the Predictors of Good Functional Outcome by Rank of Baseline NIHSS

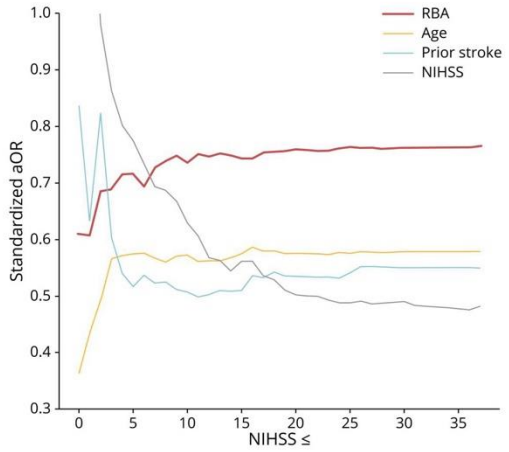

RBA had a detrimental impact on achieving a good functional outcome especially in patients with low NIHSS. aOR = adjusted odds ratio; NIHSS = NIH Stroke Scale; RBA = relative brain age.

Translation of the brain age biomarker to clinical care remains challenging. Indeed, most of the available neuroimaging brain age prediction methods include spatial registration to an anatomic template, which requires high-quality research-grade imaging.[2,4,24] Moreover, T1-weighted imaging is predominantly used in these pipelines but is uncommonly acquired during acute stroke MRI imaging workup. Therefore, there is a need for frameworks compatible with clinical care settings, especially in time-sensitive diseases such as stroke, featuring T2-FLAIR, given its common utilization in both the acute phase and during the follow-up.[29] Radiomics, an emerging image quantifying technology, could represent a potential solution because they require little computational power and can be applied to any digitalized medical imaging.[16] Radiomics were never assessed to predict brain age. While in previous literature, brain age is mostly predicted by volumetric information, radiomics description encompasses information that goes beyond volume, characterizing the shape and the texture of an image; consequently, radiomics can potentially capture more information. Analyses of T2-FLAIR images using radiomics are especially relevant in patients with stroke because this sequence reflects both higher age and cerebral burden of diseases.[30] Moreover, most published studies have trained their models on healthy brains, which have a uniform aging distribution unlike stroke cohorts. This aspect might be reflected by the greater errors of our predictions than in published literature, which ranges in adult cohorts from around 2.5 years, for recent complex deep learning–based methods,[31] to between 4.3 and 13.5 years for more traditional methods.[2] Moreover, there is a trend in brain age prediction literature to incorporate more and more complex and multimodal data, such as diffusion tensor imaging or functional MRI and process it within high-end deep learning frameworks.[24,32,33] We deliberately chose to tackle the challenge of leveraging clinical imaging and a lighter methodological framework with the idea of developing models that are more interpretable and may have a better chance of translating brain age biomarkers to routine clinical care.

This work has several limitations. First, our cohort included patients from 2003 to 2011, whose management might not have been fully representative of patients treated in modern stroke

care settings. Future work will assess the impact of brain age on the outcome of patients treated with up-to-date reperfusion therapies. Second, despite being drawn from a multicentric cohort using nested cross-validation, future validation of our preliminary findings in an independent cohort will further ensure the generalizability of the brain age biomarker in stroke care. Third, we could not benchmark our method against other published methods such as BrainAGE or Brain age delta[2,18] because we did not have T1-weighted images; further work could evaluate our method on reference data sets if they include T2-FLAIR imaging. Fourth, our work leveraged segmentation masks and therefore suffers from limitations related to segmentation steps. Moreover, the impact of motion artifacts or of early hemorrhagic transformation on RBA was not specifically assessed. Finally, we could not explore the relationship between T2-FLAIR radiomics-derived brain age biomarkers with more detailed outcome metrics, such as cognitive and language outcomes, or with other neuroimaging biomarkers of brain health, such as brain reserve or effective reserve.[34,35] Future studies could indeed study the relationship between radiomics brain age and cognitive reserve in patients with stroke.

To conclude, in this cohort study of 4,163 patients with ischemic stroke, using radiomics extracted from clinically acquired T2-FLAIR images, we derived RBA, a chronological age–independent biomarker describing individual biological brain age. A higher RBA was linked to the presence of cardiovascular risk factors and worse poststroke outcomes. Therefore, this newly radiomics-derived RBA may capture previously unidentified prognostic information.

Study Funding

The MRI-GENIE study was funded by NIH NINDS (R01NS086905, NSR PI). M.B was supported by the ISITE-ULNE Fundation, the Société Française de Neuroradiologie, the Société Française de Radiologie, and the Thérèse and René Planiol Fundation. A.K.B. is supported by a MGH ECOR Fund for Medical Discovery (FMD) Clinical Research Fellowship Award. MRE is supported by the American Academy of Neurology and MGH Executive Council on Research. PMR is supported by NIH K01 HL128791. TT was supported by the Helsinki University Central Hospital, Sigrid Juselius Foundation, Sahlgrenska University Hospital, and University of Gothenburg. A.G.L was supported by the Swedish Heart and Lung Foundation, Region Skåne, Lund University, Skåne University Hospital, Sparbanksstiftelsen Färs och Frosta, Fremasons Lodge of Instruction Eos in Lund, CaNVAS project was funded by NIH (US), the Swedish Government (under the Avtal om Läkarutbildning och Medicinsk Forskning, ALF); C.J. was supported by the Swedish Heart and Lung Foundation (20190203); and the Swedish state under the agreement between the Swedish government and the county councils, the ALF agreement (ALFGBG-720081) PL is supported by NIH NIBIB NAC P41EB015902; The funders had no role in design and conduct of the study; collection, management, analysis, and interpretation of the data; preparation, review, or approval of the manuscript; and decision to submit the manuscript for publication.

Disclosures

M. Etherton has received personal fees for consulting from Astra Zeneca and WorldCare Clinical Group. C. Griessenauer has received consulting honoraria from Microvention and Stryker and research funding from Medtronic and Penumbra. A. Vagal has received research funding from Cerenovus. A.G. Lindgren has received personal fees from Bayer, Astra Zeneca, BMS Pfizer, and Portola. N.S. Rost has received compensation as scientific advisory consultant from Omniox, Sanofi Genzyme, and AbbVie Inc. The other authors report no relevant disclosures. Go to Neurology.org/N for full disclosures.

Publication History

Previously published at www.researchsquare.com, https://doi.org/10.21203/rs.3.rs-923769/v1. Received by *Neurology* October 6, 2021. Accepted in final form October 6, 2022. Submitted and externally peer reviewed. The handling editor was José Merino, MD, MPhil, FAAN.

Appendix Authors

Name	Location	Contribution
Martin Bretzner, MD	J. Philip Kistler Stroke Research Center, Massachusetts General Hospital, Boston; Lille University, Inserm, CHU Lille, U1172—LilNCog—Lille Neuroscience & Cognition, France	Drafting/revision of the manuscript for content, including medical writing for content; Major role in the acquisition of data; study concept or design; analysis or interpretation of data
Anna K. Bonkhoff, MD	J. Philip Kistler Stroke Research Center, Massachusetts General Hospital, Boston	Drafting/revision of the manuscript for content, including medical writing for content; study concept or design; analysis or interpretation of data
Markus D. Schirmer, PhD	J. Philip Kistler Stroke Research Center, Massachusetts General Hospital, Boston	Major role in the acquisition of data; analysis or interpretation of data
Sungmin Hong, PhD	J. Philip Kistler Stroke Research Center, Massachusetts General Hospital, Boston	Drafting/revision of the manuscript for content, including medical writing for content; analysis or interpretation of data
Adrian Dalca, PhD	J. Philip Kistler Stroke Research Center, Massachusetts General Hospital, Boston; A.A. Martinos Center for Biomedical Imaging, Massachusetts General Hospital, Harvard Medical School; Computer Science and Artificial Intelligence Lab, Massachusetts Institute of Technology, Cambridge	Major role in the acquisition of data
Kathleen Donahue, BS	J. Philip Kistler Stroke Research Center, Massachusetts General Hospital, Boston; Computer Science and Artificial Intelligence Lab, Massachusetts Institute of Technology, Cambridge	Major role in the acquisition of data

Continued

Appendix *(continued)*

Name	Location	Contribution
Anne-Katrin Giese, MD	J. Philip Kistler Stroke Research Center, Massachusetts General Hospital, Boston	Major role in the acquisition of data
Mark R. Etherton, MD, PhD	J. Philip Kistler Stroke Research Center, Massachusetts General Hospital, Boston	Drafting/revision of the manuscript for content, including medical writing for content; Major role in the acquisition of data; analysis or interpretation of data
Pamela M. Rist, ScD	J. Philip Kistler Stroke Research Center, Massachusetts General Hospital, Boston; Division of Preventive Medicine, Department of Medicine, Brigham and Women's Hospital, Boston, MA	Drafting/revision of the manuscript for content, including medical writing for content; analysis or interpretation of data
Marco Nardin, BS	J. Philip Kistler Stroke Research Center, Massachusetts General Hospital, Boston	Major role in the acquisition of data
Robert W. Regenhardt, MD, PhD	J. Philip Kistler Stroke Research Center, Massachusetts General Hospital, Boston	Drafting/revision of the manuscript for content, including medical writing for content; analysis or interpretation of data
Xavier Leclerc, MD, PhD	Lille University, Inserm, CHU Lille, U1172—LilNCog—Lille Neuroscience & Cognition, France	Drafting/revision of the manuscript for content, including medical writing for content; analysis or interpretation of data
Renaud Lopes, PhD	Lille University, Inserm, CHU Lille, U1172—LilNCog—Lille Neuroscience & Cognition, France	Drafting/revision of the manuscript for content, including medical writing for content; study concept or design; analysis or interpretation of data
Morgan Gautherot, PhD	Lille University, CNRS, Inserm, CHU Lille, Institut Pasteur de Lille, US 41 - UMS 2014 - PLBS, France	Drafting/revision of the manuscript for content, including medical writing for content; study concept or design; analysis or interpretation of data
Clinton Wang, PhD	J. Philip Kistler Stroke Research Center, Massachusetts General Hospital, Boston	Drafting/revision of the manuscript for content, including medical writing for content; analysis or interpretation of data
Oscar R. Benavente, MD	Department of Medicine, Division of Neurology, University of British Columbia, Vancouver, British Columbia, Canada	Major role in the acquisition of data
John W. Cole, MD, MS	Department of Neurology, University of Maryland School of Medicine and Veterans Affairs Maryland Health Care System, Baltimore, MD	Major role in the acquisition of data
Amanda Donatti, PhD	School of Medical Sciences, University of Campinas (UNICAMP) and the Brazilian Institute of Neuroscience and Neurotechnology (BRAINN), Campinas, São Paulo, Brazil	Major role in the acquisition of data
Christoph Griessenauer, MD	Department of Neurosurgery, Geisinger, Danville, PA; Department of Neurosurgery, Christian Doppler Klinik, Paracelsus Medical University, Salzburg, Austria	Drafting/revision of the manuscript for content, including medical writing for content; Major role in the acquisition of data
Laura Heitsch, MD	Division of Emergency Medicine, Washington University School of Medicine, St Louis, MO; Department of Neurology, Washington University School of Medicine & Barnes-Jewish Hospital, St Louis, MO	Major role in the acquisition of data
Lukas Holmegaard, MD	Department of Clinical Neuroscience, Institute of Neuroscience and Physiology, Sahlgrenska Academy at University of Gothenburg, Gothenburg, Sweden; Department of Neurology, Sahlgrenska University Hospital, Gothenburg, Sweden	Major role in the acquisition of data
Katarina Jood, MD	Department of Clinical Neuroscience, Institute of Neuroscience and Physiology, Sahlgrenska Academy at University of Gothenburg, Gothenburg, Sweden; Department of Neurology, Sahlgrenska University Hospital, Gothenburg, Sweden	Drafting/revision of the manuscript for content, including medical writing for content; Major role in the acquisition of data
Jordi Jimenez-Conde, MD	Department of Neurology, Neurovascular Research Group (NEUVAS), IMIM-Hospital del Mar (Institut Hospital del Mar d'Investigacions Mèdiques), Universitat Autonoma de Barcelona, Barcelona, Spain	Major role in the acquisition of data
Steven J Kittner, MD	Department of Neurology, University of Maryland School of Medicine and Veterans Affairs Maryland Health Care System, Baltimore, MD	Major role in the acquisition of data

Appendix *(continued)*

Name	Location	Contribution
Robin Lemmens, MD	KU Leuven - University of Leuven, Department of Neurosciences, Experimental Neurology and Leuven Research Institute for Neuroscience and Disease (LIND), Leuven, Belgium; VIB, Vesalius Research Center, Laboratory of Neurobiology, University Hospitals Leuven, Department of Neurology, Leuven, Belgium	Drafting/revision of the manuscript for content, including medical writing for content; Major role in the acquisition of data
Christopher R. Levi, PhD	School of Medicine and Public Health, University of Newcastle, Newcastle, New South Wales, Australia; Department of Neurology, John Hunter Hospital, Newcastle, NSW, Australia	Major role in the acquisition of data
Patrick F. McArdle, PhD	Division of Endocrinology, Diabetes and Nutrition, Department of Medicine, University of Maryland School of Medicine, Baltimore, MD	Major role in the acquisition of data
Caitrin W. McDonough, PhD	Department of Pharmacotherapy and Translational Research and Center for Pharmacogenomics, University of Florida, Gainesville, FL	Major role in the acquisition of data
James F. Meschia, MD	Department of Neurology, Mayo Clinic, Jacksonville, FL	Major role in the acquisition of data
Chia-Ling Phuah, MD	Department of Neurology, Washington University School of Medicine & Barnes-Jewish Hospital, St Louis, MO	Major role in the acquisition of data
Arndt Rolfs, MD	Klinik und Poliklinik für Neurologie, Universitätsmedizin Rostock, Rostock, Germany	Major role in the acquisition of data
Stefan Ropele, MD	Department of Neurology, Clinical Division of Neurogeriatrics, Medical University Graz, Graz, Austria	Major role in the acquisition of data
Jonathan Rosand, MD MSc	Henry and Allison McCance Center for Brain Health, Massachusetts General Hospital; Center for Genomic Medicine, Massachusetts General Hospital, Boston, MA; Broad Institute, Cambridge, MA	Major role in the acquisition of data
Jaume Roquer, MD	Department of Neurology and Evelyn F. McKnight Brain Institute, Miller School of Medicine, University of Miami, Miami, FL	Major role in the acquisition of data

Appendix *(continued)*

Name	Location	Contribution
Tatjana Rundek, MD/ PhD	Department of Neurology and Evelyn F. McKnight Brain Institute, Miller School of Medicine, University of Miami, Miami, FL	Drafting/revision of the manuscript for content, including medical writing for content; Major role in the acquisition of data
Ralph L. Sacco, MD, MS	Department of Neurology and Evelyn F. McKnight Brain Institute, Miller School of Medicine, University of Miami, Miami, FL	Major role in the acquisition of data
Reinhold Schmidt, MD	Department of Neurology, Clinical Division of Neurogeriatrics, Medical University Graz, Graz, Austria	Major role in the acquisition of data
Pankaj Sharma, MD, PhD. FRCP	Institute of Cardiovascular Research, Royal Holloway University of London (ICR2UL), Egham, UK St Peter's and Ashford Hospitals, UK	Major role in the acquisition of data
Agnieszka Slowik, MD, PhD	Department of Neurology, Jagiellonian University Medical College, Krakow, Poland	Major role in the acquisition of data
Alessandro Sousa, MD	School of Medical Sciences, University of Campinas (UNICAMP) and the Brazilian Institute of Neuroscience and Neurotechnology (BRAINN), Campinas, São Paulo, Brazil	Major role in the acquisition of data
Tara M. Stanne, MD	Department of Clinical Neuroscience, Institute of Neuroscience and Physiology, Sahlgrenska Academy at University of Gothenburg, Gothenburg, Sweden; Department of Neurology, Sahlgrenska University Hospital, Gothenburg, Sweden	Drafting/revision of the manuscript for content, including medical writing for content; Major role in the acquisition of data
Daniel Strbian, MD	Division of Neurocritical Care & Emergency Neurology, Department of Neurology, Helsinki University Central Hospital, Helsinki, Finland	Major role in the acquisition of data
Turgut Tatlisumak, MD	Department of Clinical Neuroscience, Institute of Neuroscience and Physiology, Sahlgrenska Academy at University of Gothenburg, Gothenburg, Sweden; Department of Neurology, Sahlgrenska University Hospital, Gothenburg, Sweden	Drafting/revision of the manuscript for content, including medical writing for content; Major role in the acquisition of data
Vincent Thijs, PhD	Stroke Division, Florey Institute of Neuroscience and Mental Health, Heidelberg, Australia and Department of Neurology, Austin Health, Heidelberg, Australia	Drafting/revision of the manuscript for content, including medical writing for content; Major role in the acquisition of data

Continued

Appendix *(continued)*

Name	Location	Contribution
Achala Vagal, MD	Department of Radiology, University of Cincinnati College of Medicine, Cincinnati, OH	Drafting/revision of the manuscript for content, including medical writing for content; Major role in the acquisition of data
Johan Wasselius, MD, PhD	Department of Clinical Sciences Lund, Radiology, Lund University, Lund, Sweden; Department of Radiology, Neuroradiology, Skåne University Hospital, Malmö, Sweden	Drafting/revision of the manuscript for content, including medical writing for content; Major role in the acquisition of data
Daniel Woo, MD	Department of Neurology and Rehabilitation Medicine, University of Cincinnati College of Medicine, Cincinnati, OH	Major role in the acquisition of data
Ona Wu, PhD	A.A. Martinos Center for Biomedical Imaging, Massachusetts General Hospital, Harvard Medical School	Major role in the acquisition of data
Ramin Zand, MD	Department of Neurology, Geisinger, Danville, PA	Drafting/revision of the manuscript for content, including medical writing for content; Major role in the acquisition of data
Bradford B. Worrall, MD, MSc	Departments of Neurology and Public Health Sciences, University of Virginia, Charlottesville, VA	Drafting/revision of the manuscript for content, including medical writing for content; Major role in the acquisition of data
Jane Maguire, PhD	University of Technology Sydney, Sydney, Australia	Major role in the acquisition of data
Arne G. Lindgren, MD, PhD	Section of Neurology, Skåne University Hospital, Lund, Sweden; Department of Clinical Sciences Lund, Neurology, Lund University, Lund, Sweden	Drafting/revision of the manuscript for content, including medical writing for content; Major role in the acquisition of data
Christina Jern, MD	Institute of Biomedicine, Department of Laboratory Medicine, the Sahlgrenska Academy, University of Gothenburg, Gothenburg, Sweden; Region Västra Götaland, Sahlgrenska University Hospital, Department of Clinical Genetics and Genomics, Gothenburg, Sweden	Drafting/revision of the manuscript for content, including medical writing for content; Major role in the acquisition of data
Polina Golland, PhD	Computer Science and Artificial Intelligence Lab, Massachusetts Institute of Technology, Cambridge	Major role in the acquisition of data
Grégory Kuchcinski, MD, PhD	Lille University, Inserm, CHU Lille, U1172—LilNCog—Lille Neuroscience & Cognition, France	Drafting/revision of the manuscript for content, including medical writing for content; Major role in the acquisition of data; study concept or design; analysis or interpretation of data
Natalia S. Rost, MD, MPH	J. Philip Kistler Stroke Research Center, Massachusetts General Hospital, Boston	Drafting/revision of the manuscript for content, including medical writing for content; Major role in the acquisition of data; study concept or design; analysis or interpretation of data

References

1. Drozdowska BA, Singh S, Quinn TJ. Thinking about the future: a review of prognostic scales used in acute stroke. *Front Neurol.* 2019;10:274-274. doi: 10.3389/fneur.2019.00274
2. Franke K, Gaser C. Ten years of BrainAGE as a neuroimaging biomarker of brain aging: what insights have we gained? *Front Neurol.* 2019;10:789. doi: 10.3389/fneur.2019.00789
3. Hénon H, Pasquier F, Leys D. Poststroke dementia. *Cerebrovasc Dis (Basel, Switzerland).* 2006;22(1):61-70. doi: 10.1159/000092923
4. Ning K, Zhao L, Matloff W, Sun F, Toga AW. Association of relative brain age with tobacco smoking, alcohol consumption, and genetic variants. *Sci Rep.* 2020;10:10.
5. Kolbeinsson A, Filippi S, Panagakis Y, et al. Accelerated MRI-predicted brain ageing and its associations with cardiometabolic and brain disorders. *Sci Rep.* 2020;10:19940.
6. Stern Y, Arenaza-Urquijo EM, Bartrés-Faz D, et al. Whitepaper: defining and investigating cognitive reserve, brain reserve, and brain maintenance. *Alzheimers Demen.* 2020;16(9):1305-1311. doi: 10.1016/j.jalz.2018.07.219
7. Richard G, Kolskår K, Ulrichsen KM, et al. Brain age prediction in stroke patients: highly reliable but limited sensitivity to cognitive performance and response to cognitive training. *NeuroImage Clin.* 2020;25:102159. doi: 10.1016/j.nicl.2019.102159
8. Egorova N, Liem F, Hachinski V, Brodtmann A. Predicted brain age after stroke. *Front Aging Neurosci.* 2019;11:348-348. doi: 10.3389/fnagi.2019.00348
9. de Lange AMG, Anatürk M, Suri S, et al. Multimodal brain-age prediction and cardiovascular risk: the Whitehall II MRI sub-study. *Neuroimage.* 2020;222:117292-117292.
10. van Griethuysen JJ, Fedorov A, Parmar C, et al. Computational radiomics system to decode the radiographic phenotype. *Cancer Res.* 2017;77(21):e104–e107. doi: 10.1158/0008-5472.can-17-0339
11. Giese A-K, Schirmer MD, Dalca AV, et al. White matter hyperintensity burden in acute stroke patients differs by ischemic stroke subtype. *Neurology.* 2020;95(1):e79–e88. doi: 10.1212/wnl.0000000000009728
12. Bonkhoff AK, Schirmer MD, Bretzner M, et al. Outcome after acute ischemic stroke is linked to sex-specific lesion patterns. *Nat Commun.* 2021;12(1):3289. doi: 10.1038/s41467-021-23492-3
13. Hong S, Giese AK, Schirmer MD, et al. Excessive white matter hyperintensity increases susceptibility to poor functional outcomes after acute ischemic stroke. *Front Neurol.* 2021;12:700616. doi: 10.3389/fneur.2021.700616
14. Schirmer MD, Dalca AV, Sridharan R, et al. White matter hyperintensity quantification in large-scale clinical acute ischemic stroke cohorts – the MRI-GENIE study. *NeuroImage: Clin.* 2019;23:101884. doi: 10.1016/j.nicl.2019.101884
15. Dubost F, Bruijne M de, Nardin M, et al. Multi-atlas image registration of clinical data with automated quality assessment using ventricle segmentation. *Med Image Anal.* 2020;63:101698. doi: 10.1016/j.media.2020.101698
16. Lambin P, Leijenaar RTH, Deist TM, et al. Radiomics: the bridge between medical imaging and personalized medicine. *Nat Rev Clin Oncol.* 2017;14(12):749-762. doi: 10.1038/nrclinonc.2017.141
17. Mongan J, Moy L, Kahn CE. Checklist for artificial intelligence in medical imaging (CLAIM): a guide for authors and reviewers. *Radiol Artif Intelligence.* 2020;2:e200029.
18. Smith SM, Vidaurre D, Alfaro-Almagro F, Nichols TE, Miller KL. Estimation of brain age delta from brain imaging. *Neuroimage.* 2019;200:528-539. doi: 10.1016/j.neuroimage.2019.06.017
19. Pedregosa F, Varoquaux G, Gramfort A, et al. Scikit-learn: machine learning in Python. *J Mach Learn Res.* 2011;12:2825-2830.
20. Seabold S, Perktold J. Statsmodels: econometric and statistical modeling with Python. In: van der Walt S, Millman J, editors. *Proceedings of the 9th Python in Science Conference;* 2010:92-96.
21. Groot AE, Treurniet KM, Jansen IGH, et al. Endovascular treatment in older adults with acute ischemic stroke in the MR CLEAN Registry. *Neurology.* 2020;95:e131–e139.
22. Goyal M, Menon BK, van Zwam WH, et al. Endovascular thrombectomy after large-vessel ischaemic stroke: a meta-analysis of individual patient data from five randomised trials. *Lancet.* 2016;387(10029):1723-1731. doi: 10.1016/s0140-6736(16)00163-x
23. Regenhardt RW, Young MJ, Etherton MR, et al. Toward a more inclusive paradigm: thrombectomy for stroke patients with pre-existing disabilities. *J NeuroInterventional Surg.* 2020;13(10):865-868. doi: 10.1136/neurintsurg-2020-016783

24. Cole JH. Multimodality neuroimaging brain-age in UK biobank: relationship to biomedical, lifestyle, and cognitive factors. *Neurobiol Aging*. 2020;92:34-42. doi: 10.1016/j.neurobiolaging.2020.03.014
25. Gorelick Philip B, Furie Karen L, Costantino Iadecola, et al. Defining optimal brain health in adults: a presidential advisory from the American Heart Association/American Stroke Association. *Stroke*. 2017;48:e284–e303.
26. Franke K, Gaser C, Manor B, Novak V. Advanced BrainAGE in older adults with type 2 diabetes mellitus. *Front Aging Neurosci*. 2013;5:90-90. doi: 10.3389/fnagi.2013.00090
27. Regenhardt RW, Takase H, Lo EH, Lin DJ. Translating concepts of neural repair after stroke: structural and functional targets for recovery. *Restorative Neurol Neurosci*. 2020;38(1):67-92. doi: 10.3233/rnn-190978
28. Steffener J, Habeck C, O'Shea D, Razlighi Q, Bherer L, Stern Y. Differences between chronological and brain age are related to education and self-reported physical activity. *Neurobiol Aging*. 2016;40:138-144. doi: 10.1016/j.neurobiolaging.2016.01.014
29. Regenhardt RW, Bretzner M, Zanon Zotin MC, et al. Radiomic signature of DWI-FLAIR mismatch in large vessel occlusion stroke. *J Neuroimaging*. 2022;32(1):63-67. doi: 10.1111/jon.12928
30. Bretzner M, Bonkhoff AK, Schirmer MD, et al. MRI radiomic signature of white matter hyperintensities is associated with clinical phenotypes. *Front Neurosci*. 2021;15:691244. doi: 10.3389/fnins.2021.691244
31. Peng H, Gong W, Beckmann CF, Vedaldi A, Smith SM. Accurate brain age prediction with lightweight deep neural networks. *Med Image Anal*. 2021;68:101871. doi: 10.1016/j.media.2020.101871
32. Liem F, Varoquaux G, Kynast J, et al. Predicting brain-age from multimodal imaging data captures cognitive impairment. *NeuroImage*. 2017;148:179-188. doi: 10.1016/j.neuroimage.2016.11.005
33. Cole JH, Poudel RPK, Tsagkrasoulis D, et al. Predicting brain age with deep learning from raw imaging data results in a reliable and heritable biomarker. *NeuroImage*. 2017;163:115-124. doi: 10.1016/j.neuroimage.2017.07.059
34. Schirmer MD, Etherton MD PhD MR, Dalca PhD AV, et al. Effective reserve: a latent variable to improve outcome prediction in stroke. *J Stroke Cerebrovasc Dis*. 2019;28(1):63-69. doi: 10.1016/j.jstrokecerebrovasdis.2018.09.003
35. Sumowski JF, Rocca MA, Leavitt VM, et al. Brain reserve and cognitive reserve protect against cognitive decline over 4.5 years in MS. *Neurology*. 2014;82(20):1776-1783. doi: 10.1212/wnl.0000000000000433

Supplemental materials

eAppendix 1. Supplemental analysis: Inter-center variability in brain age prediction performances study

Hypothesis: Brain age prediction performances vary between centers.

Methods: We iteratively held out one center for testing and trained on the 16 other centers. Out-of-sample brain age prediction performance was measured using the coefficient of determination (R2) of a linear regression between chronological age and predicted brain age. Correlation between the prediction performances and the difference in chronological age between the training and test sites were performed using Pearson's correlation.

Results: Predictions performances per held-out center are shown in eTable 1. Distributions of the chronological age and predicted age per held-out center are shown in eFigure 2. Briefly, and as expected, when patients from the held-out center had a mean chronological age that was significantly different from the training centers, predictions performances were poorer. Predictions performance (R2) were strongly correlated with the difference between chronological ages in the training and held-out testing centers ($r=0.90$, $p=8.5e-7$). Overall, individual held-out R2 values were lower than that in the main analysis.

Interpretation: When predicting brain age in centers whose patients' chronological age significantly differs from the training centers' patients, the model performances were not as good; probably because the model was not trained to recognize those patients' brain trophicity accurately enough. This result is in favor of working on large and heterogeneous cohorts such as MRIGENIE but also limits the interpretation of our results that could generalize only to comparable stroke populations.

eTable 1: Predictions performances and sample sizes per center.

	1	**2**	**3**	**4**	**5**	**6**	**7**	**8**	**9**	**10**	**11**	**12**	**13**	**14**	**15**	**16**	**17**
n	340	158	446	249	61	115	59	211	162	210	121	441	205	81	44	244	1015
R2	0.67	0.48	0.61	0.53	-2.04	-0.11	0.60	0.33	0.22	0.47	0.63	0.56	0.47	0.62	0.27	-1.65	0.49
True Age	64.9	64.3	64.9	61.9	42.1	70.5	63.5	64.1	51.9	60.5	62.3	67.0	61.8	53.6	67.4	41.3	67.6
Predicted age	63.8	62.6	63.6	63.5	49.6	63.2	58.9	67.9	56.3	63.8	60.5	64.4	60.2	52.4	62.3	50.3	65.7
Training age	62.6	62.7	62.5	62.9	63.1	62.6	62.8	62.7	63.2	62.9	62.8	62.3	62.8	63.0	62.7	64.1	61.2

eFigure 2: Boxplot of the distributions of age and results inter-site cross-validation brain age predictions.

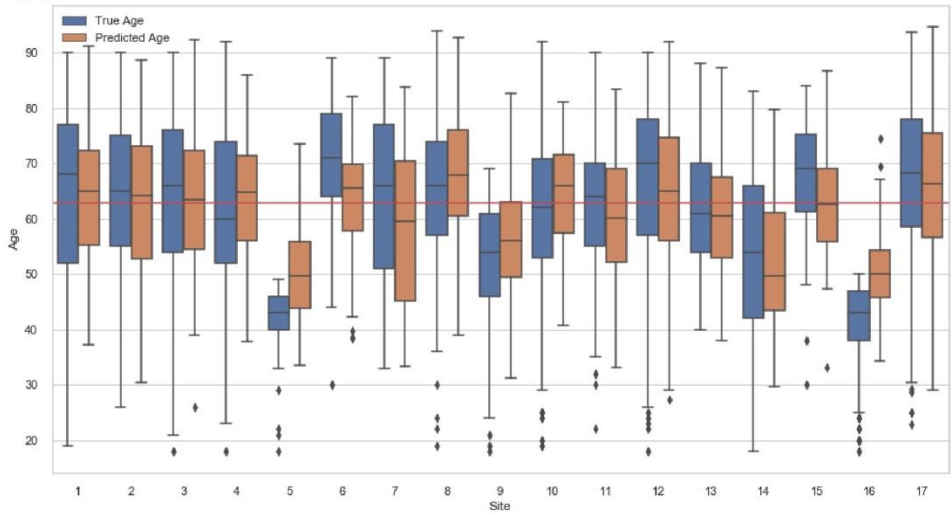

Legend: Mean age of the whole cohort (red line).

eAppendix 2. Supplemental analysis:

Question: Which T2-FLAIR radiomics are relevant for brain age prediction?

Methods: We recorded the T2-FLAIR radiomics selected in each of the 5 folds of the cross-validation as they were the most relevant variable for brain age prediction. We also recorded their respective ElasticNet linear regression coefficients for interpretation. We computed the mean, absolute mean, standard deviation and coefficient of variation of these coefficients. A variable with a positive coefficient will participate to a higher relative brain age (RBA) and therefore captures neuroimaging attributes of an older looking brain, whereas a negative coefficient will participate in producing a negative RBA and therefore a younger looking brain. As a confirmatory analysis, we computed the Pearson correlation between RBA and white matter hyperintensities (WMH) burden and brain volume.

Results: Selected and therefore relevant radiomics for brain age prediction are shown in eTable 2. Briefly, brains that were more filled and more homogeneous in T2-FLAIR were predictive of lower brain age; brains that were heterogeneous, atrophic, and had intensities profiles skewed toward high intensities in T2-FLAIR were predictive of higher brain age. RBA was negatively correlated with brain volume ($r=-0.19$, $p<0.001$) and positively correlated with WMH burden ($r=0.17$, $p<0.001$).

Interpretation: Radiomics relevant for brain age prediction were capturing neuroimaging textural aspect on T2-FLAIR related to atrophy and parenchymal heterogeneity. This was confirmed by the significant correlation between RBA and brain volume and WMH burden.

eTable 2: Coefficient of variation of the selected radiomics for brain age prediction

Radiomics	Mean value	Standard Deviation	Coefficient of Variation	Absolute mean value
original_shape_Sphericity	-3.79	0.52	37.63%	3.79
log-sigma-2-0-mm-3D_glszm_GrayLevelNonUniformityNormalized	-3.61	0.55	27.61%	3.61
wavelet-LH_firstorder_Median	3.04	0.6	24.44%	3.04
log-sigma-2-0-mm-3D_firstorder_Median	-3.04	0.66	20.79%	3.04
diagnostics_Image-interpolated_Mean	-2.72	0.2	16.60%	2.72
original_firstorder_10Percentile	-2.68	0.19	17.64%	2.68
log-sigma-3-0-mm-3D_glrlm_RunVariance	-2.57	0.39	43.80%	2.57
original_shape_MajorAxisLength	-2.53	0.57	9.54%	2.53
wavelet-HL_firstorder_Mean	2.4	0.34	47.02%	2.4
log-sigma-2-0-mm-3D_glcm_MaximumProbability	2.38	0.37	48.21%	2.38
log-sigma-2-0-mm-3D_firstorder_InterquartileRange	-2.31	0.27	27.20%	2.31
log-sigma-2-0-mm-3D_firstorder_Skewness	2.19	0.46	18.35%	2.19
wavelet-LH_glcm_Imc2	-2.16	0.43	34.38%	2.16
wavelet-LH_firstorder_Skewness	-2.08	0.19	40.63%	2.08
log-sigma-1-0-mm-3D_firstorder_Kurtosis	-1.99	0.8	19.77%	1.99
log-sigma-1-0-mm-3D_glcm_ClusterShade	-1.98	0.25	45.87%	1.98
log-sigma-3-0-mm-3D_glszm_GrayLevelNonUniformityNormalized	-1.95	0.66	22.52%	1.95
log-sigma-1-0-mm-3D_glcm_Imc1	1.88	0.42	19.14%	1.88
original_firstorder_Median	1.86	0.45	33.66%	1.86
log-sigma-3-0-mm-3D_firstorder_Median	-1.77	0.72	15.41%	1.77
log-sigma-3-0-mm-3D_glrlm_LongRunEmphasis	-1.73	0.3	39.18%	1.73
log-sigma-2-0-mm-3D_glszm_GrayLevelNonUniformity	-1.72	0.55	25.01%	1.72
log-sigma-1-0-mm-3D_glcm_Imc2	-1.71	0.25	34.13%	1.71
log-sigma-2-0-mm-3D_firstorder_RobustMeanAbsoluteDeviation	-1.69	0.28	37.74%	1.69
lbp-2D_glcm_ClusterProminence	1.6	0.26	49.92%	1.6
lbp-2D_glcm_ClusterTendency	1.53	0.15	22.57%	1.53
original_glszm_SmallAreaHighGrayLevelEmphasis	-1.51	0.24	36.93%	1.51
log-sigma-1-0-mm-3D_glcm_Idmn	-1.51	0.24	15.99%	1.51
wavelet-HL_glcm_Imc1	1.5	0.38	32.23%	1.5
lbp-2D_glrlm_LowGrayLevelRunEmphasis	-1.47	0.28	16.65%	1.47
original_shape_LeastAxisLength	-1.45	0.41	42.83%	1.45

Radiomics	Mean value	Standard Deviation	Coefficient of Variation	Absolute mean value
log-sigma-2-0-mm-3D_gldm_DependenceEntropy	1.41	0.39	15.66%	1.41
log-sigma-3-0-mm-3D_firstorder_RootMeanSquared	-1.35	0.13	21.82%	1.35
log-sigma-3-0-mm-3D_glcm_Imc1	1.35	0.51	16.48%	1.35
original_shape_SurfaceArea	1.35	0.51	24.59%	1.35
log-sigma-1-0-mm-3D_glszm_LargeAreaHighGrayLevelEmphasis	-1.34	0.33	26.58%	1.34
log-sigma-2-0-mm-3D_glszm_ZoneEntropy	1.34	0.22	28.67%	1.34
log-sigma-3-0-mm-3D_ngtdm_Busyness	1.34	0.72	14.29%	1.34
log-sigma-2-0-mm-3D_glrlm_RunEntropy	1.32	0.17	40.46%	1.32
log-sigma-1-0-mm-3D_firstorder_RootMeanSquared	1.31	0.32	78.95%	1.31
log-sigma-3-0-mm-3D_firstorder_10Percentile	1.3	0.43	14.10%	1.3
lbp-2D_gldm_DependenceEntropy	1.3	0.38	24.04%	1.3
wavelet-HL_glcm_ClusterProminence	-1.28	0.48	44.19%	1.28
log-sigma-3-0-mm-3D_glcm_Idn	-1.27	0.32	46.54%	1.27
wavelet-HL_gldm_LargeDependenceLowGrayLevelEmphasis	1.24	0.55	38.13%	1.24
original_gldm_GrayLevelNonUniformity	1.23	0.28	63.03%	1.23
lbp-2D_glszm_SizeZoneNonUniformityNormalized	1.23	0.24	25.31%	1.23
original_glszm_HighGrayLevelZoneEmphasis	-1.2	0.19	31.95%	1.2
wavelet-HL_glcm_MaximumProbability	1.18	0.22	18.94%	1.18
diagnostics_Mask-interpolated_Mean	1.14	0.38	64.59%	1.14
original_glcm_Idmn	1.14	0.46	19.61%	1.14
wavelet-HL_gldm_DependenceVariance	1.14	0.31	44.99%	1.14
lbp-2D_glcm_Imc1	-1.14	0.42	28.25%	1.14
original_shape_SurfaceVolumeRatio	1.12	0.39	41.66%	1.12
wavelet-HH_glcm_Imc1	-1.12	0.51	54.08%	1.12
wavelet-HL_firstorder_Skewness	-1.1	0.37	36.29%	1.1
log-sigma-2-0-mm-3D_glcm_InverseVariance	1.09	0.15	19.99%	1.09
original_glrlm_GrayLevelNonUniformity	1.08	0.21	16.18%	1.08
original_glcm_MaximumProbability	1.04	0.44	40.29%	1.04
log-sigma-2-0-mm-3D_glcm_ClusterShade	1.01	0.29	44.52%	1.01
original_glszm_ZoneEntropy	1.01	0.43	26.94%	1.01
log-sigma-2-0-mm-3D_gldm_LargeDependenceHighGrayLevelEmphasis	0.99	0.51	12.73%	0.99
log-sigma-1-0-mm-3D_glszm_SizeZoneNonUniformity	0.97	0.42	42.44%	0.97

Radiomics	Mean value	Standard Deviation	Coefficient of Variation	Absolute mean value
original_gldm_SmallDependenceHighGrayLevelEmphasis	-0.96	0.48	22.49%	0.96
log-sigma-3-0-mm-3D_glcm_Imc2	-0.95	0.5	32.81%	0.95
wavelet-HH_firstorder_Kurtosis	0.95	0.15	11.77%	0.95
wavelet-HH_glcm_Idmn	0.9	0.38	38.02%	0.9
wavelet-LH_glcm_Imc1	0.89	0.57	16.28%	0.89
wavelet-HL_firstorder_RootMeanSquared	0.87	0.21	16.08%	0.87
diagnostics_Image-original_Maximum	-0.87	0.24	37.68%	0.87
log-sigma-3-0-mm-3D_firstorder_Mean	-0.86	0.13	7.38%	0.86
lbp-2D_glszm_SmallAreaLowGrayLevelEmphasis	0.86	0.28	14.69%	0.86
wavelet-LH_gldm_SmallDependenceLowGrayLevelEmphasis	-0.83	0.3	51.77%	0.83
log-sigma-3-0-mm-3D_glrlm_GrayLevelNonUniformityNormalized	-0.79	0.5	29.19%	0.79
log-sigma-1-0-mm-3D_firstorder_Median	-0.76	0.13	7.11%	0.76
log-sigma-3-0-mm-3D_firstorder_Maximum	-0.75	0.28	22.45%	0.75
original_glcm_SumEntropy	0.75	0.29	26.05%	0.75
log-sigma-1-0-mm-3D_gldm_SmallDependenceHighGrayLevelEmphasis	0.74	0.27	53.15%	0.74
original_shape_Maximum2DDiameterColumn	-0.74	0.17	8.94%	0.74
log-sigma-1-0-mm-3D_firstorder_90Percentile	0.74	0.31	22.56%	0.74
log-sigma-1-0-mm-3D_ngtdm_Contrast	0.73	0.35	53.37%	0.73
log-sigma-3-0-mm-3D_glcm_Correlation	-0.7	0.31	34.13%	0.7
original_gldm_LargeDependenceHighGrayLevelEmphasis	0.69	0.37	42.52%	0.69
log-sigma-1-0-mm-3D_firstorder_Maximum	0.68	0.32	22.56%	0.68
log-sigma-1-0-mm-3D_glcm_Idn	-0.68	0.18	33.90%	0.68
log-sigma-3-0-mm-3D_ngtdm_Strength	0.66	0.18	12.68%	0.66
original_shape_Maximum3DDiameter	0.63	0.29	40.09%	0.63
log-sigma-2-0-mm-3D_firstorder_MeanAbsoluteDeviation	-0.57	0.23	24.41%	0.57
original_glrlm_ShortRunHighGrayLevelEmphasis	-0.53	0.28	36.18%	0.53
lbp-2D_glcm_Correlation	0.52	0.41	51.38%	0.52
wavelet-HH_firstorder_Mean	-0.51	0.2	14.76%	0.51
log-sigma-2-0-mm-3D_gldm_DependenceNonUniformityNormalized	-0.5	0.23	9.25%	0.5

Radiomics	Mean value	Standard Deviation	Coefficient of Variation	Absolute mean value
wavelet-HH_gldm_LargeDependenceLowGrayLevelEmphasis	0.49	0.11	15.23%	0.49
diagnostics_Mask-original_VolumeNum	-0.48	0.11	13.73%	0.48
diagnostics_Image-interpolated_Minimum	0.38	0.13	15.37%	0.38

eMethods: PyRadiomics extraction parameters.

```
setting:
  normalize: False
  binWidth: 5
  label: 1
  correctMask: True
  force2D: True
  force2Ddimension: 0
  padDistance: 5
  preCrop: True
  resampledPixelSpacing: [1, 1, 6]
  interpolator: 'sitkBSpline'
  weightingNorm:
  geometryTolerance: 0.001
imageType:
  Original: {}
  LoG: {'sigma' : [1.0, 2.0, 3.0]}
  LBP2D:
    force2Ddimension : 0
    lbp2DRadius : 1
    lbp2DSamples : 9
    lbp2DMethod : 'uniform'
  Wavelet:
    binWidth: 5
    level : 3
featureClass:
  shape:
  firstorder: []
  glcm:
    - 'Autocorrelation'
    - 'JointAverage'
    - 'ClusterProminence'
    - 'ClusterShade'
    - 'ClusterTendency'
    - 'Contrast'
    - 'Correlation'
    - 'DifferenceAverage'
    - 'DifferenceEntropy'
    - 'DifferenceVariance'
    - 'JointEnergy'
    - 'JointEntropy'
    - 'Imc1'
    - 'Imc2'
    - 'Idm'
    - 'Idmn'
    - 'Id'
    - 'Idn'
    - 'InverseVariance'
    - 'MaximumProbability'
    - 'SumEntropy'
    - 'SumSquares'
  glrlm:
```

glszm:
gldm:
ngtdm:

eFigure 1: Nested cross-validation resampling architecture.

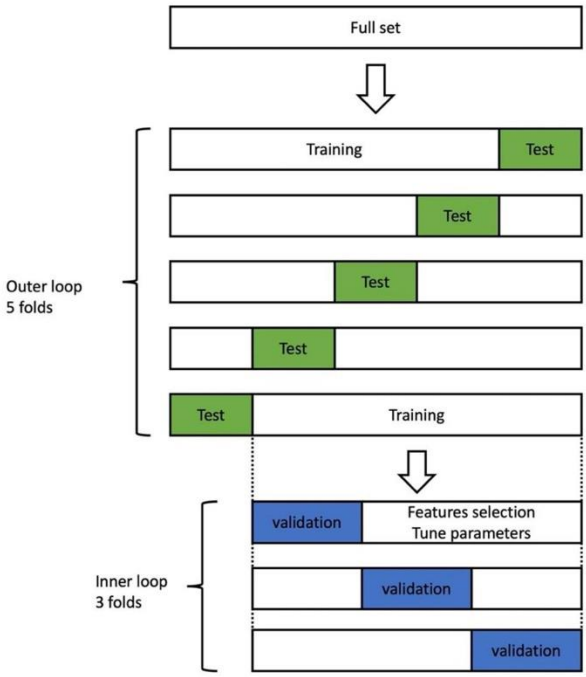

Legend: We used an ElasticNet linear regression model for both feature selection and radiomics-based brain age inference. Feature selection and model parameters tuning was done within the 3-fold inner loop and brain age inference was done within the outer loop. Packages: numpy, pandas, sklearn, pyradiomics

eFigure 3: Examples of Relative Brain Age (RBA) predictions

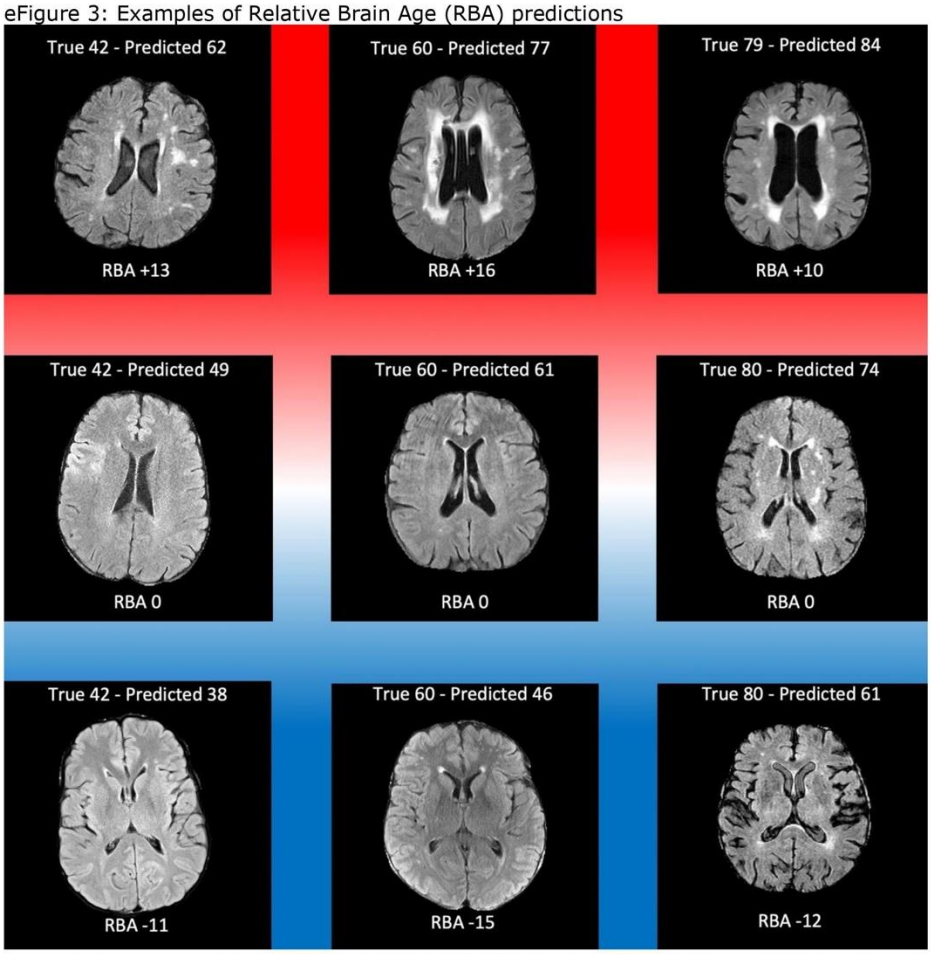

Legend: Examples of stroke patients T2-FLAIR MRI during the 4th, 6th, and 8th decades of life with their respective True chronological age, Predicted Brain Age, and RBA. For each decade, brain scans of patients with higher, neutral, and lower RBA are displayed.

eAppendix 3 RQS Checklist

Image protocol quality - well-documented image protocols (for example, contrast, slice thickness, energy, etc.) and/or usage of public image protocols allow reproducibility/replicability

- ☐ protocols well documented
- ☐ public protocol used
- ☑ none

Multiple segmentations - possible actions are: segmentation by different physicians/algorithms/software, perturbing segmentations by (random) noise, segmentation at different breathing cycles. Analyse feature robustness to segmentation variabilities

- ○ yes
- ◉ no

Phantom study on all scanners - detect inter-scanner differences and vendor-dependent features. Analyse feature robustness to these sources of variability

- ◉ yes
- ○ no

Imaging at multiple time points - collect images of individuals at additional time points. Analyse feature robustness to temporal variabilities (for example, organ movement, organ expansion/shrinkage)

- ○ yes
- ◉ no

Feature reduction or adjustment for multiple testing - decreases the risk of overfitting. Overfitting is inevitable if the number of features exceeds the number of samples. Consider feature robustness when selecting features

- ◉ Either measure is implemented
- ○ Neither measure is implemented

Multivariable analysis with non radiomics features (for example, EGFR mutation) - is expected to provide a more holistic model. Permits correlating/inferencing between radiomics and non radiomics features

- ◉ yes
- ○ no

Detect and discuss biological correlates - demonstration of phenotypic differences (possibly associated with underlying gene–protein expression patterns) deepens understanding of radiomics and biology

- ◉ yes
- ○ no

Cut-off analyses - determine risk groups by either the median, a previously published cut-off or report a continuous risk variable. Reduces the risk of reporting overly optimistic results

- ◉ yes
- ○ no

Discrimination statistics - report discrimination statistics (for example, C-statistic, ROC curve, AUC) and their statistical significance (for example, p-values, confidence intervals). One can also apply resampling method (for example, bootstrapping, cross-validation)

- ☑ a discrimination statistic and its statistical significance are reported

- [x] a resampling method technique is also applied

- [ ] none

Calibration statistics - report calibration statistics (for example, Calibration-in-the-large/slope, calibration plots) and their statistical significance (for example, P-values, confidence intervals). One can also apply resampling method (for example, bootstrapping, cross-validation)

- [ ] a calibration statistic and its statistical significance are reported

- [x] a resampling method technique is applied

- [ ] none

Prospective study registered in a trial database - provides the highest level of evidence supporting the clinical validity and usefulness of the radiomics biomarker

- ( ) yes

- (•) no

Validation - the validation is performed without retraining and without adaptation of the cut-off value, provides crucial information with regard to credible clinical performance

- [ ] No validation

- [ ] validation is based on a dataset from the same institute

- [ ] validation is based on a dataset from another institute

- [ ] validation is based on two datasets from two distinct institutes

- [ ] the study validates a previously published signature

- [x] validation is based on three or more datasets from distinct institutes

Comparison to 'gold standard' - assess the extent to which the model agrees with/is superior to the current 'gold standard' method (for example, TNM-staging for survival prediction). This comparison shows the added value of radiomics

- ( ) yes

- (•) no

Potential clinical utility - report on the current and potential application of the model in a clinical setting (for example, decision curve analysis).

- (•) yes

- ( ) no

Cost-effectiveness analysis - report on the cost-effectiveness of the clinical application (for example, QALYs generated)

- ( ) yes

- (•) no

Open science and data - make code and data publicly available. Open science facilitates knowledge transfer and reproducibility of the study

- [ ] scans are open source
- [ ] region of interest segmentations are open source
- [x] the code is open sourced
- [ ] radiomics features are calculated on a set of representative ROIs and the calculated features and representative ROIs are open source

Total score

18
(50.00%)

eAppendix 4. CLAIM: Checklist for Artificial Intelligence in Medical Imaging

Section / Topic	No.	Item	
TITLE / ABSTRACT			
	1	Identification as a study of AI methodology, specifying the category of technology used (e.g., deep learning)	**Yes**
	2	Structured summary of study design, methods, results, and conclusions	**Yes**
INTRODUCTION			
	3	Scientific and clinical background, including the intended use and clinical role of the AI approach	**P1**
	4	Study objectives and hypotheses	**P1**
METHODS			
Study Design	**5**	Prospective or retrospective study	**P2**
	6	Study goal, such as model creation, exploratory study, feasibility study, non-inferiority trial	**P2**
Data	**7**	Data sources	**P2**
	8	Eligibility criteria: how, where, and when potentially eligible participants or studies were identified (e.g., symptoms, results from previous tests, inclusion in registry, patient-care setting, location, dates)	**P2**
	9	Data pre-processing steps	**P3**
	10	Selection of data subsets, if applicable	**NA**
	11	Definitions of data elements, with references to Common Data Elements	**NA**
	12	De-identification methods	**NA**
	13	How missing data were handled	**P3**
Ground Truth	**14**	Definition of ground truth reference standard, in sufficient detail to allow replication	**P4**
	15	Rationale for choosing the reference standard (if alternatives exist)	**NA**
	16	Source of ground-truth annotations; qualifications and preparation of annotators	**P4**
	17	Annotation tools	**NA**
	18	Measurement of inter- and intrarater variability; methods to mitigate variability and/or resolve discrepancies	**NA**
Data Partitions	**19**	Intended sample size and how it was determined	**P3**
	20	How data were assigned to partitions; specify proportions	**P4**
	21	Level at which partitions are disjoint (e.g., image, study, patient, institution)	**P4**

Model	**22**	Detailed description of model, including inputs, outputs, all intermediate layers and connections	**P4**
	23	Software libraries, frameworks, and packages	**P6**
	24	Initialization of model parameters (e.g., randomization, transfer learning)	**NA**
Training	**25**	Details of training approach, including data augmentation, hyperparameters, number of models trained	**P4**
	26	Method of selecting the final model	**P4**
	27	Ensembling techniques, if applicable	**NA**
Evaluation	**28**	Metrics of model performance	**P4**
	29	Statistical measures of significance and uncertainty (e.g., confidence intervals)	**NA**
	30	Robustness or sensitivity analysis	**P4**
	31	Methods for explainability or interpretability (e.g., saliency maps), and how they were validated	**NA**
	32	Validation or testing on external data	**NA**
RESULTS			
Data	**33**	Flow of participants or cases, using a diagram to indicate inclusion and exclusion	**supp**
	34	Demographic and clinical characteristics of cases in each partition	**P7**
Model performance	**35**	Performance metrics for optimal model(s) on all data partitions	**P8**
	36	Estimates of diagnostic accuracy and their precision (such as 95% confidence intervals)	**P7-8**
	37	Failure analysis of incorrectly classified cases	**NA**
DISCUSSION			
	38	Study limitations, including potential bias, statistical uncertainty, and generalizability	**P15**
	39	Implications for practice, including the intended use and/or clinical role	**P13-14**
OTHER INFORMATION			
	40	Registration number and name of registry	**P2**
	41	Where the full study protocol can be accessed	**P2**
	42	Sources of funding and other support; role of funders	**P15-16**

Mongan J, Moy L, Kahn CE Jr. Checklist for Artificial Intelligence in Medical Imaging (CLAIM): a guide for authors and reviewers. Radiol Artif Intell 2020; 2(2):e200029. https://doi.org/10.1148/ryai.2020200029

Discussion

Synthèse générale

La prise en charge de l'AVC évolue rapidement et l'imagerie occupe une place centrale guidant la plupart des décisions thérapeutiques. Son interprétation est donc lourde de sanctions et le besoin d'outils objectifs d'aide à la décision est indéniable. A travers les travaux présentés ici, nous avons pu aborder certaines pistes de solutions pour aiguiller certaines d'entre elles.

En travaillant à la croisée des chemins des méthodes de pointes que sont l'IRM, l'intelligence artificielle, et les analyses radiomics, nous avons développé des biomarqueurs personnalisés pour caractériser l'AVC et la santé cérébrale à partir d'imageries de routine. Nous avons proposé des méthodes innovantes pour caractériser la discordance DWI-FLAIR, mesurer la santé cérébrale de manière globale au-delà des altérations visibles, comprendre les déterminants d'une sénescence cérébrale accélérée, et surtout, quantifier l'impact pronostic d'un âge cérébral élevé sur la récupération fonctionnelle après un AVC. Ainsi, nous avons tenté d'apprécier l'effet du temps sur les patients victimes d'AVC ischémique, que l'échelle soit en heures sur la lésion ischémique, ou bien en années sur la santé cérébrale. Nos travaux portent des implications concrètes pour une personnalisation de la prise en soin des patients et l'espoir d'une transition facilitée à la clinique.

Un des changements de paradigme les plus disruptifs dans la prise en charge de l'AVC a été celui du temps. Pendant deux décennies, le temps a guidé les indications thérapeutiques laissant pour compte les patients se présentant après la barre fatidique des 4h30 après le début des symptômes. Lors des débuts de la thrombectomie mécanique, le temps était lui aussi un critère important, n'étant indiqué que dans les 6 premières heures. Dans un traitement comme dans l'autre, les patients présentant un AVC du réveil se voyaient exclus, posant un réel problème clinique : en effet, 1 patient sur 5 présente un AVC du réveil.[46] Ce n'est qu'à la publication des études DAWN, WAKE-UP, et DEFUSE3 que le temps a cessé de diriger les indications.[8,9,11] L'imagerie cérébrale avancée, via les techniques de discordance DWI-FLAIR (DAWN, WAKE-UP) et de perfusion (DEFUSE3), a donc permis un bond thérapeutique dans la prise en charge de l'AVC, permettant de passer du paradigme de l'horloge à celui de l'horloge biologique,

s'affranchissant donc du temps. On n'inspecte plus la montre en projetant des probabilités pronostiques dépendantes du temps, mais on examine la résilience particulière d'un individu à l'ischémie cérébrale. Alors que dans l'imagerie de perfusion la lecture est devenue automatisée par des logiciels d'intelligence artificielle comme RapidAI (iSchemaView, Inc, Golden, CO 80401, USA) et que les critères d'indication ont été standardisés, l'interprétation de la discordance DWI-FLAIR reste subjective. Notre étude a montré qu'il était possible de quantifier cette discordance et de produire un biomarqueur grâce à l'analyse de texture radiomics. De plus, notre signature radiomics reste simple, n'étant constituée que de deux variables. Certains auteurs ont montré que la comparaison du signal FLAIR intra-lésionnel et controlatéral était également possible.[47] Cependant elle nécessite une intervention manuelle substantielle pour positionner un ROI au bon endroit dans la lésion ischémique ainsi qu'en miroir dans l'hémisphère controlatéral, puis de calculer un ratio. Notre méthode peut être complètement automatisée et on pourrait la conceptualiser comme une brique logicielle intégrée dans une suite qui comporterait une segmentation automatique de la lésion ischémique. Nous proposons donc une solution d'aide à la caractérisation de la discordance DWI-FLAIR dans l'AVC ischémique du réveil ou de début inconnu.

La santé cérébrale est un objectif de l'Organisation Mondiale pour la Santé, au cœur de sa feuille de route 2022-2030 sur les pathologies neurologiques.[48] Les enjeux de la santé cérébrale sont multiples, allant de la santé globale et du bien-être des individus à notre conception de la société, de son développement, et de sa productivité. Son maintien et son optimisation sont donc des objectifs structurants pour une population dont l'âge augmente progressivement. L'AVC est une pathologie fortement liée à l'âge, notamment par son incidence et son pronostic. Elle est également un des principaux contributeurs d'une mauvaise santé cérébrale mais est aussi une de ses conséquences.[1,32] Mesurer et optimiser la santé cérébrale, notamment dans des pathologies stratégiques dépendantes de l'âge, est un axe de recherche à prendre dès à présent pour dessiner la médecine de demain.

La neuroimagerie est la manière de choix pour explorer la santé cérébrale, cependant de nombreux freins empêchent les méthodes développées de se déployer dans la pratique clinique. En effet, la plupart des méthodes s'appuient sur de l'imagerie de recherche et un large fossé

sépare la qualité de l'imagerie de recherche à celle acquise lors du soin. De plus, outre la qualité de l'imagerie, le type de séquence acquise est parfois inadapté à la sévérité des patients ou à la routine clinique. C'est pour cette raison qu'il est nécessaire de développer des techniques d'inférence de la santé cérébrale pouvant exploiter les imageries acquises dans le cadre du soin.

Nous avons pu montrer que les analyses radiomics pouvaient extraire des données pertinentes à partir d'imagerie T2-FLAIR acquises dans le cadre du soin. Cette séquence est ubiquitaire dans les protocoles d'exploration des pathologies cérébrales et notamment lors du bilan initial et du suivi des patients victimes d'AVC ischémique. Il est donc pertinent de s'appuyer sur cette séquence pour sonder la santé cérébrale. La leucopathie est un biomarqueur de santé cérébral évident à la lecture du T2-FLAIR, cependant on sait, grâce à des techniques d'imagerie complexes, que des anomalies parenchymateuse s'étendent bien au-delà dans le parenchyme d'allure saine.[34] Nous avons pu répliquer ce résultat et ainsi montrer, uniquement à partir d'imagerie clinique de routine T2-FLAIR, et grâce à l'analyse radiomics de la texture, que la leucopathie ne représentait que la partie émergée de l'iceberg, capturant des altérations invisibles à l'œil nu pourtant intégrantes du continuum lésionnel cérébral. Le volume de leucopathie croit avec les facteurs de risques cardiovasculaires, mais nous avons également montré que l'expression texturale de la leucopathie au sein du parenchyme cérébral normale étaient corrélée à la présence de facteurs de risques cardiovasculaires. En outre, nos résultats étaient en faveur d'une d'expression texturale différenciée et spécifique de certains risques cardiovasculaires. Les analyses radiomics permettent donc de capturer des éléments sur l'imagerie T2-FLAIR de routine qui traduisent l'expression spécifique parenchymateuse cérébrale du profil de risque cardiovasculaire des patients.

Parmi les biomarqueurs de santé cérébrale, l'âge cérébral est un biomarqueur intuitif et attrayant. Il résulte de l'analyse de la neuroimagerie IRM et peut être obtenu classiquement de plusieurs manières, soit par analyse directe de l'image par des algorithmes d'intelligence artificielle, soit, plus fréquemment, par prédiction à partir des volumétries cérébrales.[49] Ces méthodes sont très largement basées sur l'imagerie pondérée T1, non acquise lors du bilan IRM initial des patients suspects d'AVC. Les radiomics, quant à eux, peuvent être appliquées à l'imagerie T2-FLAIR et sont donc adaptée à cette tâche, cependant leur performance dans la

prédiction de l'âge cérébral est inconnue. Le résultat le plus important notre première étude a été de montrer que la signature radiomics de l'expression latente de la leucopathie dans le parenchyme d'allure normale était corrélée à l'âge chronologique, autorisant alors l'hypothèse de l'inférence radiomics de l'âge cérébral.

Nos résultats ont montré que l'âge cérébral pouvait être produit par l'analyse radiomics du T2-FLAIR d'imageries acquises lors du soin et qu'il était pertinent dans l'étude de la santé cérébrale et la prédiction du pronostic après AVC. Au-delà de la simple preuve de concept de la faisabilité de cette méthode, nous avons pu montrer que les patients qui avaient un cerveau d'allure plus âgée avaient plus de facteurs de risques cardiovasculaires. De plus, certains de ces facteurs de risques sont modifiables ce qui ouvre la voie à un suivi en neuroimagerie de la santé cérébral ainsi qu'à des études sur le contrôle de ces facteurs de risque. De plus, nos résultats confirment les données de la littérature publiées sur l'impact négatif de l'AVC, de l'hypertension, du diabète, du tabagisme, et des pathologies cardiaques sur l'âge cérébral.[50–54] Notre projet a également montré la relation complexe qui existe entre sévérité de l'infarctus, âge cérébral, et pronostic. Avoir un cerveau d'allure plus âgée et donc en moins bonne santé cérébrale, est associé à une moins bonne récupération fonctionnelle après AVC. Comme présupposé, l'impact pronostic négatif de l'âge cérébral était prédominant dans les formes moins sévères, alors que dans les AVC graves, son effet était relativement moindre. Ce résultat est en faveur de la sensibilité de l'âge cérébral à la réserve structurelle cérébrale et donc à la résilience individuelle aux pathologies neurologiques. Ce point précis pourrait nous aiguiller chez les patients présentant un AVC peu sévère avec un NIHSS <5, situation dans laquelle il existe une équipoise thérapeutique et qui est le sujet de nombreux essais cliniques randomisés en cours évaluant l'intérêt de la thrombectomie mécanique. En effet, lorsqu'un patient souffre d'un AVC peu sévère, ses chances de récupération spontanées sont élevées. Cependant, s'il est en mauvaise santé cérébrale, on peut imaginer que ses chances de récupération sans intervention sont plus faibles et qu'il pourrait plus bénéficier d'un traitement qu'un patient en bonne santé cérébrale. De plus, il semble que les altération parenchymateuses qui conduisent à un âge cérébral plus élevé précèdent l'AVC.[17] De ce fait, l'âge cérébral pourrait être étudié comme critère d'inclusion dans des essais thérapeutiques de prévention primaire afin de tester l'hypothèse d'une réduction

de risque d'AVC. Outre la prévention primaire, la prévention tertiaire est également une hypothèse de travail, mais il reste à démontrer si l'âge cérébral peut être utilisé afin de personnaliser l'intensité de la rééducation après un AVC.[44]

Limites

Nos travaux ont de nombreuses limites qui sont principalement liées à la nature rétrospective de nos analyses. A cette limite se rajoute le décalage anachronique de la cohorte MRIGENIE. En effet, ses patients sont issus d'un amalgame de différentes cohortes dont les plus récentes ont été constituées en 2011. De plus, ils diffèrent des patients traités par thrombectomie à la fois en termes de distribution de la sévérité des AVC, de délais de prises en charge et d'IRM cérébrale, mais surtout en termes de traitement reçus. Désormais, et depuis 2015, la thrombectomie est un traitement incontournable de l'AVC et cet aspect est un frein à la généralisabilité de nos résultats.

Nous reconnaissons également une limite conceptuelle de nos résultats sur la discordance DWI-FLAIR. En effet, nous n'avons pas exploré les déterminants de l'apparition d'un hypersignal FLAIR intra-lésionnel, ce qui pourrait aider à mieux sélectionner les patients durant la phase préhospitalière. L'étude de la relation entre le temps, l'état du parenchyme cérébral, la lésion ischémique, son aspect en imagerie, et la qualité des collatérales leptoméningées pourrait également apporter des connaissances nouvelles pour la discipline. Une autre limitation concerne le manque d'intégration de la localisation des lésions ischémiques ou des biomarqueurs sus-cités dans la modélisation pronostique. Enfin, la performance de notre algorithme et son applicabilité chez des patients présentant un AVC sévère reste incertaine tant leur imagerie peut être artéfactée par les mouvements involontaires.

Perspectives

Les principales perspectives de ces travaux sont la réplication de nos résultats sur des cohortes modernes de patients victimes d'AVC ischémique. Il sera donc nécessaire de constituer une cohorte d'imagerie des patients traités à Lille par thrombectomie mécanique pour un AVC ischémique.

Nous validerons notre signature radiomics de la discordance DWI-FLAIR sur la cohorte des patients traités par thrombectomie à Lille afin de tester la robustesse et la validité de notre signature radiomics de la discordance DWI-FLAIR. Enfin, nous pourrons tester l'impact de ce biomarqueur personnalisé quantitatif sur la prise en charge de l'AVC du réveil, à la fois en termes de pronostic, mais également sur d'optimisation du temps, la standardisation des décisions, et le confort des praticiens impliqués dans cette filière.

Les perspectives de notre étude sur l'âge cérébral passent également par sa réplication sur les patients traités par thrombectomie mécanique à Lille. Ces efforts de réplication ont d'ores et déjà débuté et les résultats préliminaires seront présentés ci-dessous.

Ces deux efforts de réplications seront pour moi l'opportunité d'encadrer des étudiants en master, et des thèses de radiologues. Deux étudiants en licence pour la santé et un étudiant en master 1 sont déjà positionnés pour aider à la constitution de la cohorte cet été, et un étudiant en master 2 explorera à partir de novembre 2023 l'âge cérébral chez ces patients, notamment pour aider les décisions d'hémicraniectomie.

Résultats préliminaires de l'âge cérébral sur la cohorte de Lille

Afin de déterminer si l'âge cérébral est un biomarqueur pertinent dans la prise en charge moderne de l'AVC, nous avons débuté la constitution une cohorte de patients traités par thrombectomie mécanique au CHU de Lille. Cette entreprise a été financée par la European Society of Radiology et par la European Institute for Biomedical Imaging Research dans le cadre de leur programme « Seed Grant ». Nous avons également déposé ce projet durant la campagne d'appel à projets GIRCI Nord-Ouest « Aide à l'émergence » 2023.

En 2019, 458 patients ont été traités par thrombectomie mécanique au CHU de Lille. Après exclusions des patients pour imagerie manquantes, corrompues, ou de qualité non-satisfaisante, 371 patients ont été analysés. L'algorithme de segmentation de la leucopathie, du parenchyme cérébral, et des ventricules est toujours en cours de transfert entre le Mass Generral Brigham et le CHU de Lille. Nous avons donc opté pour une stratégie alternative : nous avons extrait les volumétries cérébrales parcellisées à partir de l'imagerie T2-FLAIR grâce à SynthSeg, un outil puissant récemment déployé dans l'environnement FreeSurfer.[55,56] Nous avons ensuite répliqué l'analyse en substituant ce vecteur de volumétries cérébrales aux radiomics, prédit l'âge cérébral à partir de ces volumes corticaux et sous corticaux, et dérivé l'âge cérébral relatif (Figure 3). Enfin, de manière similaire, nous avons analysé les déterminants cliniques d'un cerveau d'allure plus âgé en réalisant une régression linéaire multiple de l'âge cérébral relatif à l'aide des variables cliniques. Enfin, pour tester si l'âge cérébral avancé est un facteur pronostic pertinent même dans la prise en charge moderne de l'AVC, nous avons réalisé une régression logistique multivariée de pronostic à l'aide des variables cliniques, de l'âge cérébral relatif, et des variables de traitement.

Figure 3 : L'âge cérébral relatif à partir de volumétries issues de l'imagerie 2D T2-FLAIR

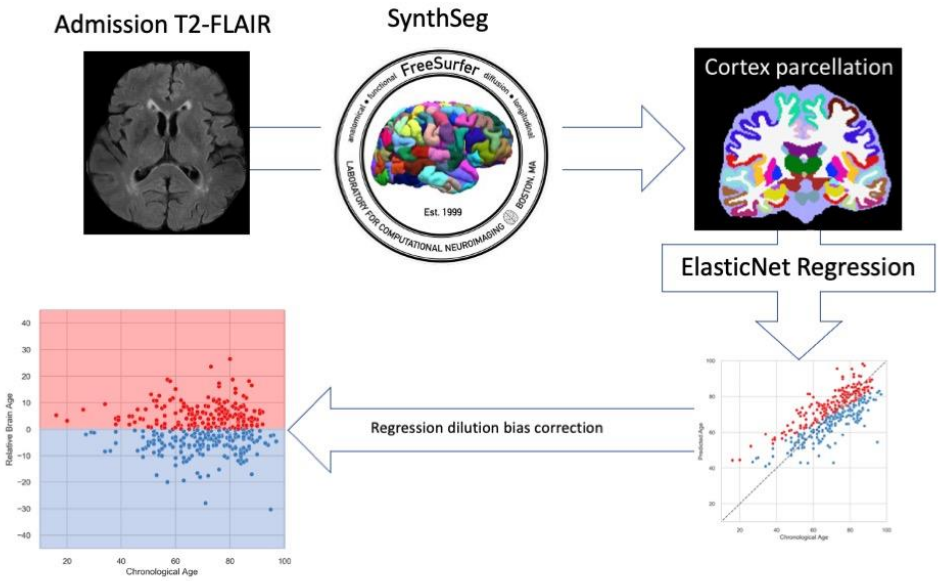

Premièrement, les caractéristiques de la cohorte étaient sans particularité et superposables à celles de la littérature portant sur la thrombectomie mécanique (âge moyen = 70 ans, 54% femmes, NIHSS médian = 16, 47% thrombolysés, 75% de recanalisation satisfaisante, 34% de bon pronostic fonctionnel).

Deuxièmement, nous avons montré que les données volumétriques corticales et sous-corticales peuvent êtes extraites de séquences 2D T2-FLAIR et pouvaient être utilisées pour prédire l'âge cérébral.

Troisièmement, l'analyse multivariée des déterminants cliniques de l'âge cérébral relatif a retrouvé des facteurs de risques similaires que lors de notre analyse conduite dans MRIGENIE (Table 1).

Enfin, nous avons trouvé que l'âge cérébral avancé était un facteur de risque de mauvais pronostic après AVC chez les patients traités par thrombectomie, indépendamment de l'âge chronologique, de la sévérité de l'AVC, ou bien de la qualité de la recanalisation. (Table 2)

Table 1 : Analyse multivariée des déterminants clinique de l'âge cérébral relatif

	coef.	P>|t|	[0.025	0.975]
Hypertension	2.69	<0.001	1.03	4.35
Diabetes mellitus	2.09	0.03	0.26	3.92

Variables testées : Age, sexe, hypertension, diabète, fibrillation atriale, dyslipidémie, tabagisme, occlusion en tandem, AVC du réveil, poids, pression artérielle systolique, pression artérielle diastolique, glycémie. Modèle : régression linéaire.

Table 2 : Analyse multivariée du pronostic après AVC

	Coefficient std.	Odds-ratio	95% CI	P>|z|
Age	-0.75	0.47	0.36 - 0.62	<0.001
Age cérébral relatif	**-0.39**	**0.68**	**0.52 - 0.89**	**0.005**
NIHSS	-0.60	0.54	0.41 - 0.73	<0.001
Thrombolyse	0.80	2.23	1.33 - 3.74	0.002
Recanalisation	1.88	6.55	2.88 - 14.90	<0.001
Temps de procédure	-0.53	0.59	0.43 - 0.80	0.001

Variables testées : temps imagerie-thrombectomie, thrombolyse, recanalisation satisfaisantee, temps de procédure, age, sexe, hypertension, diabète, fibrillation atriale, dyslipidémie, tabagisme, occlusion en tandem, AVC du réveil, poids, pression artérielle systolique, pression artérielle diastolique, glycémie. Modèle : régression logistique.

Ces résultats sont préliminaires et seront étoffé lors l'expansion de la cohorte locale des patients traités par thrombectomie. De plus, une comparaison entre les prédictions de l'âge cérébral par radiomics et par volumétrie cérébrale sera effectuée afin de déterminer méthode la plus adaptée. Enfin, une publication est prévue dans *European Radiology*, comme mandaté par la bourse reçue pour conduire ce travail.

Conclusion

J'ai eu le plaisir de partager ces quatre années de thèse entre Boston et Lille, et d'acquérir des connaissances et des compétences en recherche en neuroimagerie appliquées à l'AVC ischémique. J'ai aimé travailler sur à l'intersection de la radiologie, de l'intelligence artificielle, et des neurosciences. J'ai pu tenter de répondre à certaines des questions qui émaillent la prise en charge de ces patients dans notre quotidien au CHU de Lille. J'ai particulièrement tiré une grande fierté de produire des résultats à l'aide d'imagerie acquises dans le cadre du soin, personnellement convaincu du caractère essentiel d'une telle approche.

Premièrement, nous avons pu développer une méthode radiomics pour caractériser le signal FLAIR de l'infarctus et ainsi poser la première pierre d'un effort de standardisation dans son interprétation.

Deuxièmement, nous avons montré, grâce à l'approche radiomics couplée aux méthodes d'apprentissage machine, que l'imagerie clinique constituait une véritable source de données exploitables. Ainsi, nous avons montré que l'analyse radiomics d'images T2-FLAIR de patients victimes d'AVC permettait de capturer la charge lésionnelle cérébrale et de prédire l'âge cérébral.

Enfin, nous avons montré l'intérêt de l'âge cérébral comme biomarqueur personnalisé de santé cérébrale chez les patients victimes d'AVC ischémiques capturant à la fois les conséquences encéphaliques du profil cardiovasculaire individuel, et surtout impactant le pronostic après AVC.

Références

1. Feigin VL, Stark BA, Johnson CO, et al. Global, regional, and national burden of stroke and its risk factors, 1990–2019: a systematic analysis for the Global Burden of Disease Study 2019. The Lancet Neurology. 2021;20:795–820.

2. Adams HP, Bendixen BH, Kappelle LJ, et al. Classification of subtype of acute ischemic stroke. Definitions for use in a multicenter clinical trial. TOAST. Trial of Org 10172 in Acute Stroke Treatment. Stroke. 1993;24:35–41.

3. Flueckiger P, Longstreth W, Herrington D, Yeboah J. Revised Framingham Stroke Risk Score, Nontraditional Risk Markers, and Incident Stroke in a Multiethnic Cohort. Stroke. American Heart Association; 2018;49:363–369.

4. Powers WJ, Rabinstein AA, Ackerson T, et al. Guidelines for the Early Management of Patients With Acute Ischemic Stroke: 2019 Update to the 2018 Guidelines for the Early Management of Acute Ischemic Stroke: A Guideline for Healthcare Professionals From the American Heart Association/American Stroke Association. Stroke. American Heart Association; 2019;50:e344–e418.

5. Demeestere J, Wouters A, Christensen S, Lemmens R, Lansberg MG. Review of Perfusion Imaging in Acute Ischemic Stroke. Stroke. American Heart Association; 2020;51:1017–1024.

6. Emberson J, Lees KR, Lyden P, et al. Effect of treatment delay, age, and stroke severity on the effects of intravenous thrombolysis with alteplase for acute ischaemic stroke: a meta-analysis of individual patient data from randomised trials. The Lancet. 2014;384:1929–1935.

7. Goyal M, Menon BK, van Zwam WH, et al. Endovascular thrombectomy after large-vessel ischaemic stroke: a meta-analysis of individual patient data from five randomised trials. Lancet. 2016;387:1723–1731.

8. Nogueira RG, Jadhav AP, Haussen DC, et al. Thrombectomy 6 to 24 Hours after Stroke with a Mismatch between Deficit and Infarct. N Engl J Med. Epub 2017 Nov 11.

9. Albers GW, Marks MP, Kemp S, et al. Thrombectomy for Stroke at 6 to 16 Hours with Selection by Perfusion Imaging. New England Journal of Medicine. 2018;378:708–718.

10. Rocha M, Jovin TG. Fast Versus Slow Progressors of Infarct Growth in Large Vessel Occlusion Stroke: Clinical and Research Implications. Stroke. 2017;48:2621–2627.

11. Thomalla G, Fiebach JB, Østergaard L, et al. A multicenter, randomized, double-blind, placebo-controlled trial to test efficacy and safety of magnetic resonance imaging-based thrombolysis in wake-up stroke (WAKE-UP). Int J Stroke. 2014;9:829–836.

12. Thomalla G, Cheng B, Ebinger M, et al. DWI-FLAIR mismatch for the identification of patients with acute ischaemic stroke within 4·5 h of symptom onset (PRE-FLAIR): a multicentre observational study. The Lancet Neurology. 2011;10:978–986.

13. Drozdowska BA, Singh S, Quinn TJ. Thinking About the Future: A Review of Prognostic Scales Used in Acute Stroke. Front Neurol. Frontiers Media S.A.; 2019;10:274–274.

14. Boulouis G, Bricout N, Benhassen W, et al. White matter hyperintensity burden in patients with ischemic stroke treated with thrombectomy. Neurology. 2019;93:e1498–e1506.

15. Groot AE, Treurniet KM, Jansen IGH, et al. Endovascular treatment in older adults with acute ischemic stroke in the MR CLEAN Registry. Neurology. Wolters Kluwer Health, Inc. on behalf of the American Academy of Neurology; 2020;95:e131–e139.

16. Etherton MR, Wu O, Cougo P, et al. Integrity of normal-appearing white matter and functional outcomes after acute ischemic stroke. Neurology. 2017;88:1701–1708.

17. Werden E, Cumming T, Li Q, et al. Structural MRI markers of brain aging early after ischemic stroke. Neurology. 2017;89:116–124.

18. Lambin P, Leijenaar RTH, Deist TM, et al. Radiomics: the bridge between medical imaging and personalized medicine. Nat Rev Clin Oncol. 2017;14:749–762.

19. Chen Q, Xia T, Zhang M, Xia N, Liu J, Yang Y. Radiomics in Stroke Neuroimaging: Techniques, Applications, and Challenges. Aging and Disease. 2021;12:12.

20. Giese A-K, Schirmer MD, Donahue KL, et al. Design and rationale for examining neuroimaging genetics in ischemic stroke: The MRI-GENIE study. Neurol Genet. 2017;3:e180.

21. Haralick RM, Shanmugam K, Dinstein I. Textural Features for Image Classification. IEEE Transactions on Systems, Man, and Cybernetics. 1973;SMC-3:610–621.

22. Lambin P, Rios-Velazquez E, Leijenaar R, et al. Radiomics: Extracting more information from medical images using advanced feature analysis. European Journal of Cancer. 2012;48:441–446.

23. Aerts HJWL, Velazquez ER, Leijenaar RTH, et al. Decoding tumour phenotype by noninvasive imaging using a quantitative radiomics approach. Nature Communications. 2014;5:4006.

24. Gillies RJ, Kinahan PE, Hricak H. Radiomics: Images Are More than Pictures, They Are Data. Radiology. Radiological Society of North America; 2015;278:563–577.

25. Fournier L, Costaridou L, Bidaut L, et al. Incorporating radiomics into clinical trials: expert consensus endorsed by the European Society of Radiology on considerations for data-driven compared to biologically driven quantitative biomarkers. Eur Radiol. 2021;31:6001–6012.

26. Ligero M, Jordi-Ollero O, Bernatowicz K, et al. Minimizing acquisition-related radiomics variability by image resampling and batch effect correction to allow for large-scale data analysis. Eur Radiol. Epub 2020 Sep 9.

27. Haarburger C, Müller-Franzes G, Weninger L, Kuhl C, Truhn D, Merhof D. Radiomics feature reproducibility under inter-rater variability in segmentations of CT images. Sci Rep. Nature Publishing Group; 2020;10:12688.

28. Duron L, Balvay D, Perre SV, et al. Gray-level discretization impacts reproducible MRI radiomics texture features. PLOS ONE. 2019;14:e0213459.

29. Park JE, Park SY, Kim HJ, Kim HS. Reproducibility and Generalizability in Radiomics Modeling: Possible Strategies in Radiologic and Statistical Perspectives. Korean Journal Of Radiology. 2019;20:1124–1137.

30. Bretzner M, Bonkhoff AK, Schirmer MD, et al. Radiomics-Derived Brain Age Predicts Functional Outcome After Acute Ischemic Stroke. Neurology. 2023;100:e822–e833.

31. Schirmer MD, Etherton MR, Dalca AV, et al. Effective reserve: a latent variable to improve outcome prediction in stroke. J Stroke Cerebrovasc Dis. 2019;28:63–69.

32. Gardener H, Wright CB, Rundek T, Sacco RL. Brain health and shared risk factors for dementia and stroke. Nat Rev Neurol. 2015;11:651–657.

33. Maillard P, Fletcher E, Harvey D, et al. White matter hyperintensity penumbra. Stroke. 2011;42:1917–1922.

34. Maniega SM, Valdés Hernández MC, Clayden JD, et al. White matter hyperintensities and normal-appearing white matter integrity in the aging brain. Neurobiol Aging. 2015;36:909–918.

35. Schirmer MD, Dalca AV, Sridharan R, et al. White matter hyperintensity quantification in large-scale clinical acute ischemic stroke cohorts – The MRI-GENIE study. NeuroImage: Clinical. 2019;23:101884.

36. Cox SR, Lyall DM, Ritchie SJ, et al. Associations between vascular risk factors and brain MRI indices in UK Biobank. European Heart Journal. 2019;40:2290–2300.

37. Dickie DA, Valdés Hernández M del C, Makin SD, et al. The brain health index: Towards a combined measure of neurovascular and neurodegenerative structural brain injury. International Journal of Stroke. SAGE Publications; 2018;13:849–856.

38. Beaudet G, Tsuchida A, Petit L, et al. Age-Related Changes of Peak Width Skeletonized Mean Diffusivity (PSMD) Across the Adult Lifespan: A Multi-Cohort Study. Frontiers in Psychiatry. 2020;11:342.

39. Fjell AM, McEvoy L, Holland D, Dale AM, Walhovd KB. What is normal in normal aging? Effects of aging, amyloid and Alzheimer's disease on the cerebral cortex and the hippocampus. Progress in Neurobiology. 2014;117:20–40.

40. Franke K, Gaser C. Ten Years of BrainAGE as a Neuroimaging Biomarker of Brain Aging: What Insights Have We Gained? Front Neurol. 2019;10:789.

41. Bashyam VM, Erus G, Doshi J, et al. MRI signatures of brain age and disease over the lifespan based on a deep brain network and 14 468 individuals worldwide. Brain. 2020;143:2312–2324.

42. Cole JH, Poudel RPK, Tsagkrasoulis D, et al. Predicting brain age with deep learning from raw imaging data results in a reliable and heritable biomarker. NeuroImage. 2017;163:115–124.

43. Egorova N, Liem F, Hachinski V, Brodtmann A. Predicted Brain Age After Stroke. Front Aging Neurosci. Frontiers Media S.A.; 2019;11:348–348.

44. Richard G, Kolskår K, Ulrichsen KM, et al. Brain age prediction in stroke patients: Highly reliable but limited sensitivity to cognitive performance and response to cognitive training. NeuroImage: Clinical. 2020;25:102159.

45. Beheshti I, Nugent S, Potvin O, Duchesne S. Bias-adjustment in neuroimaging-based brain age frameworks: A robust scheme. Neuroimage Clin. 2019;24:102063.

46. Mackey J, Kleindorfer D, Sucharew H, et al. Population-based study of wake-up strokes. Neurology. 2011;76:1662–1667.

47. Schwamm LH, Wu O, Song SS, et al. Intravenous thrombolysis in unwitnessed stroke onset: MR WITNESS trial results: Thrombolysis in Stroke. Ann Neurol. 2018;83:980–993.

48. Optimizing brain health across the life course: WHO position paper [online]. Accessed at: https://www.who.int/publications-detail-redirect/9789240054561. Accessed February 28, 2023.

49. Lombardi A, Monaco A, Donvito G, Amoroso N, Bellotti R, Tangaro S. Brain Age Prediction With Morphological Features Using Deep Neural Networks: Results From Predictive Analytic Competition 2019. Front Psychiatry. 2020;11:619629.

50. Franke K, Gaser C, Manor B, Novak V. Advanced BrainAGE in older adults with type 2 diabetes mellitus. Front Aging Neurosci. Frontiers Media S.A.; 2013;5:90–90.

51. Steffener J, Habeck C, O'Shea D, Razlighi Q, Bherer L, Stern Y. Differences between chronological and brain age are related to education and self-reported physical activity. Neurobiol Aging. 2016;40:138–144.

52. de Lange A-MG, Anatürk M, Suri S, et al. Multimodal brain-age prediction and cardiovascular risk: The Whitehall II MRI sub-study. NeuroImage. 2020;222:117292.

53. Cole JH. Multimodality neuroimaging brain-age in UK biobank: relationship to biomedical, lifestyle, and cognitive factors. Neurobiol Aging. 2020;92:34–42.

54. Ning K, Zhao L, Matloff W, Sun F, Toga AW. Association of relative brain age with tobacco smoking, alcohol consumption, and genetic variants. Scientific Reports. Nature Publishing Group; 2020;10:10.

55. Billot B, Greve DN, Puonti O, et al. SynthSeg: Segmentation of brain MRI scans of any contrast and resolution without retraining. Medical Image Analysis. 2023;86:102789.

56. Fischl B. FreeSurfer. Neuroimage. 2012;62:774–781.